

This item was submitted to [Loughborough's Research Repository](#) by the author.  
Items in Figshare are protected by copyright, with all rights reserved, unless otherwise indicated.

## A study of discrete nonlinear systems

PLEASE CITE THE PUBLISHED VERSION

PUBLISHER

© H.S. Dhillon

PUBLISHER STATEMENT

This work is made available according to the conditions of the Creative Commons Attribution-NonCommercial-NoDerivatives 4.0 International (CC BY-NC-ND 4.0) licence. Full details of this licence are available at:  
<https://creativecommons.org/licenses/by-nc-nd/4.0/>

LICENCE

CC BY-NC-ND 4.0

REPOSITORY RECORD

Dhillon, Harjinder S.. 2019. "A Study of Discrete Nonlinear Systems". figshare.  
<https://hdl.handle.net/2134/34292>.



## Pilkington Library

Author/Filing Title ..... DHILLON .....

Vol. No. .... Class Mark ..... T .....

**Please note that fines are charged on ALL  
overdue items.**

**FOR REFERENCE ONLY**

0402507991



# BRITISH THESIS SERVICE

**DX235021**

Awarding Body : Loughborough  
Thesis By : DHILLON Harjinder Singh  
Thesis Title : A STUDY OF DISCRETE NONLINEAR SYSTEMS

We have assigned this thesis the number given at the top of this sheet.

**THE BRITISH LIBRARY  
DOCUMENT SUPPLY CENTRE**



# **A Study Of Discrete Nonlinear Systems**

by

HARJINDER SINGH DHILLON

A Doctoral Thesis


Submitted in partial fulfilment of the requirements

for the award of

Doctor of Philosophy of Loughborough University

April 2001

©by H. S. Dhillon, 2001.

 Loughborough University Pitt Rivers Library	
Date	Mar 02
Class	
Acc No.	0402507991

To my mother,  
For more than I can express.

## Abstract

An investigation of various spatially discrete time-independent nonlinear models was undertaken. These models are generically applicable to many different physical systems including electron-phonon interactions in solids, magnetic multilayers, layered superconductors and classical lattice systems.

To characterise the possible magnetic structures created on magnetic multilayers a model has been formulated and studied. The Euler-Lagrange equation for this model is a discrete version of the Sine-Gordon equation. Solutions of this equation are generated by applying the methods of Chaotic Dynamics - treating the space variable associated with the layer number as a discrete time variable. The states found indicate periodic, quasiperiodic and chaotic structures.

Analytic solutions to the discrete nonlinear Schrödinger Equation (DNSE) with cubic nonlinearity are presented in the strong coupling limit. Using these as a starting point, a procedure is developed to determine the wave function and the energy eigenvalue for moderate coupling. The energy eigenvalues of the different structures of the wave function are found to be in excellent agreement with the exact strong coupling result.

The solutions to the DNSE indicate commensurate and incommensurate spatial structures associated with different localisation patterns of the wave function. The states which arise may be fractal, periodic, quasiperiodic or chaotic.

This work is then extended to solve a first order discrete nonlinear equation. The exact solutions for both the first and second order discrete nonlinear equations with cubic nonlinearity suggests that this method of studying discrete nonlinear equations may be applied to solve discrete equations with any order difference and cubic nonlinearity.



## Acknowledgements

Any endeavour consists of many interactions with the people surrounding and supporting you. In particular, this thesis would not have existed without the support of a great number of people surrounding me. I would like to thank all the people who have supported me and made this endeavour possible.

I would especially like to express my sincere thanks to my supervisor Professor F. V. Kusmartsev for his excellent guidance, encouragement, patience, support and friendship during the course of my PhD. It has been a greatly beneficial experience to work with you and gain such a valuable insight into theoretical Physics.

I wish to thank the Department Of Physics at Loughborough University for the opportunity to undertake this postgraduate research study. I thank all the members of staff especially Bharat Chavda, Dr. N. E. Hussey, Dr. K.-U. Neumann, Dr. M. B. Sobnack, Prof. K. R. A. Ziebeck and the ever helpful and smiling Maureen McKenzie.

I thank Prof. K. E. Kürten for some very stimulating discussions.

I am grateful to the Engineering and Physical Sciences Research Council for the financial support which enabled me to undertake this postgraduate research.

Sincere thanks must also go to Dr. D. E. G. Williams. I can only offer my appreciation for your support, discussions, insight and witticisms throughout the time I knew you and the influence you had on my decision to do a PhD.

Special thanks go to everyone who has made my time as a research student enjoyable. This includes everyone at Aikido, Darshan Vaidya, Dave Yewlett & Lucy Whetton, Gerry Rassias, Irina Gorbunova, Jon Taylor & Emma Bell, Magdalena Sokalska, Martin Butterfield, Martyn Pendlebury & Mavis Gingoore, Mohammed Al-Busaidy, Oscar Fernandez, Paul Spencer, Panagiotis Kottas, Robert Chorzepa, Sebastian Dressler, Stefan Hilbert, Tilmann Hickel, Tim Smith and Siaw Foon Lee. Thanks must also go to everyone else I've known whilst at University including Dan Jackson and Farhad Ali.

I would like to offer my penultimate word of thanks to my family and my wife. I am extremely grateful for your unconditional love and support – not just during

the course of my PhD but throughout my life. Thank you.

And ultimately, for everything, I thank God.

## **List Of Publications**

### **Exotic Structures On Magnetic Multilayers**

Journal of Magnetism and Magnetic Materials

Volume **198-199**, Page 743 (1999)

F. V. Kusmartsev, H. S. Dhillon, M. D. Crapper

### **Electron Locking In Layered Structures In A Longitudinal Magnetic Field**

Physical Review B

Volume **60**, Page 6208 (1999)

F. V. Kusmartsev, H. S. Dhillon

### **Electron Locking In Layered Structures**

Physica B

Volume **284**, Page 1780 (2000)

H. S. Dhillon, F. V. Kusmartsev

### **Fractal And Chaotic Solutions To The Discrete Nonlinear Schrödinger Equation In Classical And Quantum Systems**

Journal of Nonlinear Mathematical Physics

Volume **8**, Page 38 (2001)

H. S. Dhillon, F. V. Kusmartsev, K. E. Kürten

# Contents

<b>1</b>	<b>Introduction</b>	<b>9</b>
<b>2</b>	<b>Exotic Structures On Magnetic Multilayers</b>	<b>13</b>
2.1	Introduction To Magnetism . . . . .	13
2.1.1	Diamagnetism . . . . .	15
2.1.2	Paramagnetism . . . . .	15
2.1.3	Ferromagnetism . . . . .	16
2.1.4	Antiferromagnetism . . . . .	17
2.1.5	Ferrimagnetism . . . . .	18
2.2	Magnetic Multilayers . . . . .	19
2.3	Modelling The Interaction Of Magnetic Multilayers . . . . .	21
2.4	Structures Arising In Magnetic Multilayers . . . . .	25
2.5	Iterated Maps . . . . .	33
2.6	Results Of Iterated Maps . . . . .	34
2.6.1	Dependence On $\phi_0$ . . . . .	34
2.6.2	Dependence on $\beta$ . . . . .	49
2.7	Summary Of Interactions In Magnetic Multilayers . . . . .	68
2.8	Developing The Model . . . . .	70
<b>3</b>	<b>Solutions Of The Discrete Nonlinear Schrödinger Equation</b>	<b>72</b>
3.1	Introduction To The Discrete Nonlinear Schrödinger Equation . . . . .	72
3.2	The Hamiltonian And The DNSE . . . . .	74
3.3	Iterated Maps . . . . .	76
3.4	Exact Solutions Of The DNSE . . . . .	78
3.5	First Order Perturbation Corrections . . . . .	88
3.6	Exact Numerical Solutions For Finite $c$ . . . . .	92
3.7	Results . . . . .	95
3.7.1	Periodic Structures . . . . .	95
3.7.2	Quasiperiodic Structures . . . . .	101

3.7.3	Chaotic Structures . . . . .	108
3.7.4	Fractal Structures . . . . .	116
3.8	Summary . . . . .	120
<b>4</b>	<b>Solutions To A First Order Discrete Cubic Equation</b>	<b>124</b>
4.1	Exact Solutions Of The Discrete Equation . . . . .	124
<b>5</b>	<b>Conclusion and Outlook</b>	<b>130</b>
5.1	Conclusion . . . . .	130
5.2	Future Work . . . . .	132
5.2.1	Static Magnetic Multilayer Structures . . . . .	132
5.2.2	Influence Of A Magnetic Field On Magnetic Multilayers . . .	132
5.2.3	Dynamics Of Discrete Nonlinear Systems . . . . .	133
5.2.4	Statistical Mechanics Of Discrete Nonlinear Systems . . . . .	133
	<b>References</b>	<b>135</b>
	<b>Appendices</b>	<b>139</b>
	Appendix 1 - Mathematica Programme Used To Study Magnetic Multilayers	140
	Appendix 2 - Mathematica Programme Used To Study The DNSE . . . . .	148

*'All religions, arts and sciences are branches of the same tree.  
All these aspirations are directed toward ennobling man's life,  
lifting it from the sphere of mere physical existence  
and leading the individual towards freedom.'*

— Albert Einstein

# 1 Introduction

Research in the broad sense – the production, dissemination, understanding and realisation of new knowledge – is a subject of great importance. In essence, research contributes to satisfying the unlimited quest for discovery which is the foundation of man's endless curiosity and helps develop solutions to complex world needs.

The objective of this thesis is to contribute to man's knowledge of the world around us. In particular a detailed investigation of discrete nonlinear systems has been undertaken and the results presented at conferences and meetings and published in journals.

This work developed from my undergraduate work on 'Regular And Chaotic Wave Functions On A Lattice' [1] and chaotic structures in discrete systems. Chaos is an important branch of nonlinear dynamics because chaotic behaviour seems to be universal [2]. It is present in mechanical oscillators, electrical circuits, lasers, nonlinear optical systems, chemical reactions, nerve cells, heated fluids and weather systems. Even more importantly, this chaotic behaviour shows qualitative and quantitative universal features which are independent of the details of the particular system and corresponds to a disappearance of periodic trajectories.

Classical chaos is more often seen in discrete systems, which can be described, for example, by a discrete map. This was first done by the seminal work of Feigenbaum with the aid of iterative maps ([2] and references therein) where he showed that for a large class of iterative maps, exhibiting infinite period-doubling bifurcations, the transition to aperiodic orbits can be described by universal constants, governing the so-called Feigenbaum route to chaos.

Classical chaos corresponds to a disappearance of periodic trajectories. As classical chaotic motion is more obvious in time discrete systems, it is therefore natural to study the wave function of quantum systems, and hence the quantum analogy of this phenomenon, by considering the physical effects in materials which may be described as spatially discrete systems. The question arises whether or not it would be possible in these systems for two slightly different values of physical parameter

(for example, coupling constant) to correspond to two qualitatively different wave functions?

An illustrative example of a discrete system is that of magnetic multilayers, materials made up of thin layers of materials with different magnetic characteristics. Here we study the distribution of magnetic moments inside thin films and multilayers, the behaviour of which are very different to bulk magnetic materials. A discrete nonlinear model has been formulated to characterise possible magnetic structures which may be created on magnetic multilayers. The interlayer structures found indicate either (i) a regular periodic, (ii) a quasiperiodic change in the magnetisation or (iii) spatially chaotic (glassy) states. The periodic and quasiperiodic structures arising are a generalisation of plane defects in bulk samples, eg domain walls. The conditions at which the spatially chaotic (glassy) states may arise have been determined and the states described. The magnetic structures created depend mostly on the ratio of the magnetic anisotropy constant to the exchange constant. With the increase of this ratio the periodic structures first transform into the quasiperiodic and then into the chaotic (glassy) states. The same tendency arises with the depolarisation of the magnetic moments in the first layer deposited on the substrate.

We then go on to discuss stationary solutions of the discrete nonlinear Schrödinger equation (DNSE) with a cubic nonlinearity which is generically applicable to several quantum, electron and classical lattice systems.

As a prime example we consider a single electron which is strongly coupled with phonons on a  $1D$  chain of atoms – the (Rashba)-Holstein polaron model [3, 4] – and so describes a system which is naturally discrete in space. In the adiabatic approximation this system is conventionally described by the DNSE. Another relevant example is that of superconducting states in layered superconductors described by the same DNSE [5]. Amongst many other applications the typical example for a classical lattice is a system of coupled nonlinear oscillators [6].

The DNSE has previously been studied by making the continuum approximation and solving the resultant second order differential equation or by reformulating into the form of a  $2D$  mapping and iterating [9, 8, 7, 6]. However, we find that the DNSE



may also be solved exactly whilst maintaining the discrete nature of the equation.

The spectrum of eigenvalues of this model and the corresponding wave function is presented in the strong coupling limit. Using this as a starting point we go on to develop a procedure to calculate the wave function for moderate coupling and find that the eigenvalue of these structures of the wave function is in excellent agreement with the exact strong coupling result.

This procedure allows us to obtain (numerically) exact solutions of the DNSE directly. When applied to our typical example we find that the wave function of an electron on a deformable lattice (and other quantum or classical discrete systems) may exhibit incommensurate and irregular structures. These states are analogous to the periodic, quasiperiodic and chaotic structures found in classical chaotic dynamics.

This work is then extended to solve a first order discrete nonlinear equation. The exact solutions for both the first and second order discrete nonlinear equations with cubic nonlinearity suggests that this method of studying discrete nonlinear equations may be applied to solve discrete equations with any order difference and cubic nonlinearity.

Finally, some suggestions are made as to how the work presented in this thesis may be further extended and applied, in particular, to systems of multilayered magnetic materials.

*'I seem to have been only like a boy playing on the seashore and diverting myself in  
now and then finding a smoother pebble or prettier shell than ordinary,  
whilst the great ocean of truth lay all undiscovered before me.'*

— Isaac Newton

## 2 Exotic Structures On Magnetic Multilayers

### 2.1 Introduction To Magnetism

The study of magnetism has been described as possibly the second oldest profession in the world [10]. Unlike the oldest profession in the world, interest in the former has waxed and waned over the centuries. Magnetism is a physical phenomenon due to the interaction of magnetic (dipole) moments. The concept of a magnetic moment may be understood in simple terms as the motion of electric charges in closed paths (orbits) around a central core. A typical example is the motion of an electron in orbit around a nucleus in an atom. The current due to this orbiting electron is

$$I = \frac{e\omega}{2\pi} \quad (1)$$

where  $e$  is the charge of the electron and  $\omega$  is its angular velocity [11]. This current gives rise to an orbital magnetic moment

$$m = IA \quad (2)$$

where  $A$  is the (cross-sectional) area of the orbit. In addition to this orbital momentum, the electron also possesses an ‘intrinsic’ angular momentum called spin which is due to the electron *spinning* on its axis of rotation. The famous Stern-Gerlach experiment (1922) demonstrated that the spin of an electron is quantized and may only take two values: either spin-up ( $+\frac{1}{2}\hbar$ ) or spin-down ( $-\frac{1}{2}\hbar$ ) [12].

The magnetic moment of a free atom is principally due to the total (orbital + spin) angular momentum of the electrons in the subshells of that atom and their various interactions [13]. The Pauli Exclusion Principle forbids two electrons (fermions) being in the same quantum state and consequently different quantized energy levels must be occupied by the various electrons of an atom. This then provides an explanation of the periodic table of elements in terms of the electronic configurations of the atoms of the elements. For a completely filled shell the resultant angular momentum is zero and so there is no permanent magnetic moment [14].

The magnetic moment of a bulk solid is due to the magnetic moments of the individual atoms which make up the bulk. A useful measure of the average magnetic moment of a macroscopic system is the magnetisation,  $M$ . Consider a volume element  $\Delta V$  in a material where  $\Delta V$  is small on a macroscopic scale but is large enough to contain a large number of atoms. If  $m_i$  represents the magnetic moment of the  $i$ th atom in the volume element, then the average magnetic moment for this volume is  $\sum_i m_i$ . The magnetisation is defined as the magnetic moment per unit volume

$$\mathbf{M} = \frac{\sum_i m_i}{\Delta V} \quad (3)$$

The magnetisation describes the magnetic state of a medium or material. For example if  $\mathbf{M} = \mathbf{0}$  everywhere then no part of the medium has a magnetic moment. This can change, however, if an external magnetic field is applied.

When an external magnetic field  $\mathbf{H}$  is applied to a material it exerts a force on the electrons and so affects the bulk magnetic moment of the material. The magnetic susceptibility per unit volume  $\chi$  then gives a measure of how strongly the magnetisation is affected by an applied magnetic field

$$\mathbf{M} = \chi \mathbf{H} \quad (4)$$

As both  $\mathbf{M}$  and  $\mathbf{H}$  have the same units  $\chi$  is a dimensionless quantity [15]. The cumulative effect of both the external magnetic field and the magnetisation gives rise to the magnetic induction,  $\mathbf{B}$  (or magnetic flux density). The magnetic induction is the magnetic flux per unit area of a magnetic field perpendicular to the magnetic field and is defined as

$$\mathbf{B} = \mu_o(\mathbf{H} + \mathbf{M}) \quad (5)$$

where  $\mu_o$  is the permeability of free space.

Different materials respond differently to changes in the external magnetic field. There are five main categories of magnetic behaviour: *diamagnetic*, *paramagnetic*, *ferromagnetic*, *antiferromagnetic* and *ferrimagnetic*.

### 2.1.1 Diamagnetism

Diamagnetism is associated with the tendency of electrical charges to shield the interior of a body from an applied magnetic field. A magnetic moment directed in the direction opposite to the applied field is induced due to changes in the orbits of electrons in the atoms of the material. The susceptibility of a diamagnetic substance is negative. Also the magnetisation induced by the applied field is directly proportional to the applied field – the susceptibility remains constant. Although all substances are diamagnetic, it is a weak form of magnetism and may be (completely) masked by other, stronger forms of magnetism. One notable exception is the case of superconductors which exhibit strong diamagnetism and so expel all the magnetic field from the interior of the body. Macroscopic diamagnetic effects have also been observed in levitating frogs, nuts and a whole host of other things [17].

### 2.1.2 Paramagnetism

In paramagnetic materials, the atoms which make up the material have associated with them a net magnetic moment. In the absence of an applied field these magnetic moments are orientated randomly and the magnetisation of a paramagnetic substance is zero. However, in an applied magnetic field the magnetic moments are induced to align in the same direction as the magnetic field – the susceptibility of a paramagnetic substance is positive. Opposing the tendency for the magnetic moments to align with the magnetic field are the randomising thermal effects. Except for large magnetic fields and low temperatures, the magnetisation of a paramagnetic material is proportional to the applied field at constant temperature – the susceptibility is temperature dependent. For very large magnetic fields or at very low temperatures the magnetisation saturates as all the magnetic moments align with the applied field – the magnetisation approaches a maximum and will not increase any further.

### 2.1.3 Ferromagnetism

For both diamagnetic and paramagnetic substances the magnetisation is non-zero only if a magnetic field is applied. Ferromagnetic materials, on the other hand, can have a spontaneous magnetic moment – a non-zero magnetisation even in the absence of an applied magnetic field – below a certain temperature called the Curie temperature. Above this temperature ferromagnetic materials behave the same as paramagnetic materials. However, below the Curie temperature there is a marked difference in the behaviour of ferromagnetic materials as compared with paramagnetic materials; ferromagnetic materials may form domains. A domain is a region within a ferromagnet in which all the individual magnetic moments tend to align in the same orientation. By the very nature of these domains, the orientation of the magnetisation of different domains is different. The domains are separated by domain walls where the magnetisation changes from the orientation of one domain to the orientation of an adjacent domain. In the absence of a magnetic field, the net magnetisation of the domains can be zero and this gives rise to an unmagnetised ferromagnet. Note that in a paramagnetic material the magnetic moments are aligned randomly whereas in a ferromagnetic material there is an ordering of the magnetic moments.

The mechanism which causes the magnetic moments to align in a ferromagnetic substance is due to an exchange interaction. Essentially, this exchange interaction is due to the interaction of electrons from different atoms whose charge distributions overlap and the Pauli Exclusion Principle [16]. In ferromagnetic substances it is energetically favourable for the magnetic moments to (locally) align with each other. Note that the orientating effect of the exchange interaction is opposed by thermal fluctuations and at temperatures above the Curie temperature the alignment of magnetic moments is destroyed.

When a magnetic field is applied to a ferromagnetic material the domains in which the magnetic moments are orientated in the same direction as the magnetic field increase in size at the expense of other domains. That is, the number of magnetic moments with the same direction as the applied field increases and results

in an overall magnetisation of the material even when the applied magnetic field is removed. This can result in a non-zero magnetisation even if there is no applied magnetic field. The magnetisation is not linearly dependent on the magnetic field but rather depends on the previous treatment of the sample. This gives rise to the hysteresis effect in ferromagnets. Consequentially, the susceptibility of ferromagnetic materials is not constant. Note that the magnetisation cannot increase without limit; when all the magnetic moments of the sample are aligned with the applied magnetic field then the magnetisation has saturated.

#### 2.1.4 Antiferromagnetism

In contrast with ferromagnetic materials, the neighbouring magnetic moments of antiferromagnetic materials are aligned antiparallel to one another. That is below a certain temperature (the Néel temperature) the magnetic moments spontaneously create an ordered array in which alternate moments are equal but have opposite directions. The individual local moments sum to zero total moment and the effect of this ordering is that there is no spontaneous magnetisation.

The mechanism which causes antiferromagnetic ordering of magnetic moments is again due to the exchange interaction. In antiferromagnetic substances it is energetically favourable for the magnetic moments to orientate in directions opposite to neighbouring moments. Note that this orientating effect is also opposed by thermal fluctuations and at temperatures above the Néel temperature the antiparallel alignment of magnetic moments disappears and the antiferromagnetic material exhibits paramagnetic behaviour.

When a magnetic field is applied to an antiferromagnetic material there are two possible scenarios. The applied field could be either parallel to the axis of the magnetic moments or it could be perpendicular to the axis of the magnetic moments. Above the Néel temperature the susceptibility is independent of the direction of the field. As the temperature decreases the susceptibility increases. Just above the Néel temperature the susceptibility reaches a maximum and now begins to depend on

the direction of the magnetic field. If the magnetic field is applied perpendicular to the sample then the susceptibility decreases slightly as the temperature is decreased further. If the magnetic field is applied parallel to the axis of the magnetic moments then the susceptibility decreases much more rapidly as the temperature decreases.

#### **2.1.5 Ferrimagnetism**

Ferrimagnetic materials are another class of materials with ordered magnetic moments. Like antiferromagnetics, adjacent magnetic moments in ferrimagnetics are orientated in opposite directions. However, unlike antiferromagnetics, these magnetic moments are not equal in magnitude. The magnitude of the magnetic moments orientated in one direction is larger than the magnitude of the magnetic moments orientated in the other direction and consequently there is a permanent magnetic moment even in the absence of an applied magnetic field similar to ferromagnetics.



## 2.2 Magnetic Multilayers

Modern growth techniques, such as molecular beam epitaxy or laser ablation, allow magnetic multilayers to be built up. These consist of thin layers of materials with different magnetic characteristics; for example, magnetic layers of *Fe*, *Ni* or *Co* separated by non-magnetic layers of *Cu*. A schematic diagram of a magnetic multilayer system is shown in Figure 2.1. Multilayers of magnetic materials have exhibited a wide range of magnetic phenomena [10].

In magnetic multilayer structures, the magnetic films are grown one layer at a time. Often each layer appears as a single domain, ie all magnetic moments in that layer have the same orientation. When a second layer is grown on top of the first layer, the orientation of magnetic moments in the second layer is not necessarily the same as in the first layer. Following addition of a third layer, the magnetic moments of this layer may have yet another orientation. The orientation of the magnetic moments is usually dictated by a competition between exchange energy and anisotropy energy – which directs the magnetisation along certain crystallographic axes called directions of easy magnetisation. In bulk magnetic samples this competition gives rise to the creation of magnetic domains described above due to long-range dipole-dipole interactions.

Naturally, questions arise about what kind of magnetic structures (analogous to the Bloch domain wall) may be created by the interaction between the magnetic moments in magnetic multilayer systems and how these structures may be created.

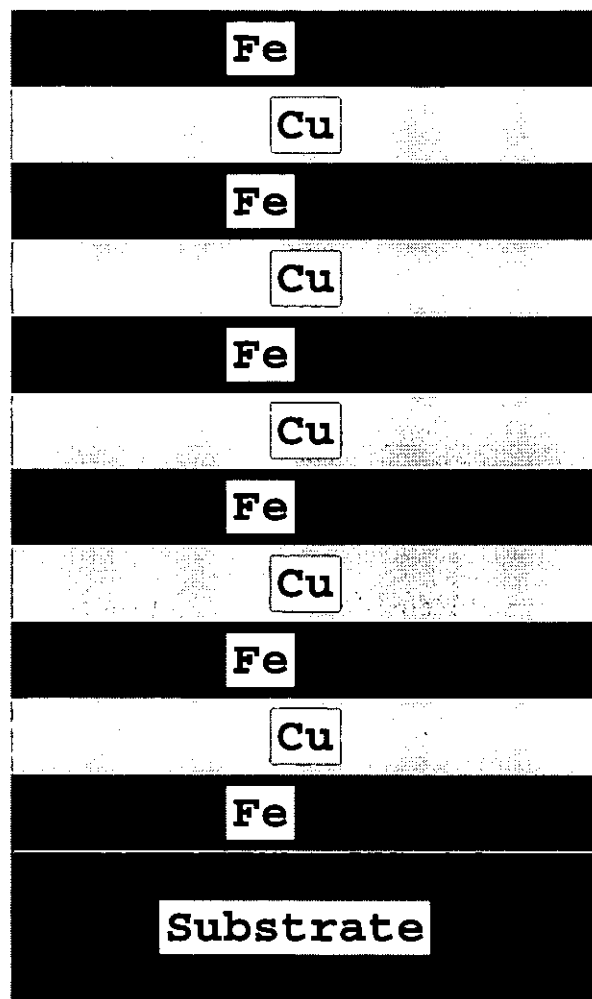


**Figure 2.1** *A schematic diagram of a magnetic multilayer system consisting of alternating layers of iron and copper.*

## 2.3 Modelling The Interaction Of Magnetic Multilayers

There are two related properties which are important for an understanding of the structure of magnetic materials. These are the domain structure and the magnetic anisotropy. The domain structure is such that for magnetic moments close to each other, it is energetically favourable for them to be aligned in the same orientation. As a large stray magnetic field would result in a highly energetic state, it is energetically favourable that magnetic moments which are relatively far away from each other are aligned in opposite directions thus decreasing the magnetostatic self-energy. This causes the formation of domains in which the direction of magnetisation is determined by the magnetic anisotropy; it is energetically favourable for the magnetisation, within a domain to align in a particular direction, usually along the easy axis. However, the very formation of these domains means that adjacent magnetic moments cannot be simply aligned in the same orientation as each other but that there must be some, perhaps very small, difference in the orientation of adjacent magnetic moments.

The characteristic length scale in many problems dealing with magnetism is the size of the domain wall in the structure. The size of these domain walls depend on the strength of the exchange coupling between the magnetic moments and the magnetic anisotropy. The division into domains and the subsequent creation of these domain walls is at the expense of exchange energy. A large exchange coupling favours a large domain wall so that the angle,  $\phi$ , between adjacent magnetic moments is small. A large anisotropy favours a small domain wall so that the angle between adjacent magnetic moments is large. If there were zero exchange coupling this would then lead to antiferromagnetic behaviour ie the angle between adjacent magnetic moments would be  $\phi = \pi$ . Thus the overall magnetic behaviour involves a balance of the exchange energy and anisotropy energy.

To describe the possible structures which may arise in a magnetic multilayer system, a discrete, nonlinear, one-dimensional model has been developed which takes into account the exchange energy, the magnetostatic energy and the anisotropy energy. The main competition is between the exchange energy  $E_{ex}$ , which favours

the alignment of the magnetic moments of atoms and the magnetic anisotropy energy  $E_{an}$ , which promotes the alignment of the magnetic moments along the easy axis of the system. The easy axis is chosen to be the direction of growth of the magnetic multilayer. The magnetostatic energy is taken into consideration by an appropriate choice of initial conditions – chosen so as not to give trivial structures (with a large magnetostatic energy) whilst modelling magnetic multilayers.

The exchange energy of a magnetic multilayer system may be described by the Heisenberg Hamiltonian [14, 16, 18]

$$H = \sum_{ij} J_{ij} \vec{s}_i \cdot \vec{s}_j \quad (6)$$

where  $J_{ij}$  is the exchange coupling between spins  $\vec{s}_i$  and  $\vec{s}_j$ . For ferromagnetic ordering  $J_{ij} < 0$  and for antiferromagnetic ordering  $J_{ij} > 0$ . A multilayer film has different exchange constants depending on whether the exchange is developed in-plane or inter-plane [19]. The nonmagnetic layers separating the magnetic layers may also contribute to the exchange coupling between magnetic layers. As exchange coupling is a short-range effect and dependent on the space between the magnetic moments the exchange forces inside each layer are much larger than the forces associated with the exchange interaction between the layers.

The anisotropy energy is usually related to a long-range spin-spin interaction or to a spin-orbital interaction of magnetic moments. It is plausible to assume that this anisotropy is much weaker than the short-range exchange coupling within each layer (this is always the case for bulk materials) and so within each layer we can conjecture a ferromagnetic structure of the magnetic moments ie each layer is a single domain with all the moments pointing in the same direction. Consequently, each layer may be considered as a single classical spin. With this assumption, the relevant terms of the Hamiltonian associated with the interlayer magnetic structure are an interlayer exchange energy and the anisotropy energy. The competition between these two terms determines the interlayer structure of the magnetic multilayer film. Thus, we study the magnetic structures created between different layers, assuming that all magnetic moments of the same layer align homogeneously. A similar model is

presented in the review [10] by Howson. Here, as an example, a uniaxially symmetric multilayer is considered with an easy axis (uniaxial) magnetic anisotropy present.

The possible structures which may arise in this system of magnetic multilayers involve a balance of the exchange energy and anisotropy energy and so the ordering between the layers will be determined by a classical Hamiltonian of the form

$$H = \sum_{ij} J_{ij} \vec{M}_i \cdot \vec{M}_j + K \sum_i M_i^z \cdot M_i^z \quad (7)$$

where  $\vec{M}_n = (M_{nx}, M_{ny}, M_{nz})$  is the magnetic spin of the  $n$ th layer and  $K$  is a constant related to the strength of the anisotropy which promotes the alignment of the magnetic moments along the easy axis of the system. It is convenient to introduce the projection of the magnetic moments along the easy axis as  $M_{nz} = M \cos \phi_n$  where  $\phi_n$  is the colatitude of the  $n$ th layer. For simplicity, only nearest-neighbour interactions between the  $n$ th and  $n + 1$  layers are considered and we assume that the exchange coupling is identical for all nearest-neighbour pairs, such that  $J_{n,n+1} = J$ . Then

$$H = JM^2 \sum_n \cos(\phi_n - \phi_{n+1}) + KM^2 \sum_n \cos^2 \phi_n \quad (8)$$

For  $\phi_n \sim \phi_{n+1}$  we may make the small angle approximation  $\cos(\phi_n - \phi_{n+1}) \approx 1 - \frac{(\phi_n - \phi_{n+1})^2}{2}$  so that,

$$H = JM^2 \sum_n 1 - \frac{JM^2}{2} \sum_n (\phi_n - \phi_{n+1})^2 + KM^2 \sum_n \cos^2 \phi_n \quad (9)$$

where the first term is a constant. The energetically favourable states of this Hamiltonian correspond to minima of this discrete nonlinear system and occur when

$$\frac{\partial H}{\partial \phi_n} = 0 \quad (10)$$

which gives

$$-\frac{JM^2}{2} (-2\phi_{n-1} + 4\phi_n - 2\phi_{n+1}) - KM^2 2 \sin \phi_n \cos \phi_n = 0 \quad (11)$$

Introducing the parameter  $\beta = \frac{2K}{J}$  (twice the ratio of the constant of anisotropy energy to the constant of exchange energy) the above equation simplifies to

$$-2\phi_{n-1} + 4\phi_n - 2\phi_{n+1} + \beta \sin 2\phi_n = 0 \quad (12)$$

which is invariant under the transformation  $\beta \rightarrow -\beta$  and  $2\phi_n \rightarrow 2\phi_n + \pi$ .

Note that upon making the substitution  $x_n = 2\phi_n$  then the system of magnetic multilayers may be described by the Euler-Lagrange equation

$$-x_{n-1} + 2x_n - x_{n+1} + \beta \sin x_n = 0 \quad (13)$$

which is a discrete version of the Sine-Gordon equation or the Frenkel-Kontorova model [18, 20]. This equation may also be analysed the same way as (12) (see below). In fact, some of the results for small  $\beta$  are reminiscent of the periodic motion of a simple pendulum in the continuum limit. However, as  $\beta$  is increased the discrete nature of the system becomes more and more important for a fuller understanding of the physics of the system.

## 2.4 Structures Arising In Magnetic Multilayers

As shown above, magnetic multilayer systems may be modelled by the discrete nonlinear equation (12). Investigating this model and solving the resultant system of equations will give possible structures which could arise in such discrete systems.

### Homogeneous Structures

The simplest solution of (12) is the trivial solution  $\phi_n = 0$  for all layers. This solution is presented in Figure 2.2 and corresponds to a homogeneous (ferromagnetic) structure with no domain walls in the magnetic multilayer system. Consequently, this type of structure will have a large magnetostatic energy. Another homogeneous solution of this system is the solution  $\phi_n = \pi$  for all layers. This corresponds to a structure with all magnetic moments orientated in the opposite sense to that shown in Figure 2.2. Other structures must also exist which will have a lower magnetostatic energy.

### Period-2 Structures

Other simple structures which could arise are the period-2 solutions where either  $\phi_n = 0, \phi_{n+1} = \pi$  (presented in Figure 2.3) or  $\phi_n = \pi/2, \phi_{n+1} = -\pi/2$ . Both of these structures correspond to antiferromagnetic structures and are independent of the value of  $\beta$ . The magnetostatic energy of these structures is minimal – ‘domain walls’ exist between adjacent layers – but the exchange energy cost will be very high.

Other period-2 structures do also exist but these are dependent on the value of  $\beta$ . For example, the period-2 solution  $\phi_n = \pi/4, \phi_{n+1} = -\pi/4$  presented in Figure 2.4 only exists for  $\beta = -2\pi$ . Similarly, other period-2 structures only exist for certain values of  $\beta$ .

From the analysis of (12) it can be seen that there are four obvious types of period-2 structures. For a period-2 structure we must have

$$4\phi_1 - 4\phi_2 + \beta \sin(2\phi_1) = 0 \quad (14)$$

and

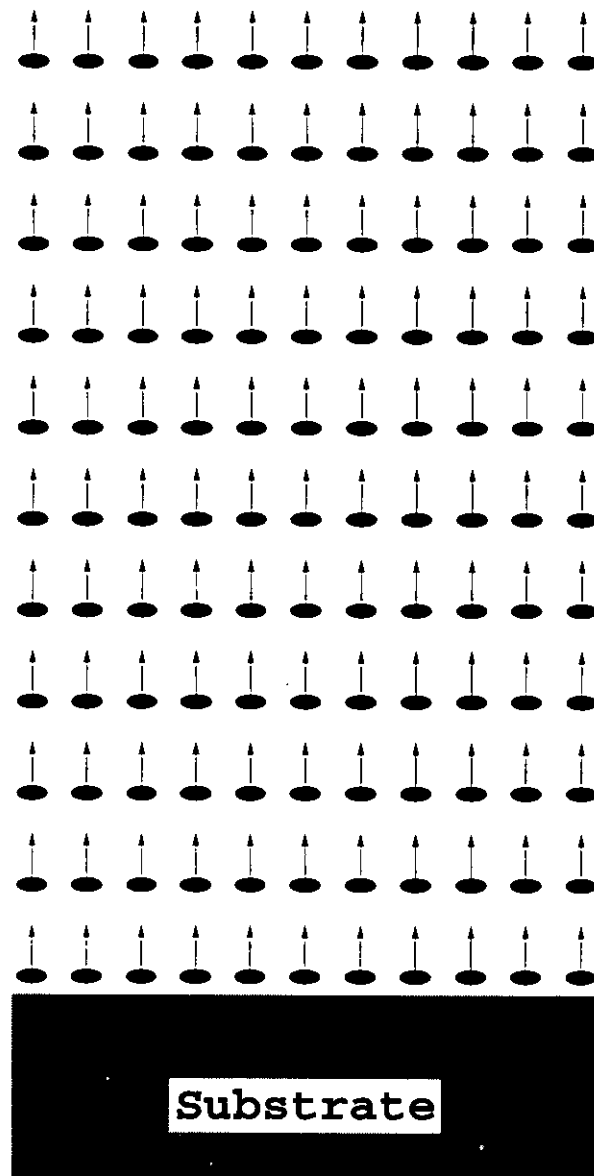


**Figure 2.2** *A ferromagnetic (homogeneous) structure in a magnetic multilayer system. The direction of magnetisation of all the layers is aligned along the easy-axis and consequently no domain walls exist within this structure. Note that each row of arrows corresponds to a single magnetic layer and that the non-magnetic layers are not shown.*



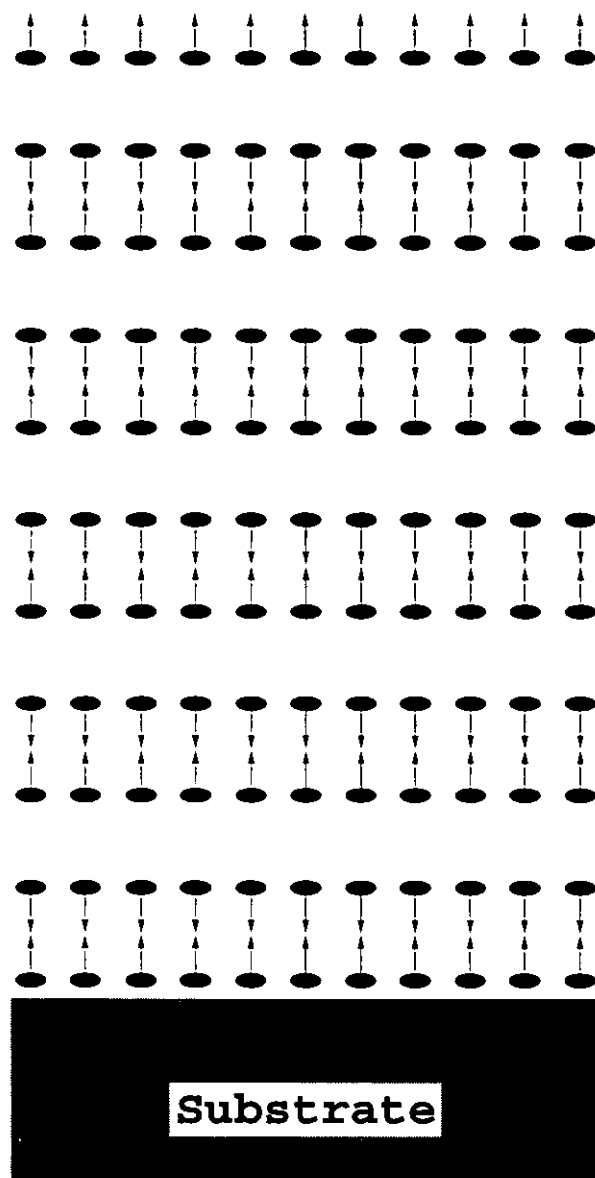


**Figure 2.3** *An antiferromagnetic structure in a magnetic multilayer system. The magnetisation of the layers is along the easy-axis but the direction of magnetisation alternates.*

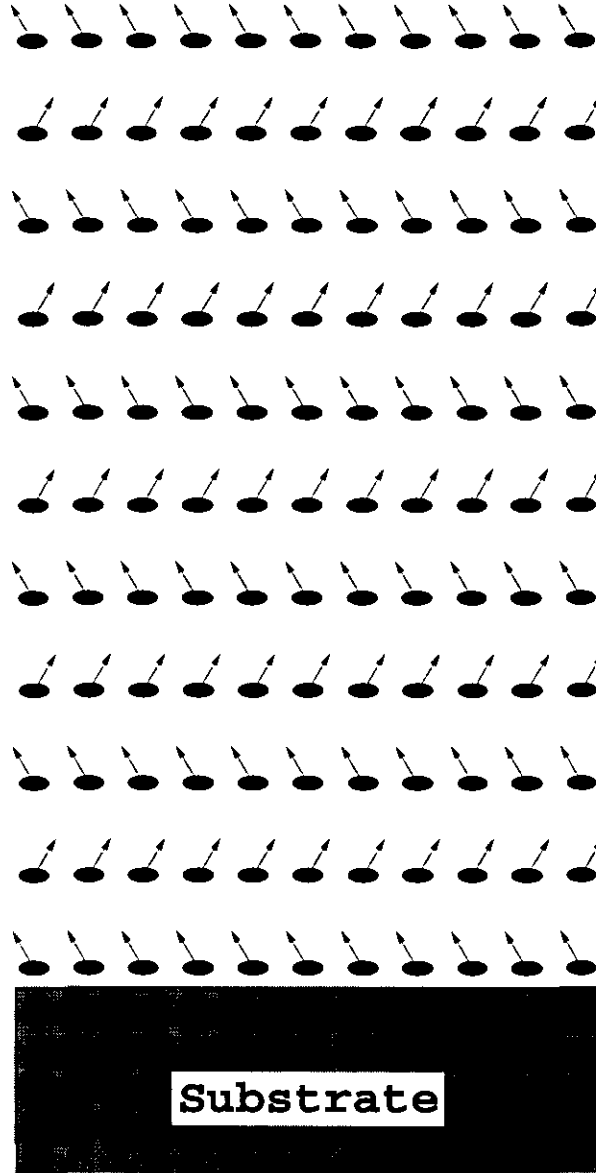


**Figure 2.4** A fan-like (spin wave) structure in a magnetic multilayer system. The direction of the projection of the magnetisation on the easy-axis is the same for all the layers but the direction of the projection of the magnetisation in the plane alternates for adjacent layers. This structure exists for  $\beta = -2\pi$  and the angle of magnetisation of a layer is either  $\pm\pi/4$ .

$$4\phi_2 - 4\phi_1 + \beta \sin(2\phi_2) = 0 \quad (15)$$

Adding (14) to (15) gives

$$\beta (\sin 2\phi_1 + \sin 2\phi_2) = 0 \quad (16)$$

which may be rewritten as

$$2\beta \sin(\phi_1 + \phi_2) \cos(\phi_1 - \phi_2) = 0 \quad (17)$$

This is satisfied (for  $\beta \neq 0$ ) when one of the following four conditions is met:  $\phi_2 = -\phi_1$ ,  $\phi_2 = \pi - \phi_1$ ,  $\phi_2 = -\pi/2 + \phi_1$  or  $\phi_2 = \pi/2 + \phi_1$ . Each of these conditions will only generate a period-2 solution for a particular value of  $\beta$ . For example, consider the condition  $\phi_2 = \pi/2 + \phi_1$ . If we choose  $\phi_1 = \pi/6$  then  $\phi_2 = 2\pi/3$ . This choice gives the period-2 structure presented in Figure 2.5 for  $\beta = 4\pi/\sqrt{3}$ . For other values of  $\beta$  this structure does not exist.

Other period-2 solutions may also exist but these are much more difficult to identify. If there is a simple relationship between  $\phi_n$  and  $\phi_{n-1}, \phi_{n+1}$  (as above) then a possible method of determining the value of  $\phi_n$  for a particular  $\beta$  is by re-arranging (12) to give

$$\frac{F(\phi_n)}{\beta} = \sin(2\phi_n) \quad (18)$$

where  $F(\phi_n) = 2\phi_{n-1} - 4\phi_n + 2\phi_{n+1}$  is a function of  $\phi_n$  only (after substituting for  $\phi_{n-1}, \phi_{n+1}$ ). In the above examples  $F(\phi_n)$  is a linear function and so the problem reduces to determining the intersect of a straight line with a graph of  $\sin(2\phi_n)$  as shown in Figure 2.6. For example, consider the period-2 solution  $\phi_{n+1} = -\phi_n$ . Substituting this into (18) yields

$$\frac{-8\phi_n}{\beta} = \sin(2\phi_n) \quad (19)$$

The solution,  $\phi_n$ , of this equation depends on the value of  $\beta$  and is determined by the intersect of the straight line  $y = -8\phi_n/\beta$  with  $y = \sin(2\phi_n)$ .

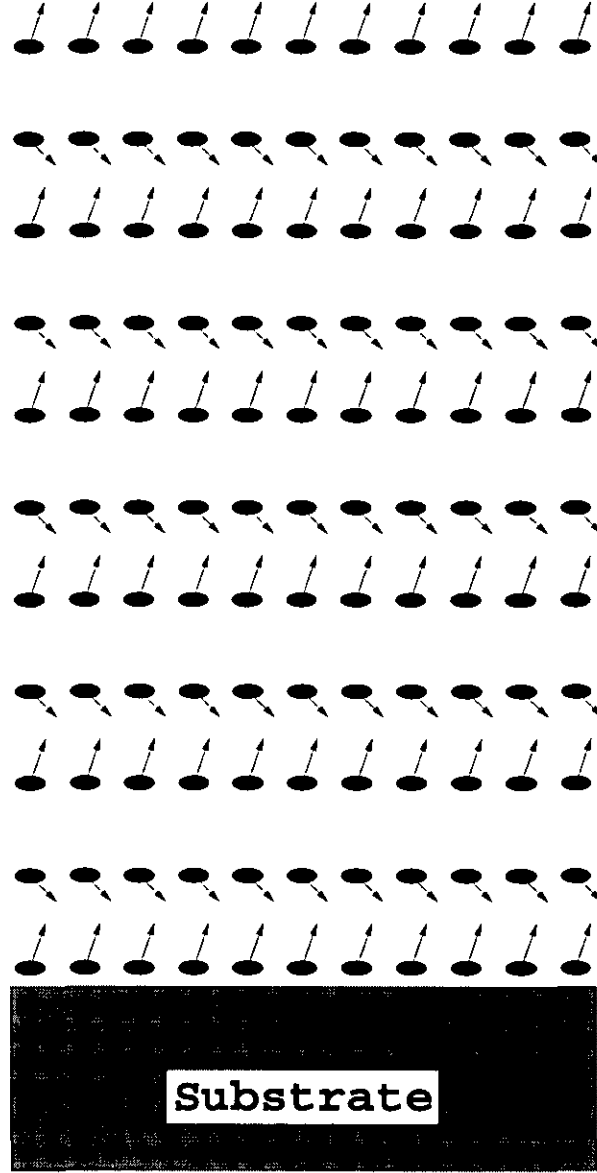


**Figure 2.5** A canted structure in a magnetic multilayer system. The direction of the projection of the magnetisation along the easy-axis alternates for adjacent layers but the direction of projection of the magnetisation in the plane is the same for all layers. This structure exists for  $\beta = 4\pi/\sqrt{3}$  and the angle of magnetisation of adjacent layers is  $\phi_1 = \pi/6$  and  $\phi_2 = 2\pi/3$ .

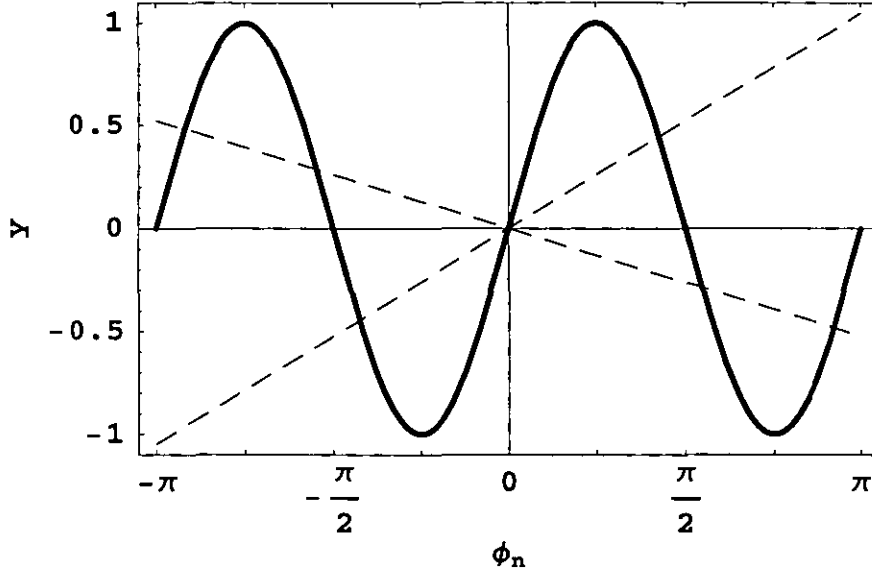


**Figure 2.6** A graph of the curve  $y = \sin(2\phi_n)$  and the straight lines  $y = -8\phi_n/\beta$  for the arbitrary values of  $\beta = -24$  and  $\beta = 48$ . The graph shows how particular period-2 structures only exist for particular values of  $\beta$ .

As an example, again consider the condition  $\phi_2 = \pi/2 + \phi_1$  for a period-2 solution. Substituting this into (18) gives

$$\frac{2\pi}{\beta} = \sin(2\phi_n) \quad (20)$$

The left hand side of this equation gives a horizontal line – the ordinate of which depends on the value of  $\beta$  – and the right hand side corresponds to a sinusoidal curve as shown in Figure 2.7.

From Figure 2.7 we see that for a period-2 solution of the form  $\phi_2 = \pi/2 + \phi_1$  to exist we require  $|\beta| \geq 2\pi$ ; for  $|\beta| < 2\pi$  this period-2 solution does not exist. Note that for  $\beta = 4\pi/\sqrt{3}$  there are 4 points of intersection of the graph of  $\sin(2\phi_n)$  with the line  $+\sqrt{3}/2$ :  $\phi_1 = -5\pi/6, \phi_1 = -2\pi/3, \phi_1 = \pi/6, \phi_1 = \pi/3$ . Similarly, there are also 4 points of intersection of the graph  $\sin(2\phi_n)$  with the line  $-\sqrt{3}/2$ :  $\phi_1 = -\pi/3, \phi_1 = -\pi/6, \phi_1 = 2\pi/3, \phi_1 = 5\pi/6$ . Between them, these eight points of intersection make up the 4 period-2 solutions  $(\phi_n, \phi_{n+1})$  for  $\beta = 4\pi/\sqrt{3}$ ,  $(-5\pi/6, -\pi/3), (-2\pi/3, -\pi/6), (\pi/6, 2\pi/3), (\pi/3, 5\pi/6)$ . If the value of  $\beta$  is changed then these particular period-2 solutions will no longer exist; there will be different

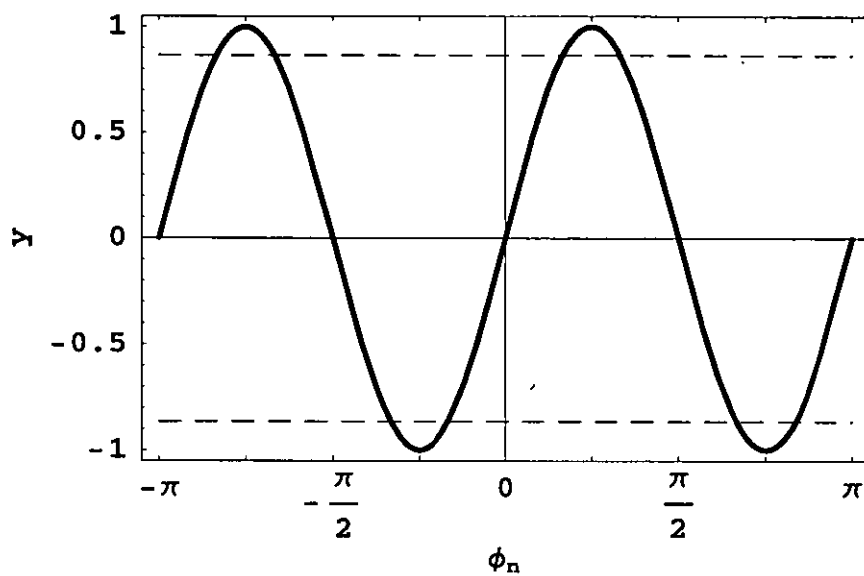


**Figure 2.7** A graph of the curve  $y = \sin(2\phi_n)$  and the straight lines  $y = 2\pi/\beta$  with  $\beta = \pm 4\pi/\sqrt{3}$ . The graph shows how a particular period-2 structure only exists for a particular value of  $\beta$ .

period-2 solutions corresponding to the new value of  $\beta$ .

## 2.5 Iterated Maps

Equation (12) appears to have an abundant amount of structures – it is feasible that lots of different types of structures exist – but it would be difficult to find them analytically. Rather than solve (12) explicitly (for a particular type of solution) an alternative approach must be adopted to identify the different types of structures which may exist in this model.

To explore the nature of possible solutions of (12), we can follow the methods used in the studies of nonlinear dynamical systems treating the space variable associated with the layer number as a discrete time variable. With such an approach [7], instead of solving (12) analytically, we can instead iterate (12) – after first representing it in the form of a  $2D$  map – and investigate the trajectories of this map. This may be done by the introduction of a parameter  $Z_n$ , such that  $Z_{n+1} = \phi_{n+1} - \phi_n$ . This gives a pair of equations which can be used to plot a  $2D$  map

$$\begin{aligned} Z_{n+1} &= Z_n + \frac{\beta}{2} \sin(2\phi_n) \\ \phi_{n+1} &= Z_{n+1} + \phi_n \end{aligned} \tag{21}$$

The initial values of  $\phi_0$  and  $\beta$  are selected by choice. We assumed  $Z_0 = 0$  for all our numerical simulations because there is no preceeding magnetic moment to interact with the magnetic moment of the first layer. The phase portraits produced from iterating (21) will help classify the type of structures obtained from the iteration procedure for different starting conditions. All the following results are for a system with 1000 iteration steps ie a 1000-layer magnetic multilayer. The Mathematica programme for this procedure is presented in Appendix 1 [21].

## 2.6 Results Of Iterated Maps

Equation (21) has been iterated for various values of  $\beta$  and  $\phi_0$  with constant  $Z_0 = 0$ . We find that there are three qualitatively different types of solutions; periodic, quasiperiodic and chaotic. The structure created depends on both the orientation  $\phi_0$  of the magnetic moments in the first layer and on the ratio  $\beta$  of the constant of anisotropy energy to the constant of exchange energy.

To understand how  $\phi_0$  and  $\beta$  affect the type of structures created in our system of magnetic multilayers we investigate the dependence of these structures on both of these variables.

### Periodic Structures

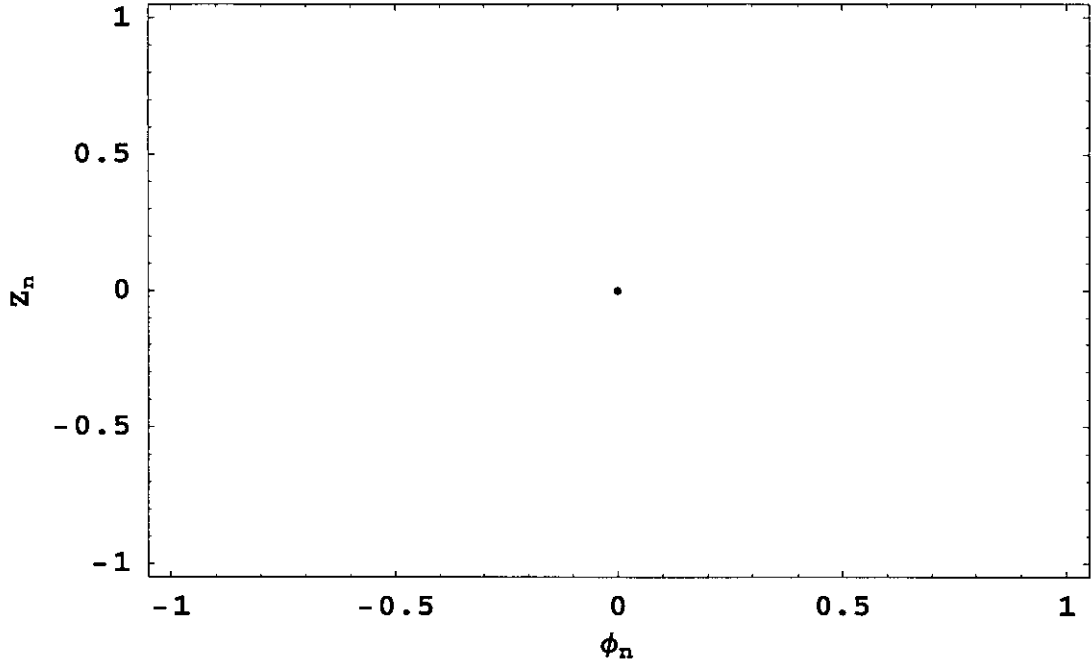
The simple homogeneous alignment of moments presented in Figure 2.2 ( $\phi_n = 0$  for all  $n$ ) is a fixed point of (12) (as is  $\phi_n = \pi$  for all  $n$ ) and does not depend on the value of  $\beta$ . However, this structure possesses a very high magnetostatic energy and can be avoided by an appropriate choice of initial conditions ( $\phi_0 \neq 0$ ). Figure 2.8 shows the phase portrait of such a structure.

This homogeneous structure requires that the magnetic moments of the first layer are all perpendicular to the substrate. In practice this is a very strict constraint. The probable influence of thermal effects will be to destroy any such alignment. If the magnetic moments in the first layer are not exactly perpendicular to the substrate then the structure created will depend on both  $\phi_0$  and  $\beta$ .

#### 2.6.1 Dependence On $\phi_0$

Similarly, the phase portrait of a period-2 structure will consist of only 2 points being visited in the phase plane. Other periodic structures do also exist. For instance with the initial conditions  $\phi_0 = 0.001$ ,  $Z_0 = 0$  and  $\beta = -1.0$  we obtain a period-6 structure. The pattern produced is regular and no deviation occurs in the periodicity. The phase portrait of this structure consists of 6 points and is presented in Figure 2.9a. Although this structure is not homogeneous, the change in the orientation of the magnetic moment of each layer throughout the period is very small as shown in





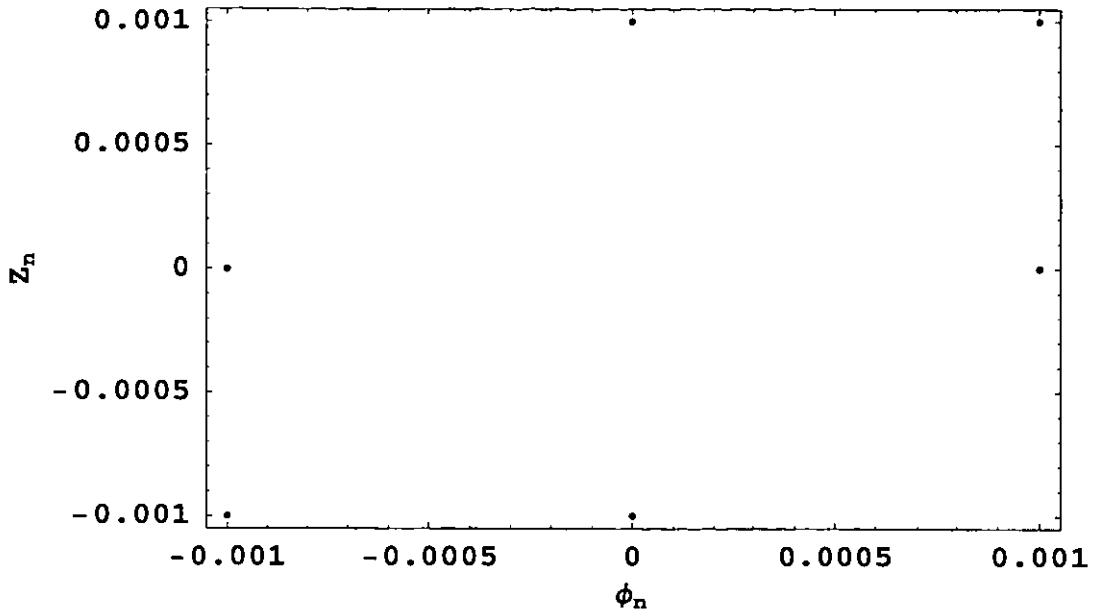
**Figure 2.8** *The phase portrait corresponding to the homogeneous solution presented in Figure 2.2 consisting of a single point at the origin in the  $\{\phi_n, Z_n\}$  phase plane. The initial conditions were  $\phi_0 = 0, Z_0 = 0$  which corresponds to a fixed point of (12).*

Figure 2.9b. This gives rise to a period-6 structure which may easily be confused with the homogeneous structure (Figure 2.2) as the difference between the two structures is not obvious, being only clearly demonstrated in the phase portraits of the two structures.

### Quasiperiodic Structures

As the angle of the magnetisation of the first layer is increased to  $\phi_0 = 0.01$  – with the anisotropy parameter kept constant – the phase portrait presented in Figure 2.10a is reminiscent of the phase portrait of the period-6 structure shown in Figure 2.9a. It is a slightly deformed period-6 orbit; there is a small deviation in the orientation of the magnetisation of every sixth layer which gives rise to the ‘weakly’ quasiperiodic structure presented in Figure 2.10a.

Again the change in the orientation of the magnetisation of subsequent layers throughout the structure is very small and so the magnetic structure presented in Figure 2.10b of this multilayer is very similar to that of the homogeneous structure.



**Figure 2.9a** *The phase portrait corresponding to the period-6 solution presented in Figure 2.9b consisting of 6 points in the  $\{\phi_n, Z_n\}$  phase plane. The initial conditions were  $\phi_0 = 0.001$ ,  $Z_0 = 0$  and  $\beta = -1.0$ .*

As  $\phi_0$  is further increased to  $\phi_0 = 0.1$  – with  $\beta = -1$  still – the phase portrait Figure 2.11a indicates a strong deformation of the period-6 structure. The phase portrait is a filled, closed loop which is an indication of a quasiperiodic orbit. The cross-section of the multilayer structure presented in Figure 2.11b shows that the orientation of the magnetic moments of the layers ‘oscillates’ gently about the easy-axis. Although this oscillation appears to repeat itself every sixth layer there are in fact small differences and so we have a quasiperiodic structure.

As the initial condition  $\phi_0$  is still further increased the amplitude of the spin waves increases. For  $\phi_0 = 1.0$  we obtain the phase portrait presented in Figure 2.12a which corresponds to the magnetic multilayer structure presented in Figure 2.12b. This cross-section of the magnetic multilayer film clearly indicates that the period-6 solution no longer exists in this structure – the magnetic structure does not repeat itself every six layers.

At  $\phi_0 = 1.15706$  there is a small but noticeable change in the phase portrait of the

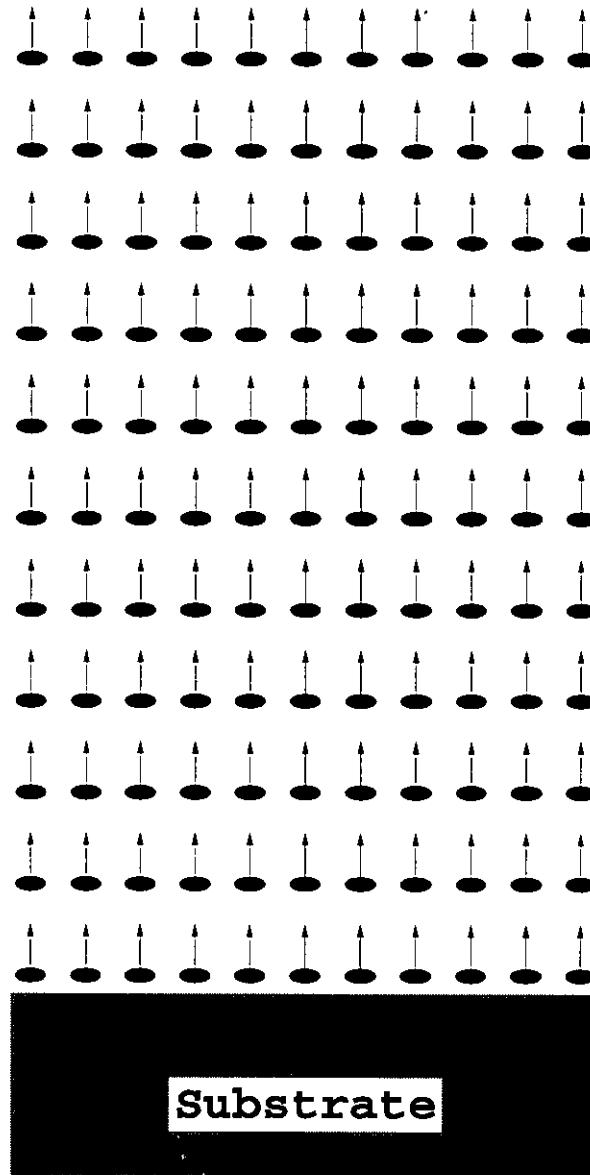


**Figure 2.9b** 11 layers of a period-6 magnetic multilayer structure which gives rise to the phase portrait presented in Figure 2.9a. This structure is very similar to that presented in Figure 2.2 because the variation in the direction of orientation of the magnetisation of each layer is extremely small.

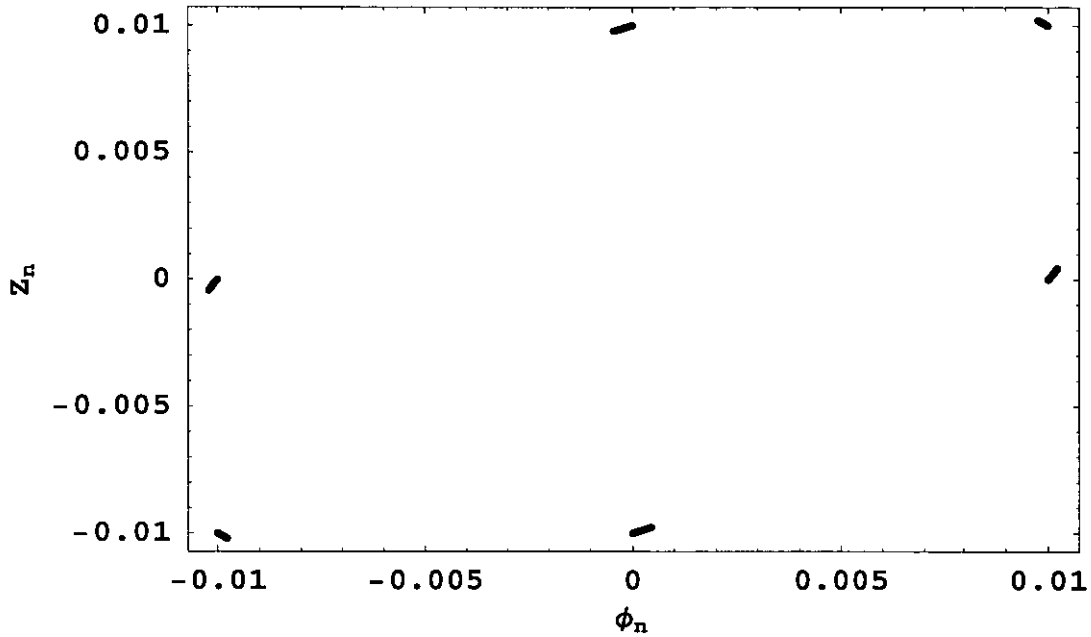


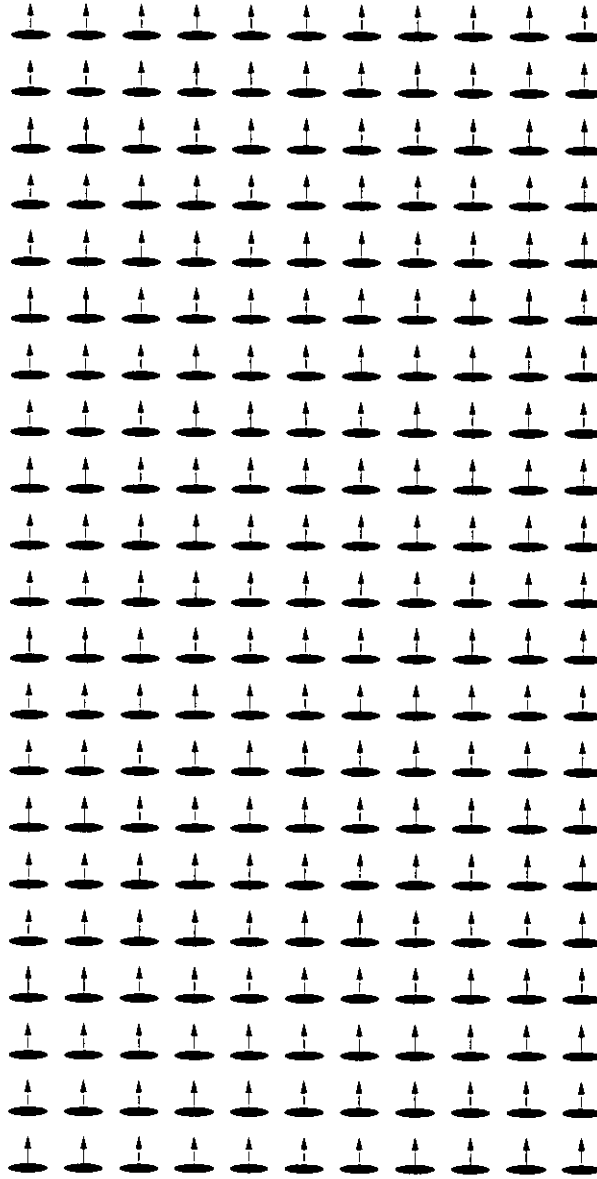
**Figure 2.10a** *The phase portrait corresponding to the structure presented in Figure 2.10b. The initial conditions were  $\phi_0 = 0.01$ ,  $Z_0 = 0$  and  $\beta = -1.0$ . This gives rise to a weakly quasiperiodic structure.*

system as the amplitude of the spin waves further increases. The previous densely filled curve presented in Figure 2.12a now becomes the broken curve presented in Figure 2.13.

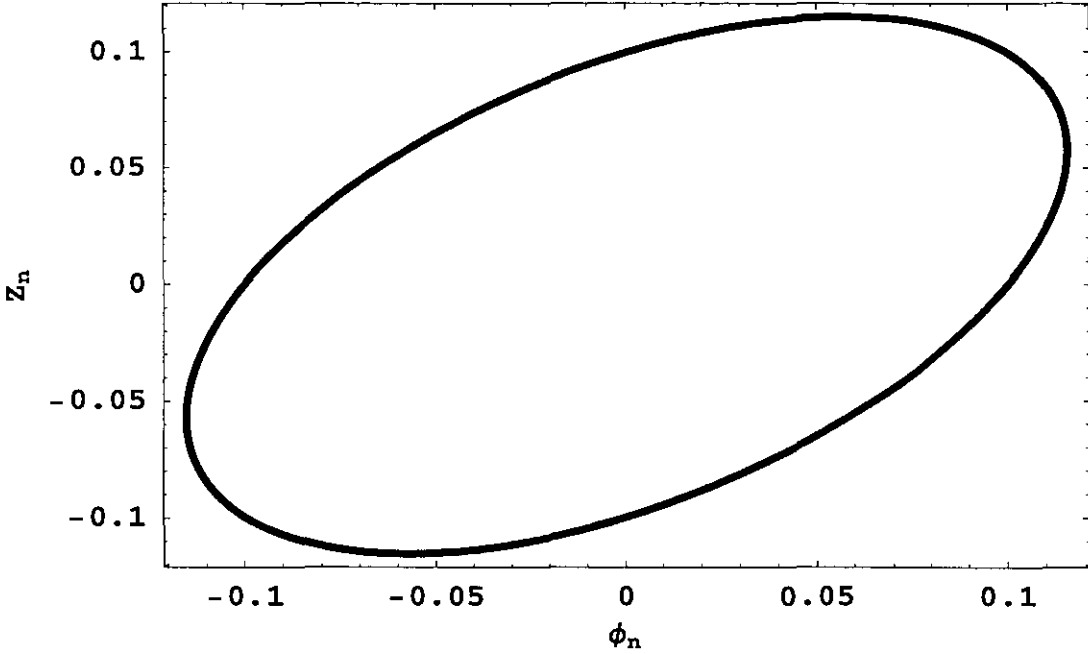
### Chaotic Structures

If we again change  $\phi_0$  by a very small amount to  $\phi_0 = 1.15707$  – which is a change of less than one thousandth of a percent – we get a very different phase portrait which is presented in Figure 2.14. There is a slight dispersion of the curve which corresponds to the amplitude of some oscillations being slightly larger than the rest. This dispersion along with the sensitive dependence on initial conditions infers the onset of chaotic behaviour within our discrete nonlinear system of magnetic multilayers.

This onset of chaotic behaviour is further demonstrated by another small change in the initial conditions to  $\phi_0 = 1.15709$  – keeping  $\beta = -1$  and  $Z_0 = 0$  – which gives a different type of phase portrait presented in Figure 2.15a.



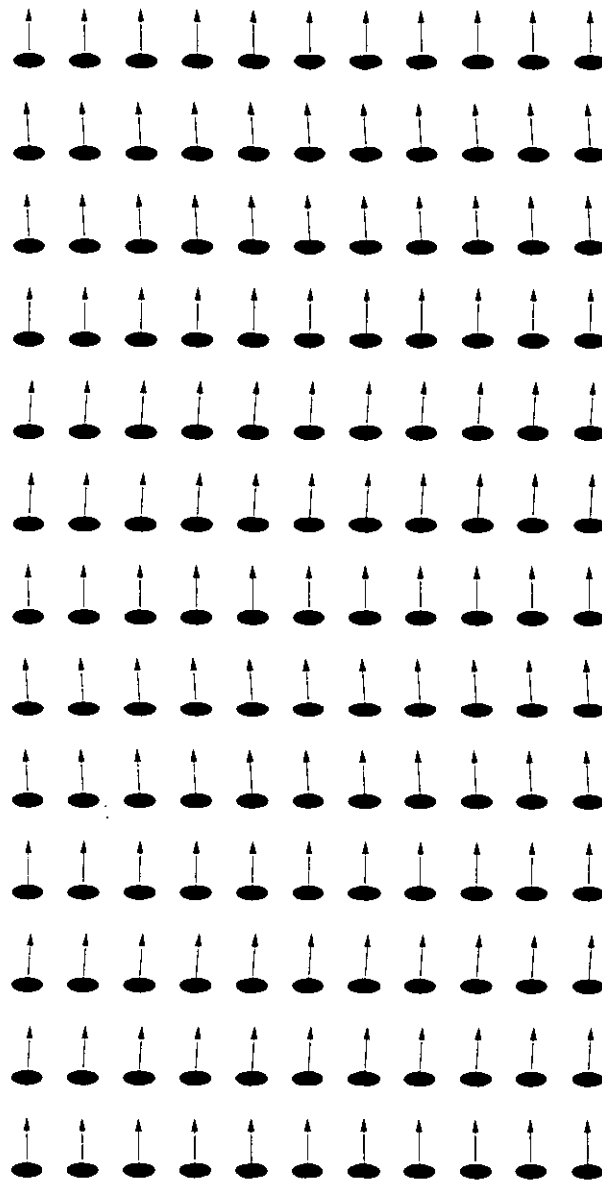
**Figure 2.10b** *Layers 680 to 700 of a 1000 layer structure which gives rise to the phase portrait presented in Figure 2.10a. The variation in the direction of orientation of the magnetisation of each layer is again very small corresponds to a weakly quasiperiodic structure.*



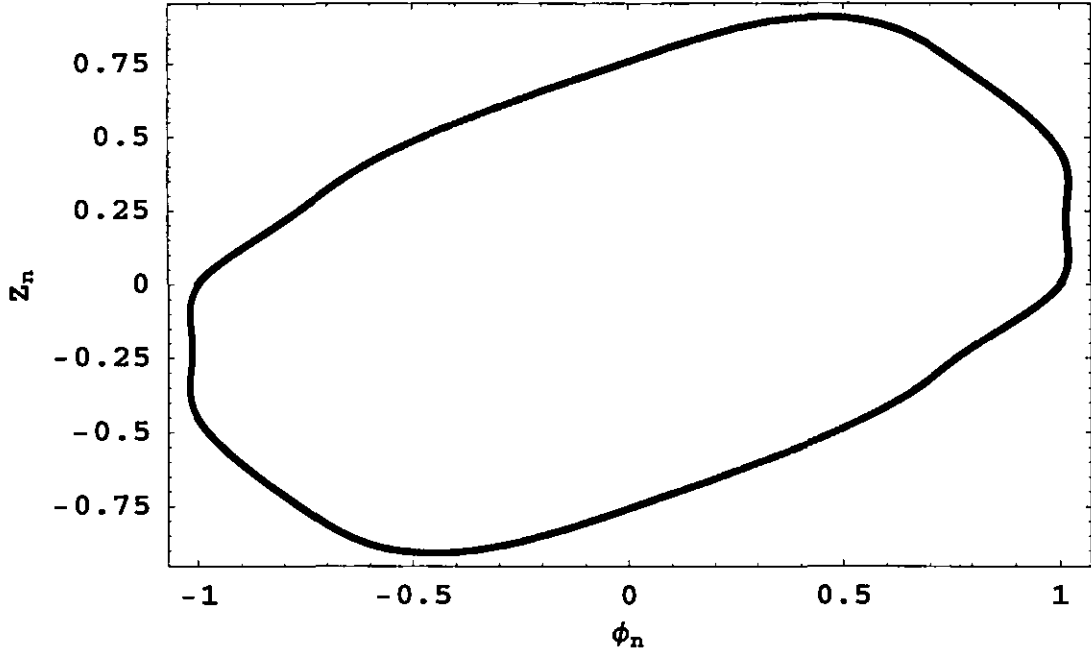
**Figure 2.11a** *The phase portrait corresponding to the structure presented in Figure 2.11b. The initial conditions were  $\phi_0 = 0.1$ ,  $Z_0 = 0$  and  $\beta = -1.0$ . This gives rise to a quasiperiodic structure.*

Figure 2.15a shows more clearly the transition to an apparently chaotic magnetic structure. Up until now all angles of the orientation of the spins were within the approximate range  $-\phi_0 \leq \phi_n \leq \phi_0$ . Now, although the orientation of the majority of the layers is still within this range, the angle of the magnetisation of some layers is closer to an angle of  $\pi$ , that is, antiparallel to the direction of growth of the magnetic multilayer structure. The cross-section of the magnetic structure presented in Figure 2.15b shows an incomplete rotation of the magnetic spins of the layers about  $\pi$ .

An interesting observation is made if the abscissa in the phase portrait presented in Figure 2.15a is shifted by  $\pi/2$ . This transformation yields the phase portrait presented in Figure 2.15c. The phase portrait of the same structure now shows a double loop (butterfly) which is a hallmark of classical chaotic motion in dynamical systems. The difference in the density of points in each of the loops (wings of the butterfly) indicates that the spins in the magnetic structure prefer to orientate themselves about the angle  $\phi = 0$  and not  $\phi = \pi$ ; this is probably due to the fact



**Figure 2.11b** *Layers 35 to 47 of a 1000 layer structure which gives rise to the quasiperiodic phase portrait presented in Figure 2.11a. The variation in the direction of orientation of the magnetisation of each layer has increased with increasing  $\phi_0$ .*



**Figure 2.12a** *Another quasiperiodic phase portrait corresponding to the structure presented in Figure 2.12b. The initial conditions were  $\phi_0 = 1.0$ ,  $Z_0 = 0$  and  $\beta = -1.0$ .*

that  $\phi_0$  is marginally closer to the former than the latter.

Starting with  $\phi_0 = 1.2$  and iterating we obtain a double loop presented in Figure 2.16a in which the density of points in each loop is about the same.  $\phi_n$  again is in the range  $-\pi/2 \leq \phi_n \leq 3\pi/2$ . In this system we have many different types of magnetic structures as shown in the Figure 2.16b. This figure represents the magnetic structure which gives rise to the phase portrait presented in Figure 2.16a. For illustrative purposes it is different to previous representations of the cross-section of a magnetic structure. Here, the left most arrow in the first row represents the magnetisation of the first layer and moving across is equivalent to progressing through the discrete magnetic system along the easy-axis. Each row of arrows represents 100 layers of the magnetic multilayer. The density of points in the top half of the phase portrait is greater than the bottom half because the clockwise rotation of spin is slightly more prevalent than the anti-clockwise, that is, there are more spin vortices than antivortices.

As  $\phi_0$  is further increased then it is noticed that the density of points in the



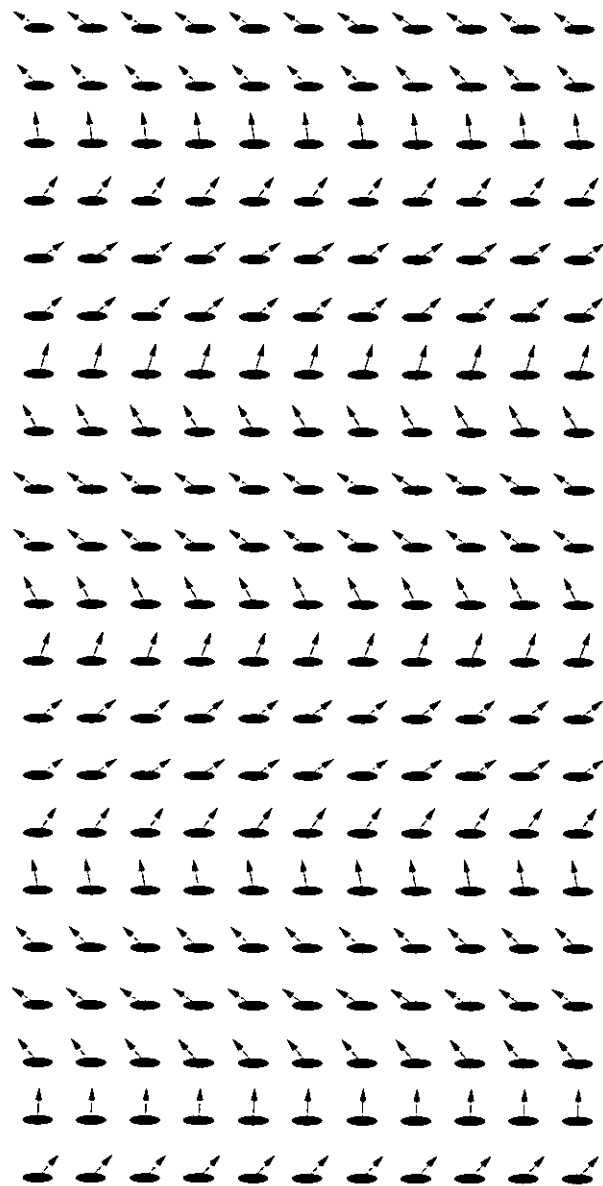


**Figure 2.12b** *Layers 35 to 55 of a 1000 layer structure which gives rise to the phase portrait presented in Figure 2.12a. The variation in the direction of orientation of the magnetisation of each layer has further increased with increasing  $\phi_0$ .*

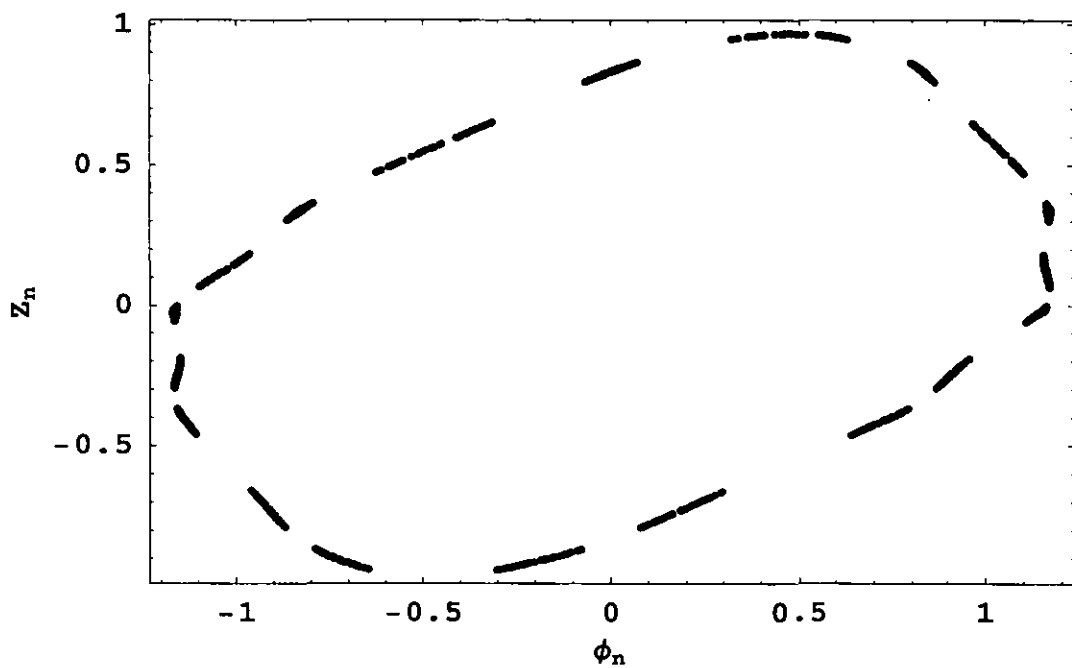


Figure 2.13 A phase portrait generated for the initial conditions  $\phi_0 = 1.15706$ ,  $Z_0 = 0$  and  $\beta = -1.0$ .

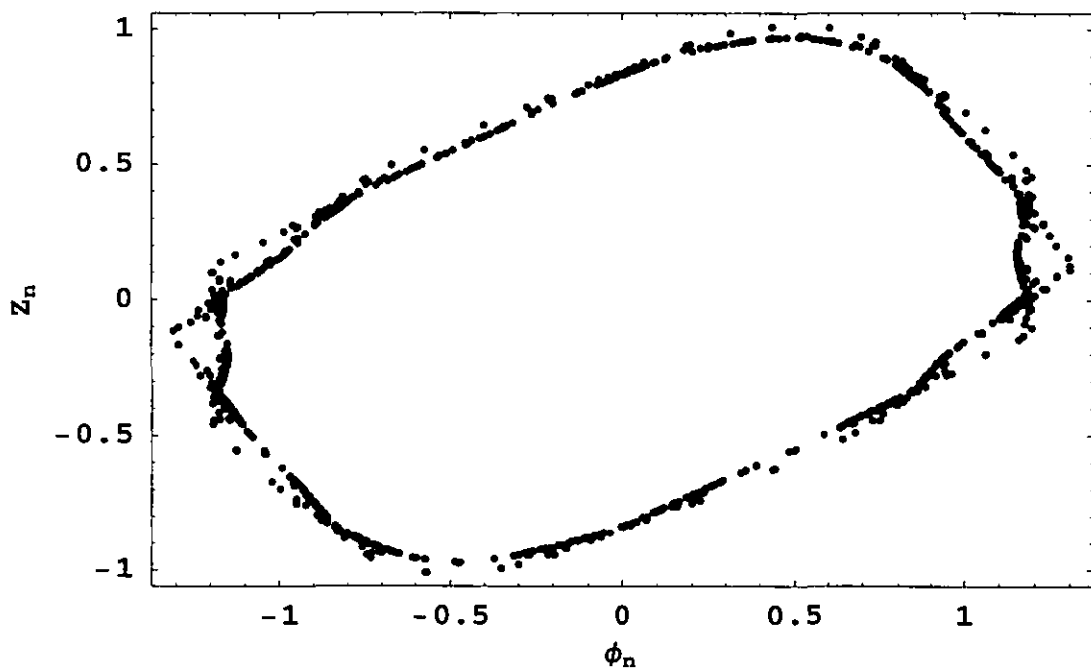


Figure 2.14 A phase portrait generated for the initial conditions  $\phi_0 = 1.15707$ ,  $Z_0 = 0$  and  $\beta = -1.0$ . This corresponds to a weakly chaotic structure.

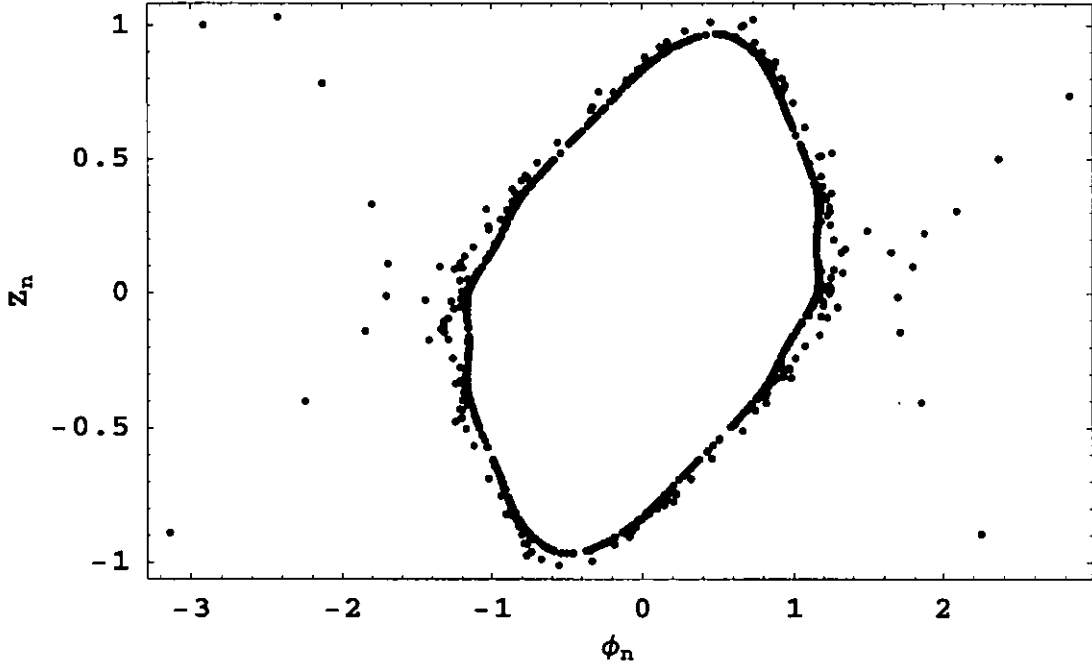
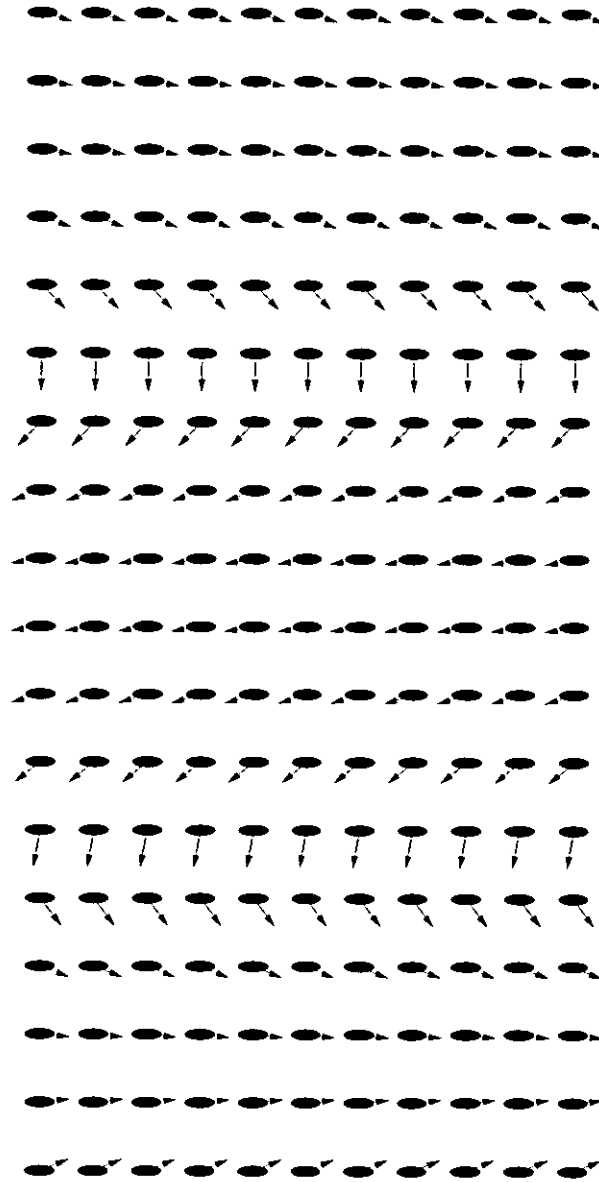


Figure 2.15a A phase portrait corresponding to the structure presented in Figure 2.15b. The initial conditions were  $\phi_0 = 1.15709$ ,  $Z_0 = 0$  and  $\beta = -1.0$ . This corresponds to another weakly chaotic structure.

bottom half of the phase portrait increases while the density of points in the top half decreases. This is demonstrated by the phase portrait presented in Figure 2.17a and implies that there are more antivortices than vortices as shown in Figure 2.17b.

With a further increase of  $\phi_0$  the behaviour remains chaotic although there is a tendency for the spins to prefer to align antiparallel to the axis of growth of the magnetic multilayer structure until at  $\phi_0 = 2.0$  the spin vortices cease to exist. Once again the only spin structure within the system is that of oscillating spins. However, unlike before the spins now prefer to align antiparallel to the easy axis. This is shown in the phase portrait presented in Figure 2.18 where the trajectory seems to be centred around the angle  $\phi = \pi$ .

This phase portrait is very similar to the phase portrait presented in Figure 2.13. The chaotic behaviour of the system appears to have vanished with the disappearance of the spin vortices. As  $\phi_0$  is further increased the behaviour of the magnetic multilayer system becomes more regular in a trend similar – but opposite



**Figure 2.15b** *Layers 980 to 997 of a 1000 layer structure which gives rise to the phase portrait presented in Figure 2.15a. As well as oscillations about the zero angle this structure shows that the relatively large value of  $\phi_0$  has given rise to some oscillations about the angle  $\pi$ .*

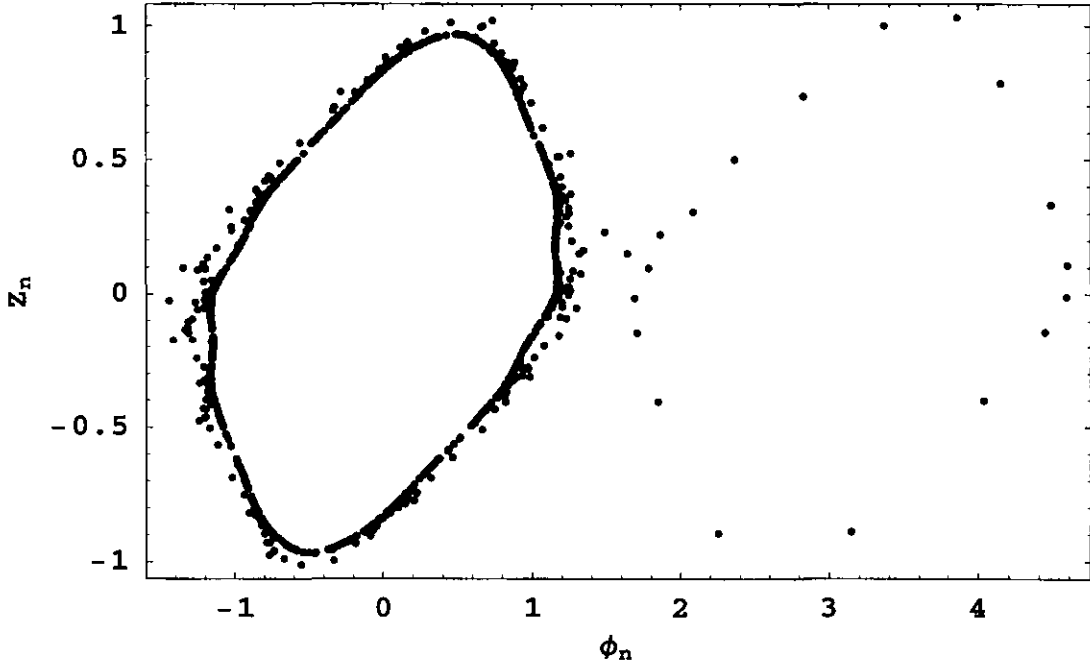


Figure 2.15c A phase portrait generated for the initial conditions  $\phi_0 = 1.15709$ ,  $Z_0 = 0$  and  $\beta = -1.0$  as in Figure 2.15a but with the abscissa shifted by  $\pi/2$ .

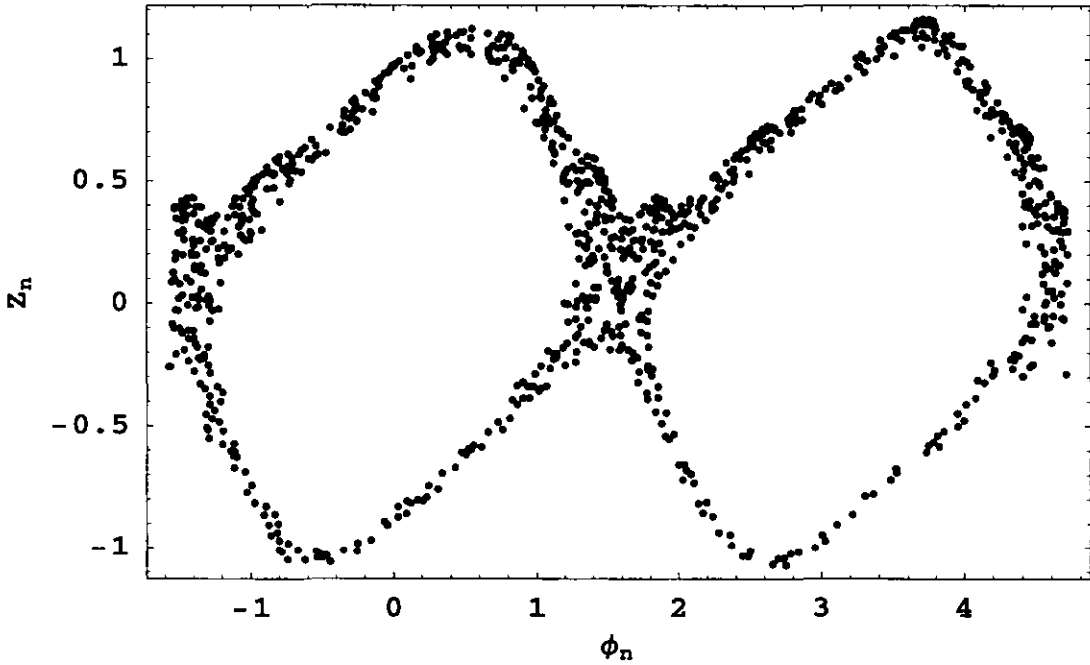
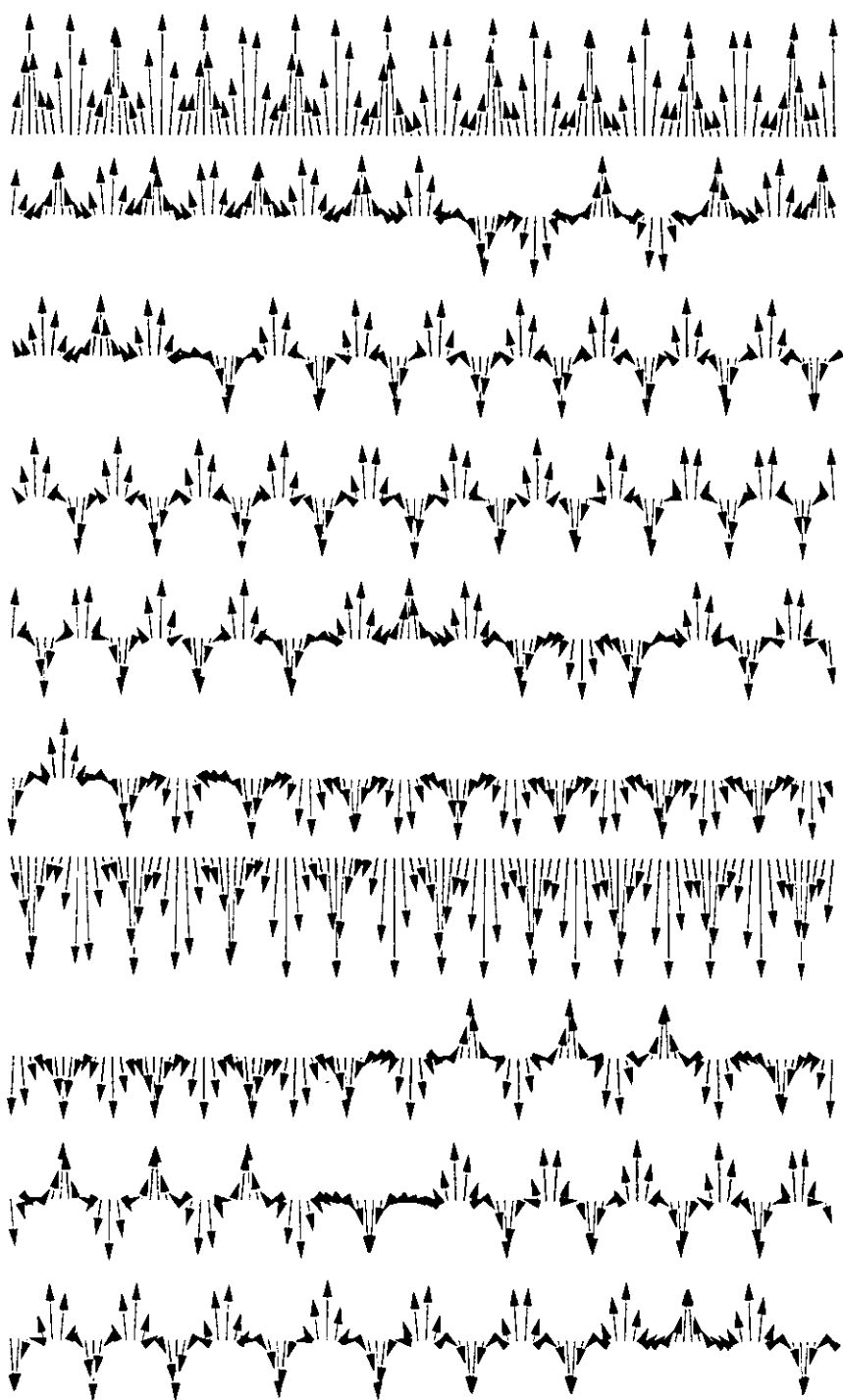
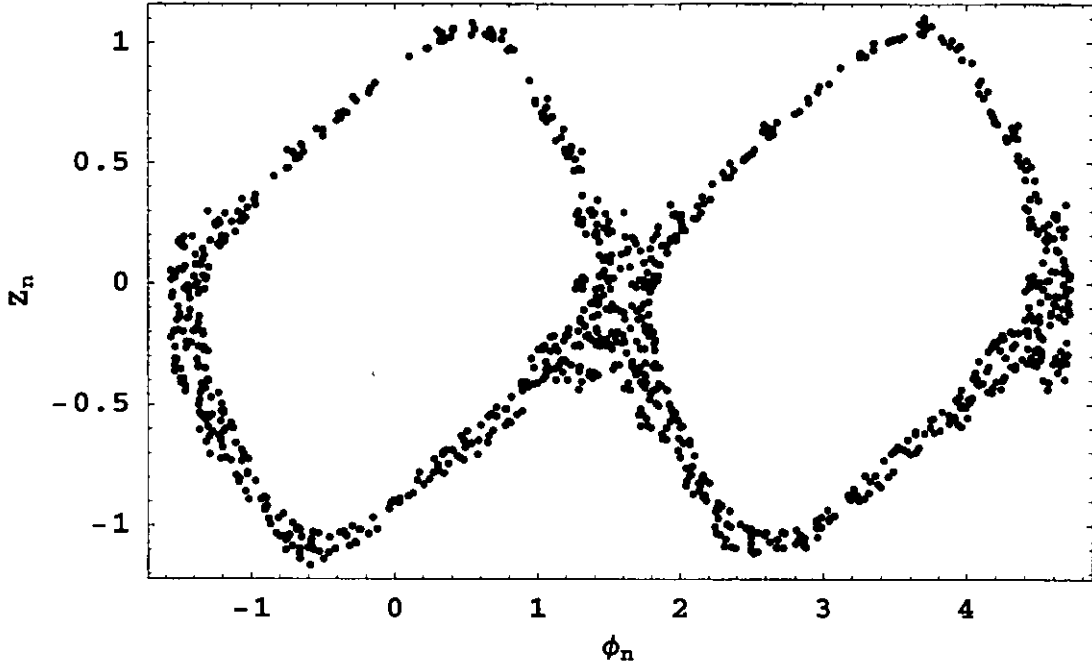


Figure 2.16a The phase portrait corresponding to the structure presented in Figure 2.16b. The initial conditions were  $\phi_0 = 1.2$ ,  $Z_0 = 0$  and  $\beta = -1.0$ . This corresponds to a chaotic structure.



**Figure 2.16b** *The 1000 layer magnetic multilayer structure which gives rise to the phase portrait presented in Figure 2.16a. Beginning in the top left, each row of arrows represents the magnetisation of 100 layers as you progress through the structure.*



**Figure 2.17a** The chaotic phase portrait corresponding to the structure presented in Figure 2.17b. The initial conditions  $\phi_0 = 1.3$ ,  $Z_0 = 0$  and  $\beta = -1.0$ .

– to when  $\phi_0$  was increased from  $\phi_0 = 0$ . The amplitude of oscillation of the spin waves decreases as the fixed point ( $\phi_0 = \pi$ ,  $Z_0 = 0$ ) is approached.

Thus, we have found that depending on the depolarisation of the magnetic moments of the first layer on the substrate, there can arise in our discrete nonlinear system of magnetic multilayers periodic, quasiperiodic and chaotic states of the system. For a constant value of  $\beta$  and a very small depolarisation of the magnetic moments of the first layer we get a regular periodic structure. With increasing  $\phi_0$  the regular structures first transform into quasiperiodic structures and then into the chaotic states.

### 2.6.2 Dependence on $\beta$

We have already mentioned that the type of structure which may arise in our system of magnetic multilayers depends on the ratio  $\beta$  of the magnetic anisotropy constant to the exchange constant.

For example, Figure 2.5 shows an analytic period-2 structure which exists for

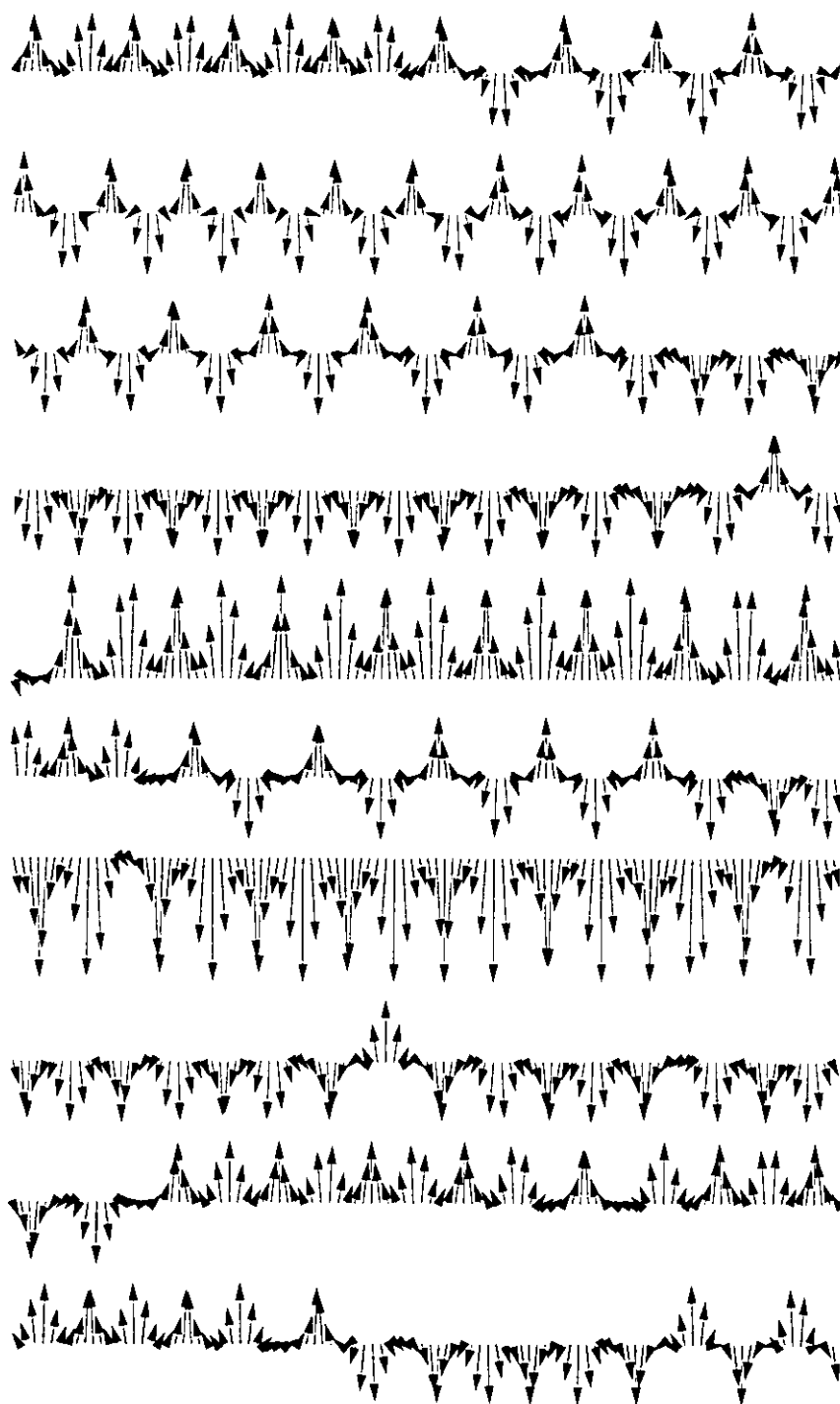
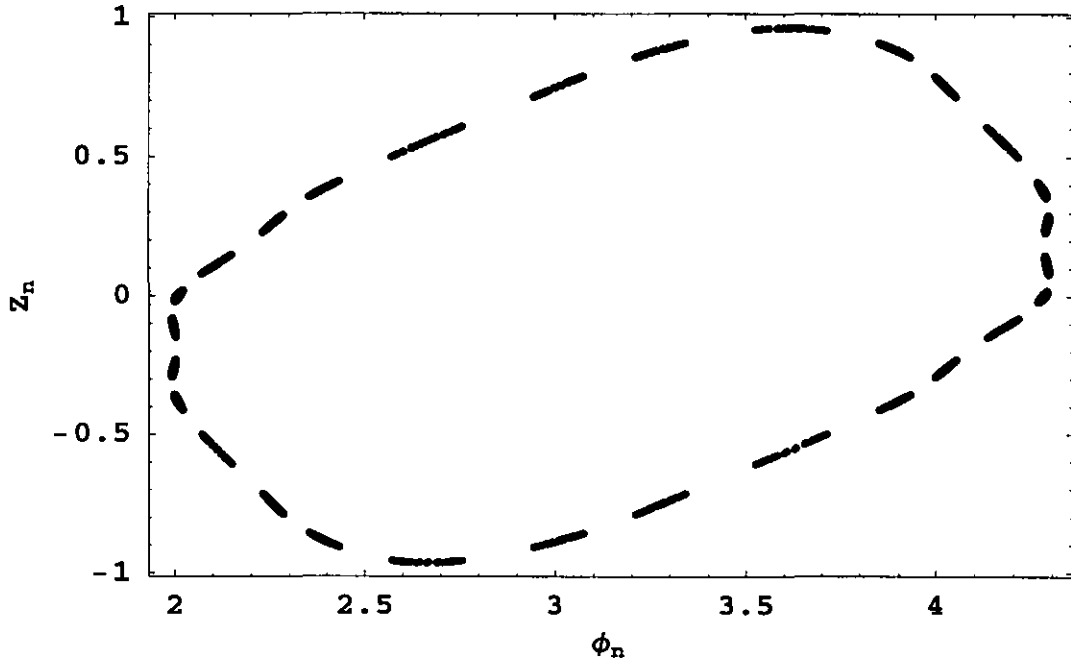


Figure 2.17b The 1000 layer magnetic multilayer structure which gives rise to the phase portrait presented in Figure 2.17a. Beginning in the top left, each row of arrows represents the magnetisation of 100 layers as you progress through the structure.





**Figure 2.18** A quasiperiodic phase portrait generated for the initial conditions  $\phi_0 = 2.0$ ,  $Z_0 = 0$  and  $\beta = -1.0$ .

$\beta = 4\pi/\sqrt{3} \approx 7.2551975$ . The phase portrait of this structure is presented in Figure 2.19.

If the value of  $\beta$  is altered slightly to  $\beta = 7.2552$  then this period-2 solution ceases to exist. In its place we obtain a completely different type of phase portrait presented in Figure 2.20a and the new structure this phase portrait corresponds to presented in Figure 2.20b. This result serves to demonstrate that specific types of solutions may only exist for particular values of the parameter  $\beta$ . For example the period-2 solution presented in Figure 2.5 ceases to exist even if  $\beta$  is changed only slightly. This can also be inferred from comparing Figure 2.19 and Figure 2.20a where a slight change in  $\beta$  gives a dramatically different phase portrait.

If we iterate with different initial conditions then we obtain different types of structures. For example with the initial condition  $\phi_0 = 0.00001$ ,  $\beta = 0.01$  and  $Z_0 = 0$  we obtain the phase portrait presented in Figure 2.21a which corresponds to a structure consisting of domains of layers separated by domain walls. The orientation of the magnetisation of the layers is the same in each domain while the

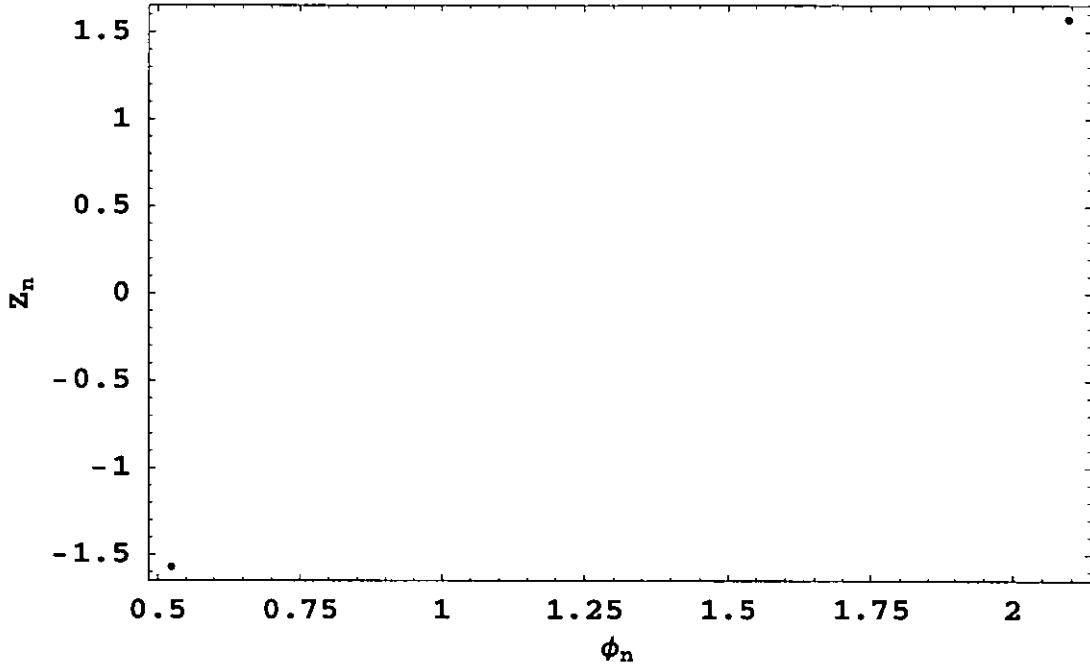


**Figure 2.19** *The phase portrait corresponding to the period-2 solution presented in Figure 2.5 consisting of just two points in the  $\{\phi_n, Z_n\}$  phase plane. The initial conditions were  $\phi_0 = \pi/6$ ,  $Z_0 = -\pi/2$  and  $\beta = 4\pi/\sqrt{3} \approx 7.2551975$ .*

orientation of the magnetisation of the layers changes gradually in a domain wall. A domain wall in a magnetic multilayer structure is presented in Figure 2.21b. For these initial conditions each domain consists of approximately 260 layers and the domain wall separating these domains consist of approximately 30 layers.

As  $\beta$  is increased to  $\beta = 0.1$  – with  $\phi_0$  unchanged – both the size of the domains and the size of the domain walls decrease. Each domain now consists of approximately 80 layers and each domain wall consists of approximately 10 layers. Figure 2.22a shows such a domain wall and the corresponding phase portrait is presented in Figure 2.22b. Note that this domain wall has the opposite sense of rotation to that presented in Figure 2.21b.

As  $\beta$  is further increased to  $\beta = 0.2$  – with  $\phi_0$  unchanged – the size of a domain decreases further to approximately 40 layers and the size of a domain wall decreases further to approximately 8 layers. This magnetic multilayer structure is presented in Figure 2.23a and the corresponding phase portrait is presented in Figure 2.23b.

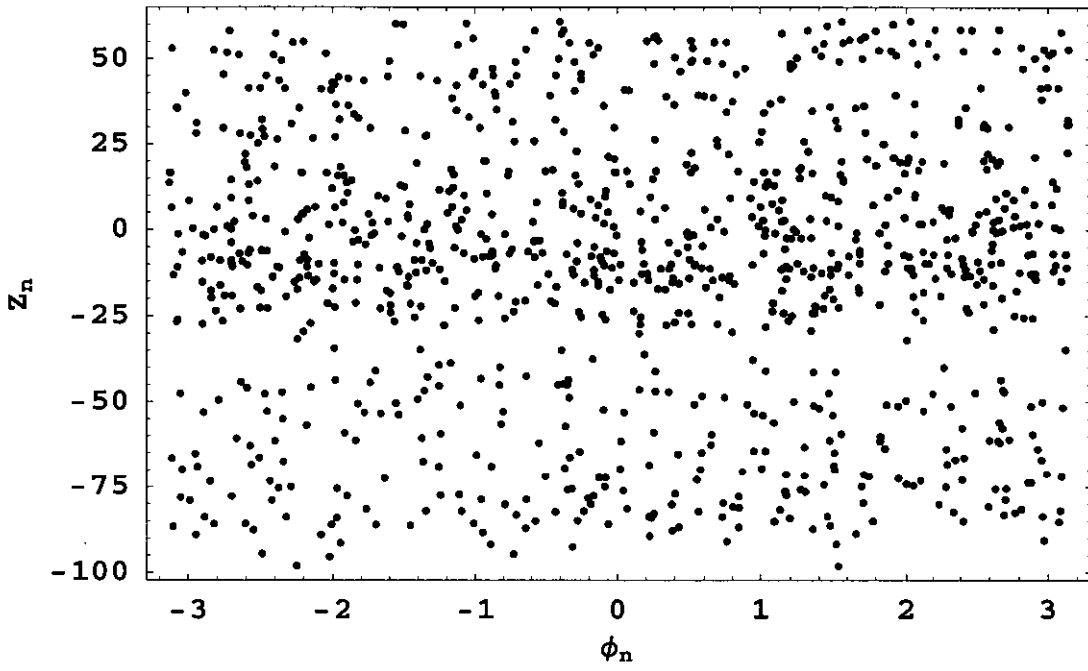


**Figure 2.20a** *The phase portrait corresponding to the magnetic multilayer structure presented in Figure 2.20b. The initial conditions were  $\phi_0 = \pi/6$ ,  $Z_0 = -\pi/2$  and  $\beta = 7.2552$ . A small change in the value of  $\beta$  gives rise to a very different phase portrait to that of the period-2 structure presented in Figure 2.19.*

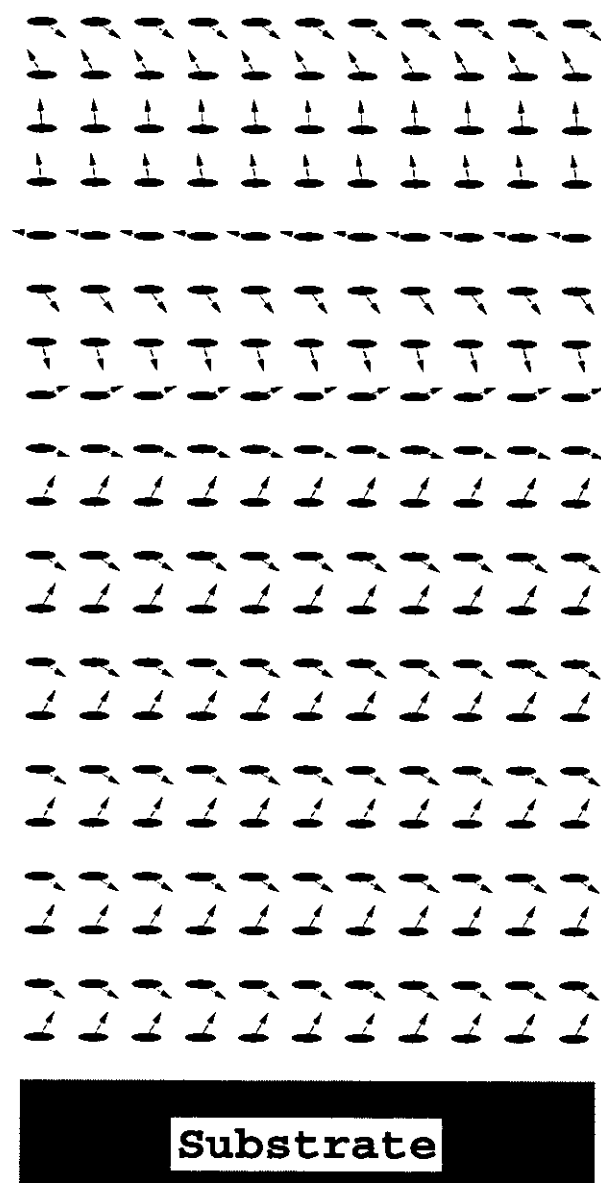


**Figure 2.20b** *Layers 1 - 20 of a cross-section of a magnetic multilayer structure which gives rise to the phase portrait presented in Figure 2.20a. This clearly indicates the disappearance of the period-2 structure presented in Figure 2.5 due to a very small change in the value of the parameter  $\beta$ .*

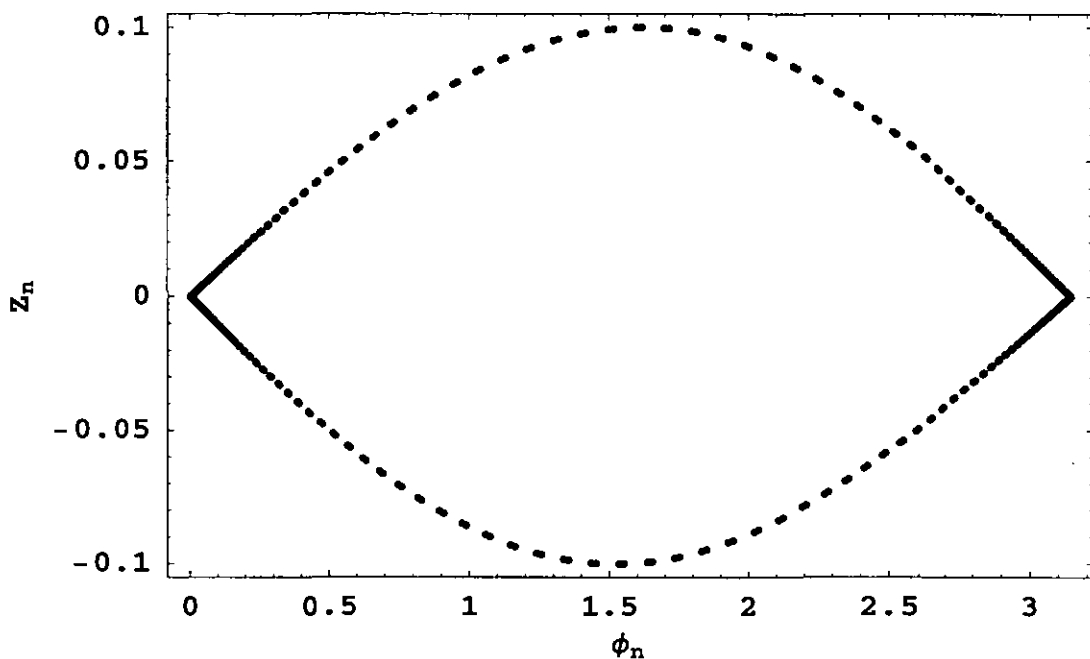


**Figure 2.21a** *The phase portrait corresponding to the structure presented in Figure 2.21b. The initial conditions were  $\phi_0 = 0.00001$ ,  $Z_0 = 0$  and  $\beta = 0.01$ . This corresponds to a domain structure in a magnetic multilayer system.*

As  $\beta$  is increased further the size of the domains and the size of the domain walls further decrease. It is also noticeable that the size of the domains and domain walls is not uniform. Different domains and domain walls have different sizes. For example with the initial condition  $\phi_0 = 0.00001$ ,  $\beta = 0.6$  and  $Z_0 = 0$  we obtain the magnetic multilayer structure presented in Figure 2.24a and the corresponding phase portrait presented in Figure 2.24b. The size of a domain is between 8 and 16 layers while the size of a domain wall is between 2 and 4 layers.

For the initial conditions  $\phi_0 = 0.00001$ ,  $\beta = 0.8$  and  $Z_0 = 0$  we obtain the phase portrait presented in Figure 2.25a and the magnetic multilayer structure it corresponds to presented in Figure 2.25b. With the increase of  $\beta$  the domains are getting smaller and smaller and the domain walls are getting closer together. Here, the size of a domain is between 5 and 8 layers while the size of a domain wall is between 1 and 2 layers. The slight dispersion in the orbit of the phase portrait of this system indicates a weakly chaotic structure.

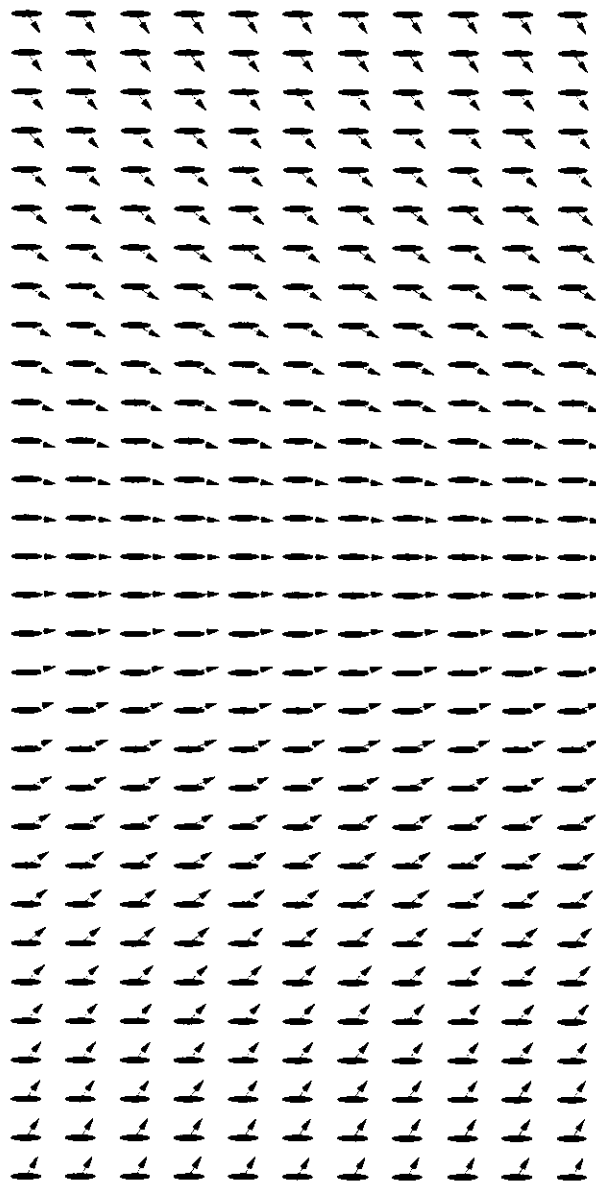


**Figure 2.21b** *Layers 630 - 660 in a 1000 layer domain structure in a magnetic multilayer system which gives rise to the phase portrait presented in Figure 2.21a. This domain wall consists of approximately 30 layers.*

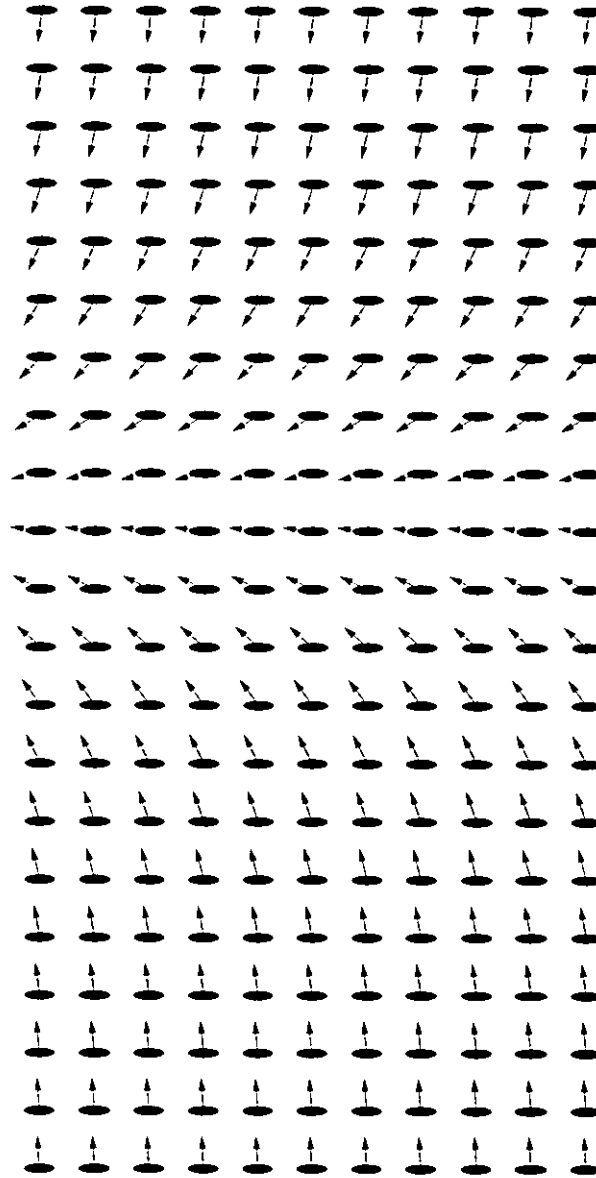


**Figure 2.22a** *Layers 195 - 215 in a 1000 layer domain structure in a magnetic multilayer system which gives rise to the phase portrait presented in Figure 2.22b. This domain wall consists of approximately 10 layers.*

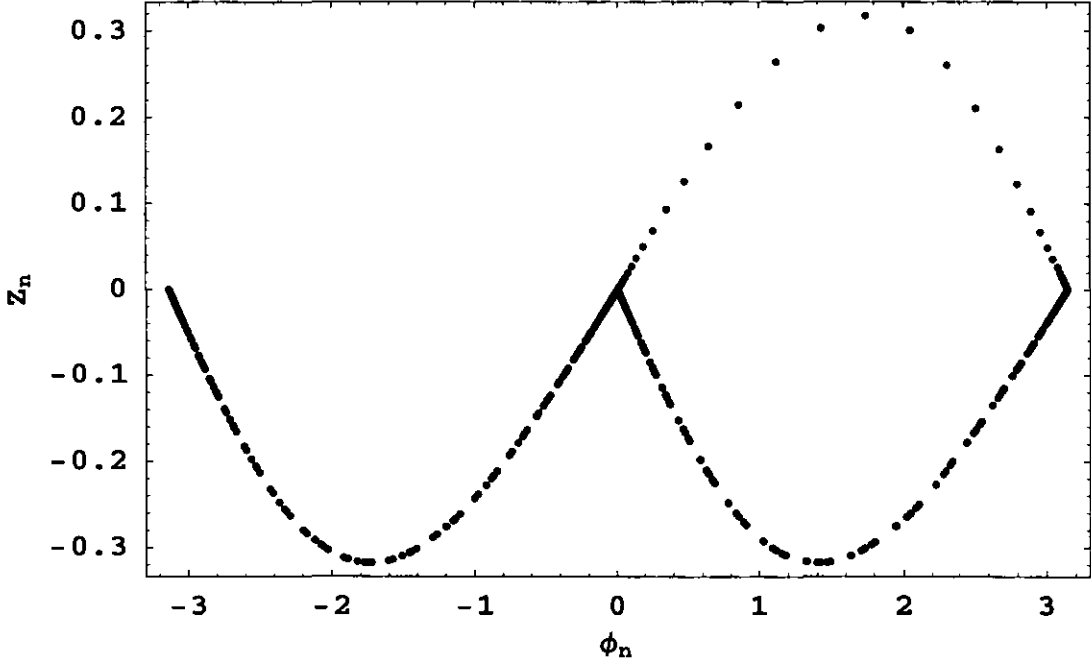


Figure 2.22b The phase portrait corresponding to the structure presented in Figure 2.22a. The initial conditions were  $\phi_0 = 0.00001$ ,  $Z_0 = 0$  and  $\beta = 0.1$ . This again corresponds to a domain structure in a magnetic multilayer system.

As  $\beta$  is further increased to  $\beta = 1.0$  – and  $\phi_0$  unchanged – the phase portrait of the system Figure 2.26a becomes further dispersed and indicates a chaotic structure. A cross-section of this magnetic multilayer structure presented in Figure 2.26b shows a magnetic spin vortex like structure. Domains of layers (and domain walls) no longer exist as now the direction of magnetisation of the layers rotates as one progresses through the magnetic multilayer structure. This rotation in the direction of magnetisation of the layers gives rise to the formation of spin vortex structures in this discrete nonlinear system.

Finally, for  $\beta = 2.0$ ,  $\phi_0 = 0.00001$  and  $Z_0 = 0$  the phase portrait of the system presented in Figure 2.27a becomes further dispersed and corresponds to a strongly chaotic structure. A cross-section of this structure is presented in Figure 2.27b. There is no apparent pattern in this structure as even spin vortices cease to exist. Instead we find a structure which is a possible candidate for a spin glass state.

Thus, we have found that depending on the ratio of the magnetic anisotropy



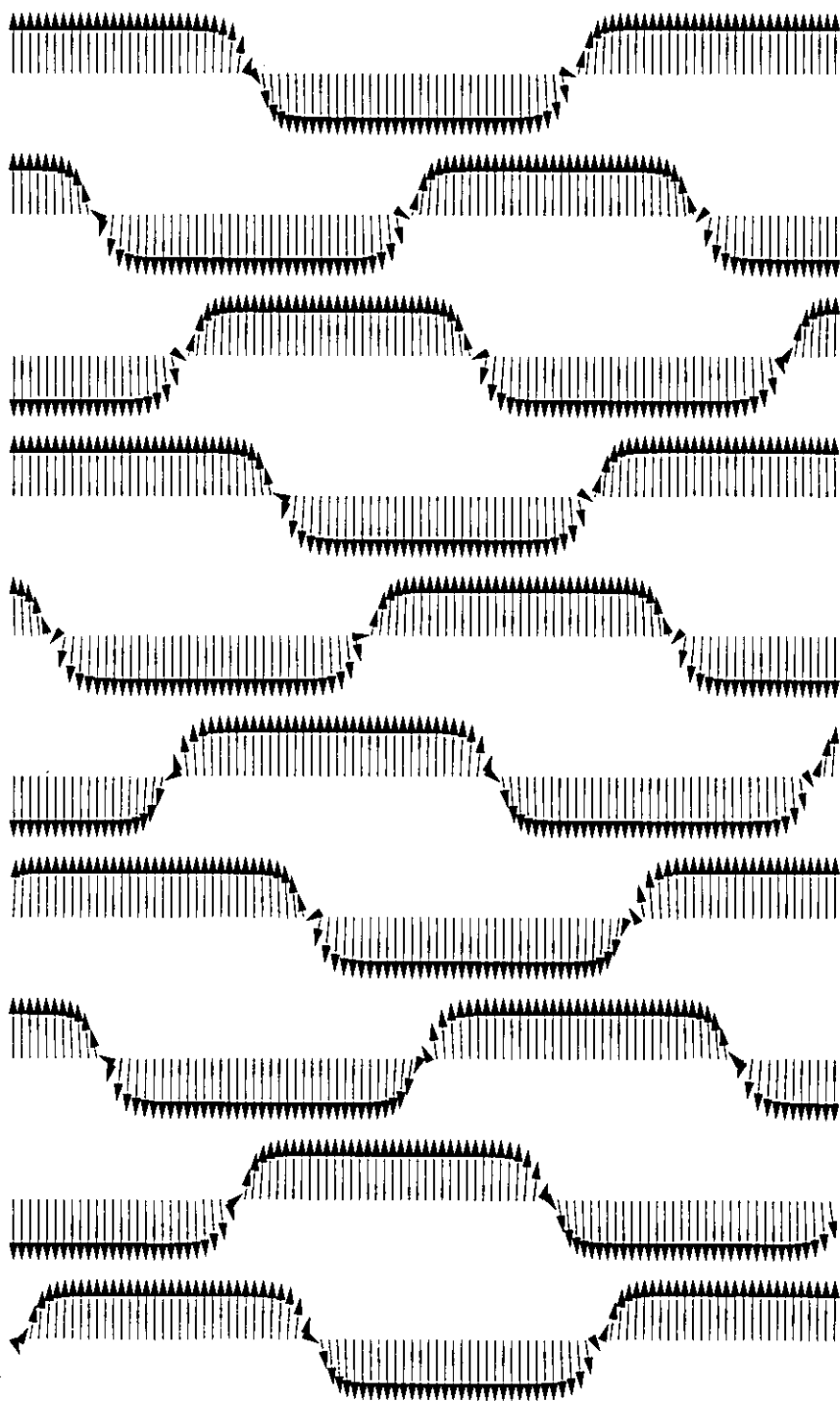


**Figure 2.23a** *The 1000 layer magnetic multilayer structure which gives rise to the phase portrait presented in Figure 2.23b. The size of a domain is approximately 40 layers and the size of a domain wall is approximately 8 layers.*

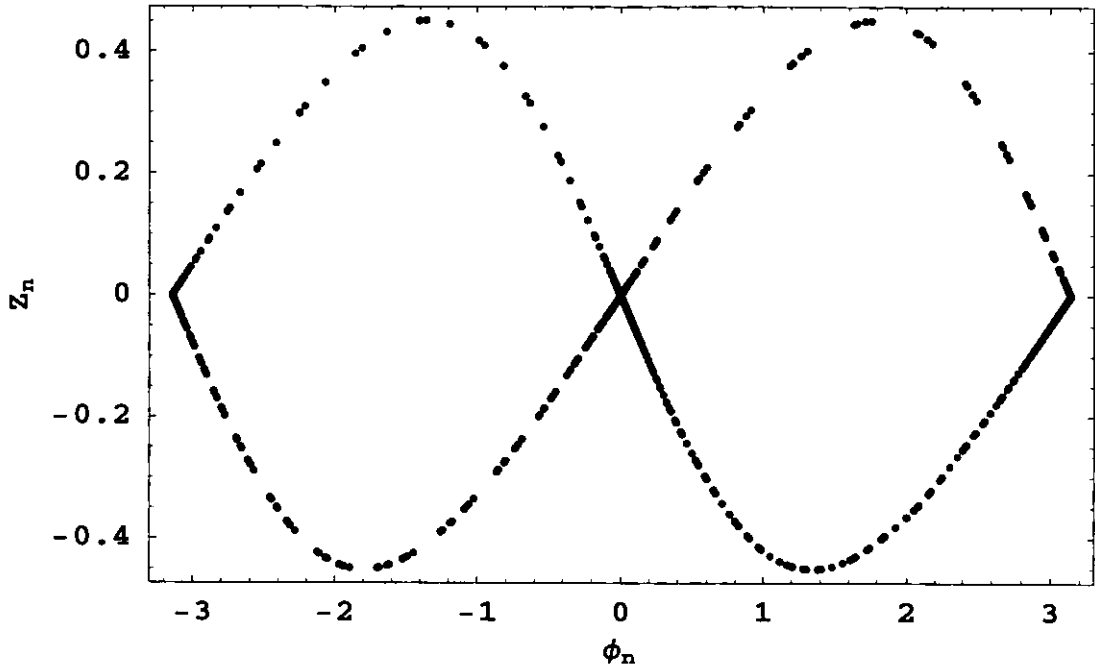


**Figure 2.23b** *The phase portrait corresponding to the structure presented in Figure 2.23a. The initial conditions were  $\phi_0 = 0.00001$ ,  $Z_0 = 0$  and  $\beta = 0.2$ .*

constant to the exchange constant there can arise in our discrete nonlinear system of magnetic multilayers periodic, quasiperiodic and chaotic states of the system. For a particular value of  $\beta$  and  $\phi_0$  the angle of depolarisation of the magnetic moments of the first layer we get a regular periodic structure. If this value of  $\beta$  is changed the regular structures transform into either quasiperiodic structures or chaotic states depending on the value of  $\beta$ .

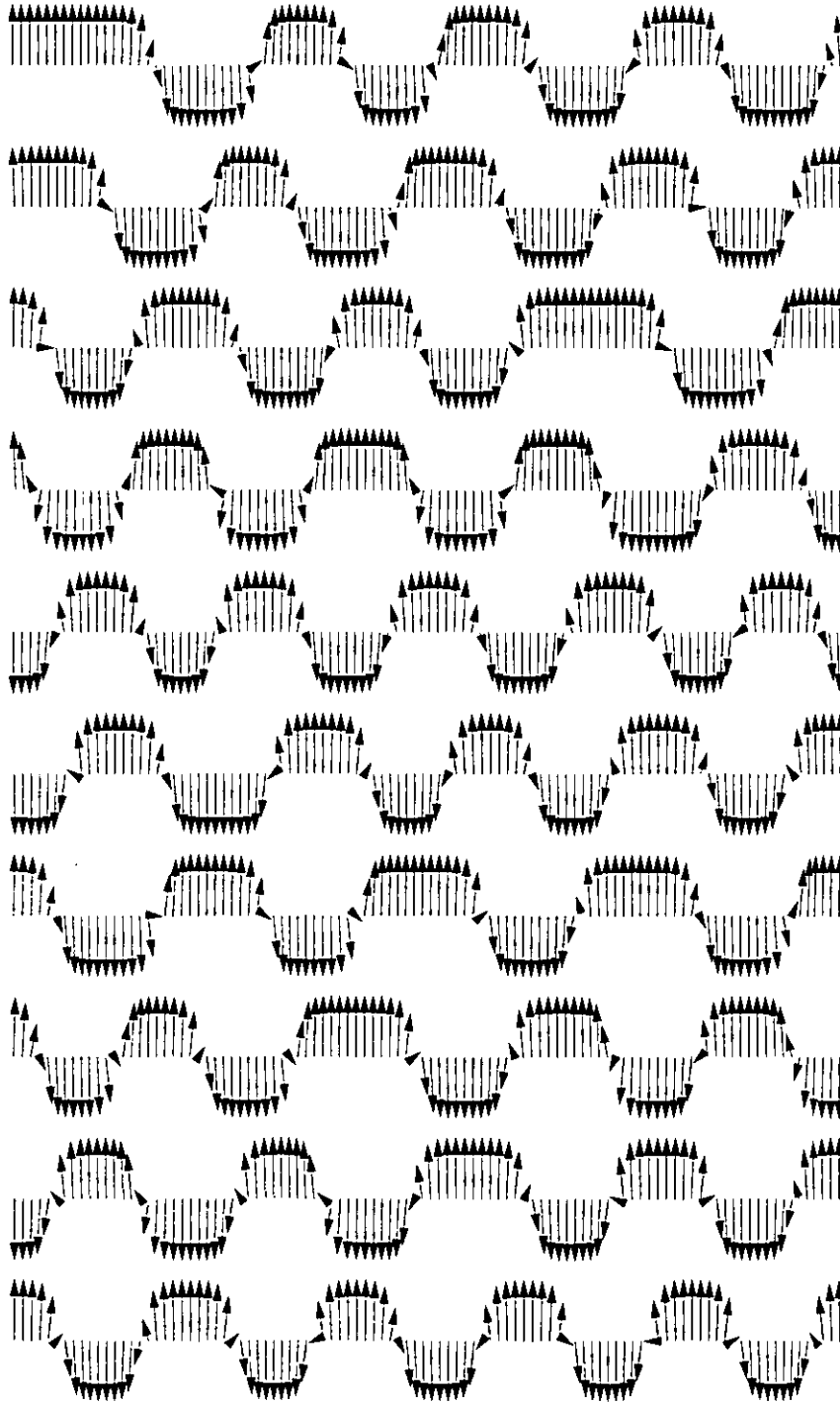


Figure 2.24a The 1000 layer magnetic multilayer structure which gives rise to the phase portrait presented in Figure 2.24b. The size of a domain can be between 8 - 16 layers and the size of a domain wall between 2 - 4 layers.

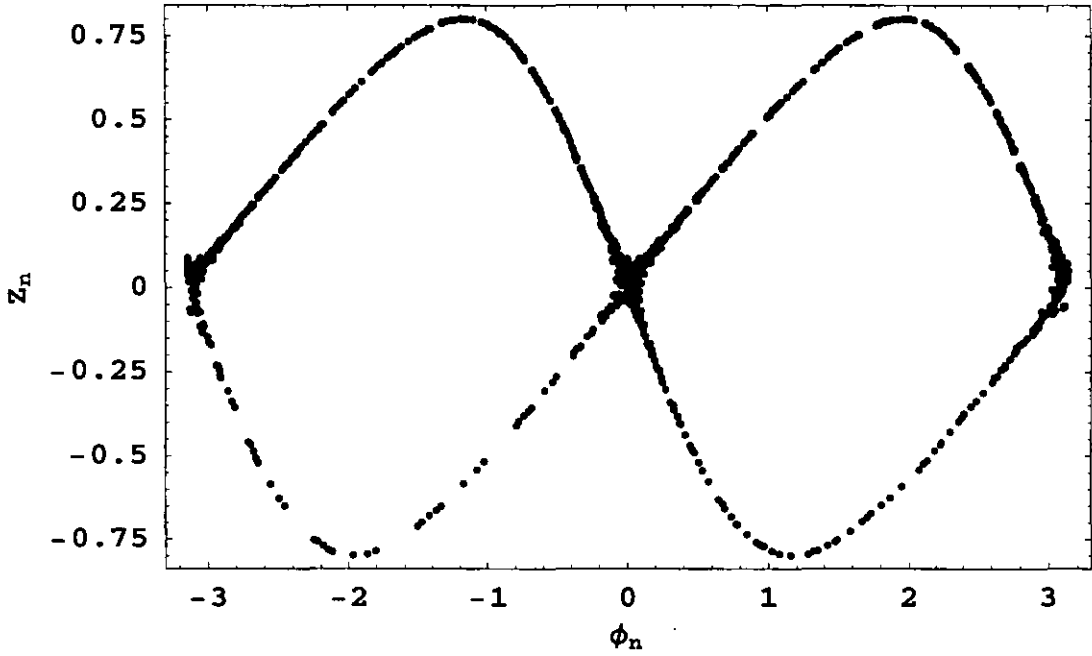


Figure 2.24b The phase portrait corresponding to the structure presented in Figure 2.24a. The initial conditions were  $\phi_0 = 0.00001$ ,  $Z_0 = 0$  and  $\beta = 0.6$ . This again corresponds to a domain structure in a magnetic multilayer system.

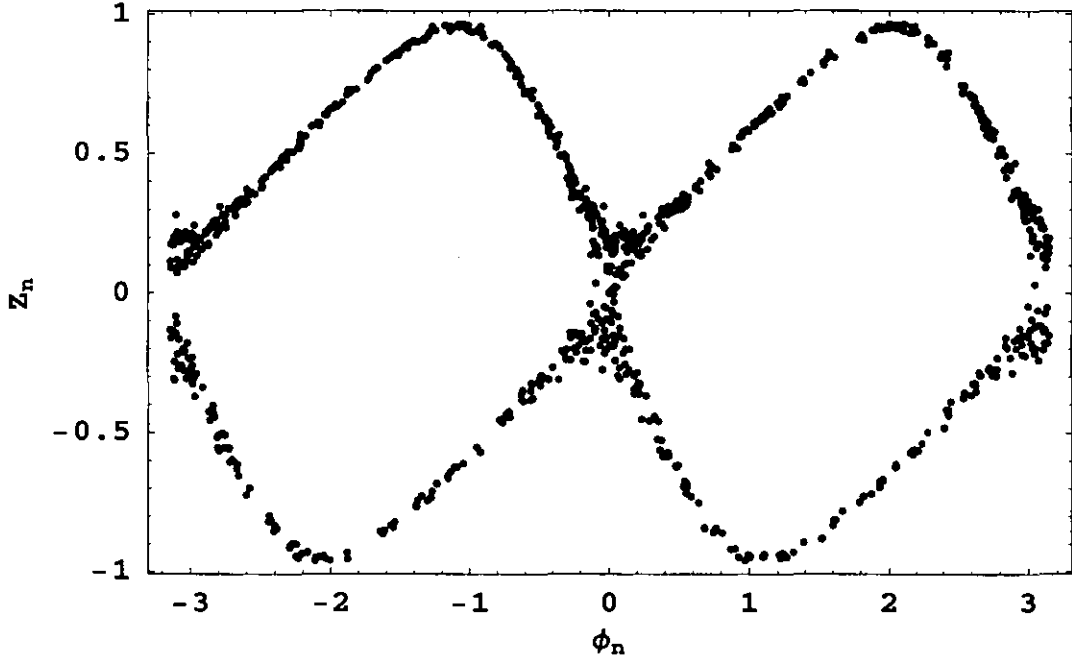
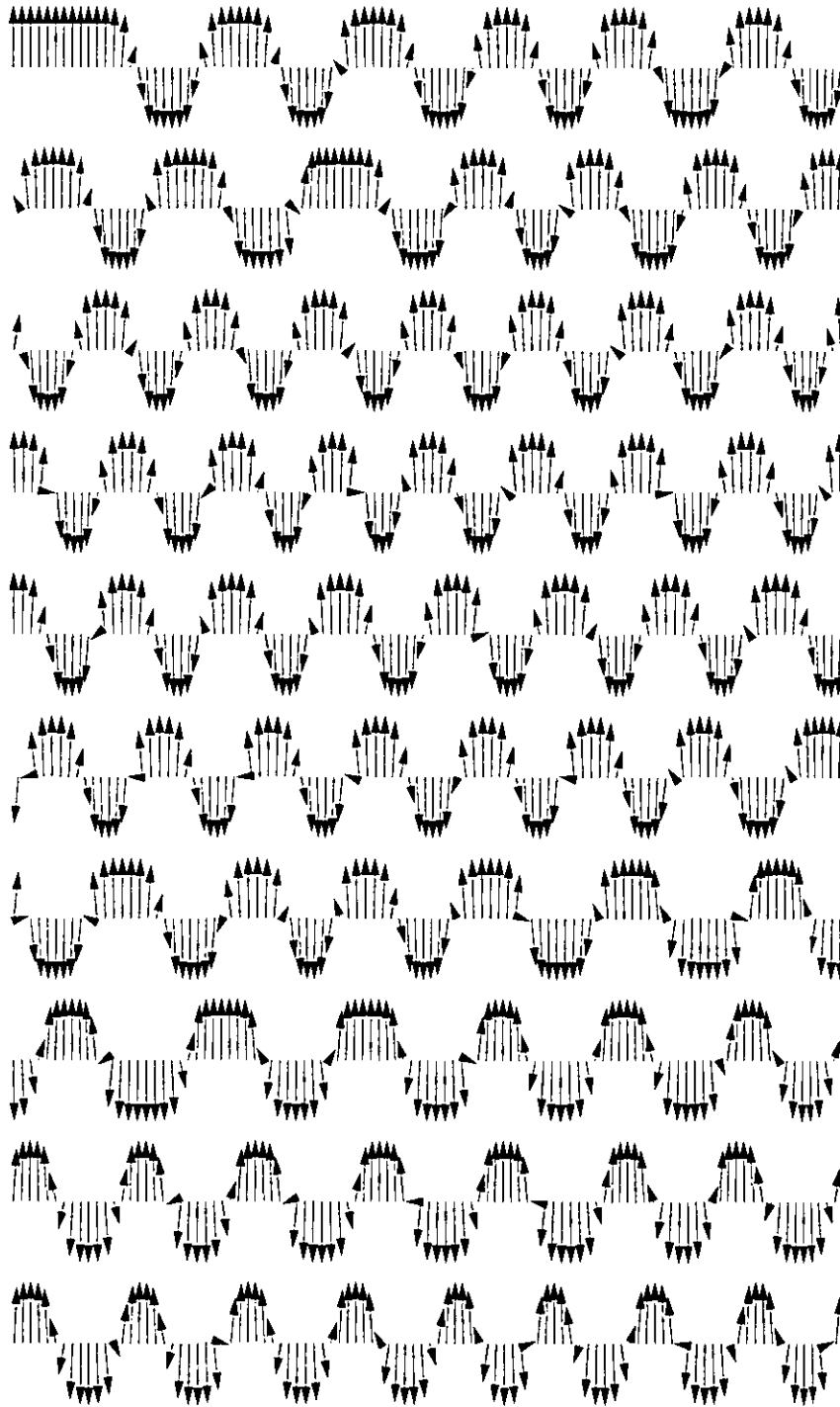
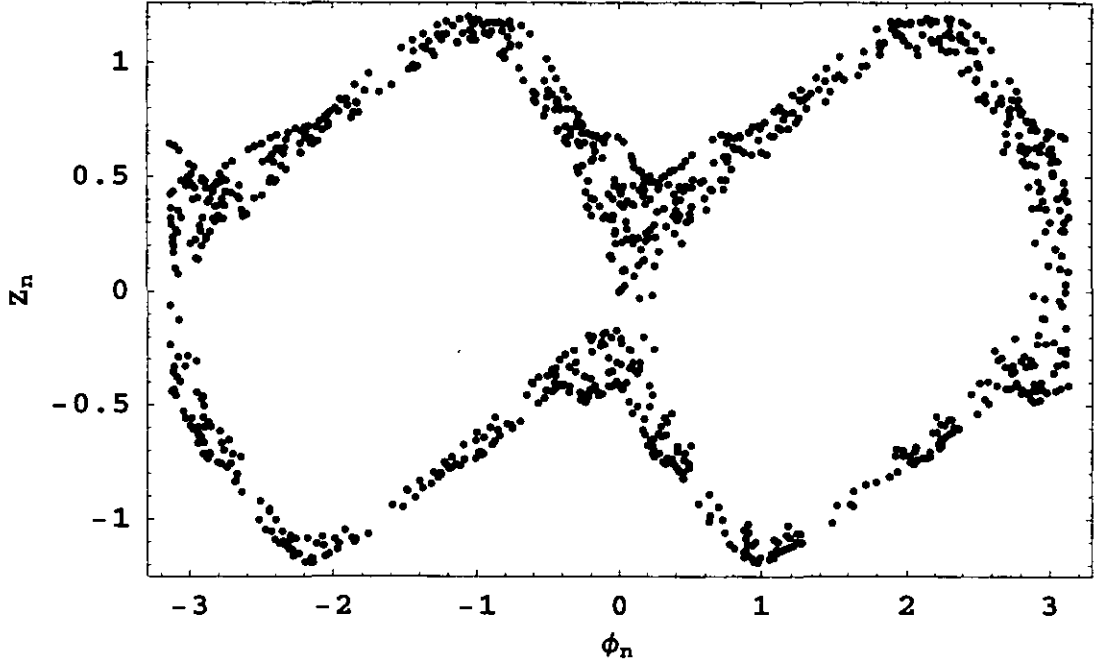


Figure 2.25a The phase portrait corresponding to the structure presented in Figure 2.25b. The initial conditions were  $\phi_0 = 0.00001$ ,  $Z_0 = 0$  and  $\beta = 0.8$ . This corresponds to a weakly chaotic domain structure in a magnetic multilayer system.



**Figure 2.25b** *The 1000 layer magnetic multilayer structure which gives rise to the phase portrait presented in Figure 2.25a. The size of a domain is between 5 - 8 layers and the size of a domain wall between 1 - 2 layers.*



**Figure 2.26a** *The phase portrait corresponding to the structure presented in Figure 2.26b. The initial conditions were  $\phi_0 = 0.00001$ ,  $Z_0 = 0$  and  $\beta = 1.0$ . This indicates a chaotic structure of magnetic spin vortices in our magnetic multilayer system.*

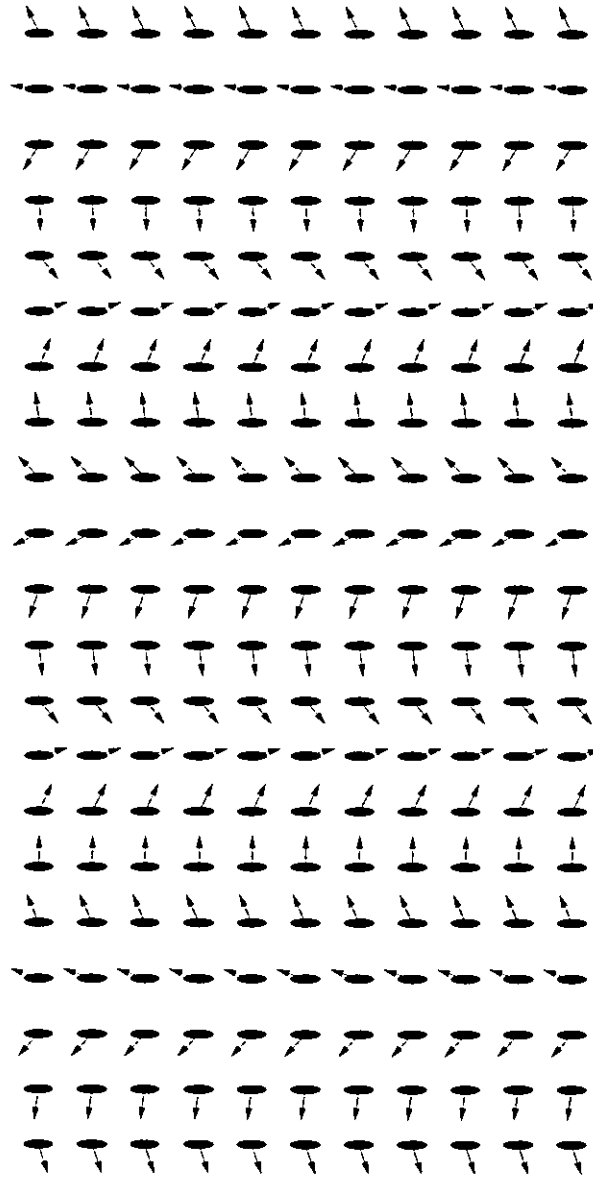


**Figure 2.26b** *Layers 195 - 215 in a 1000 layer magnetic multilayer structure which gives rise to the chaotic phase portrait presented in Figure 2.26a. A spin vortex is manifest over approximately 8 layers.*

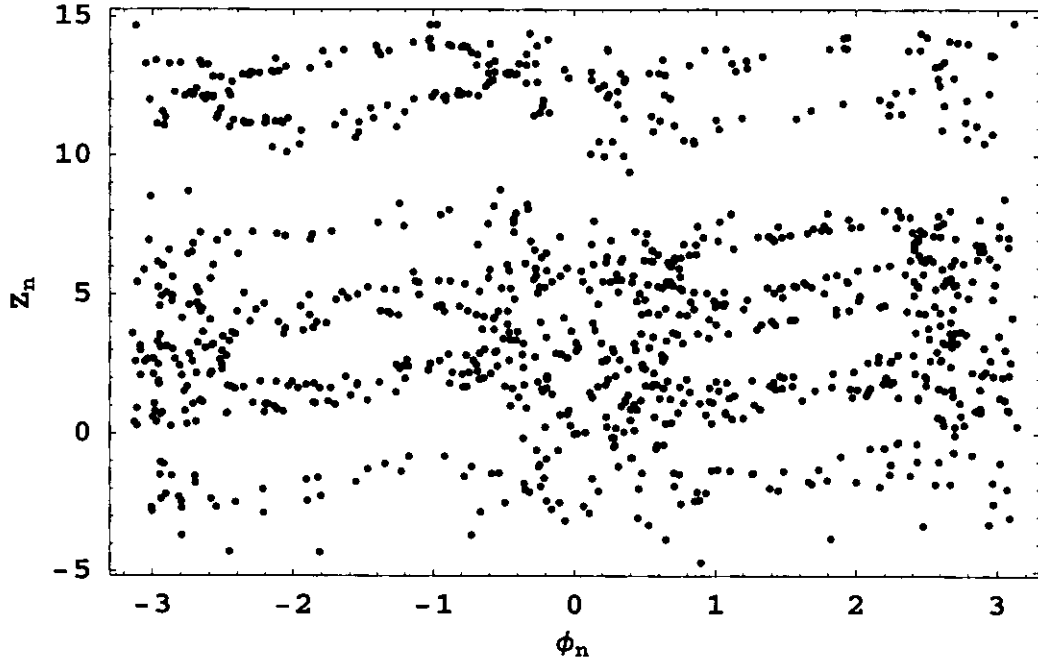


**Figure 2.27a** *The phase portrait corresponding to the structure presented in Figure 2.27b. The initial conditions were  $\phi_0 = 0.00001$ ,  $Z_0 = 0$  and  $\beta = 2.0$ . This indicates a strong chaotic structure of magnetic spins in our magnetic multilayer system.*



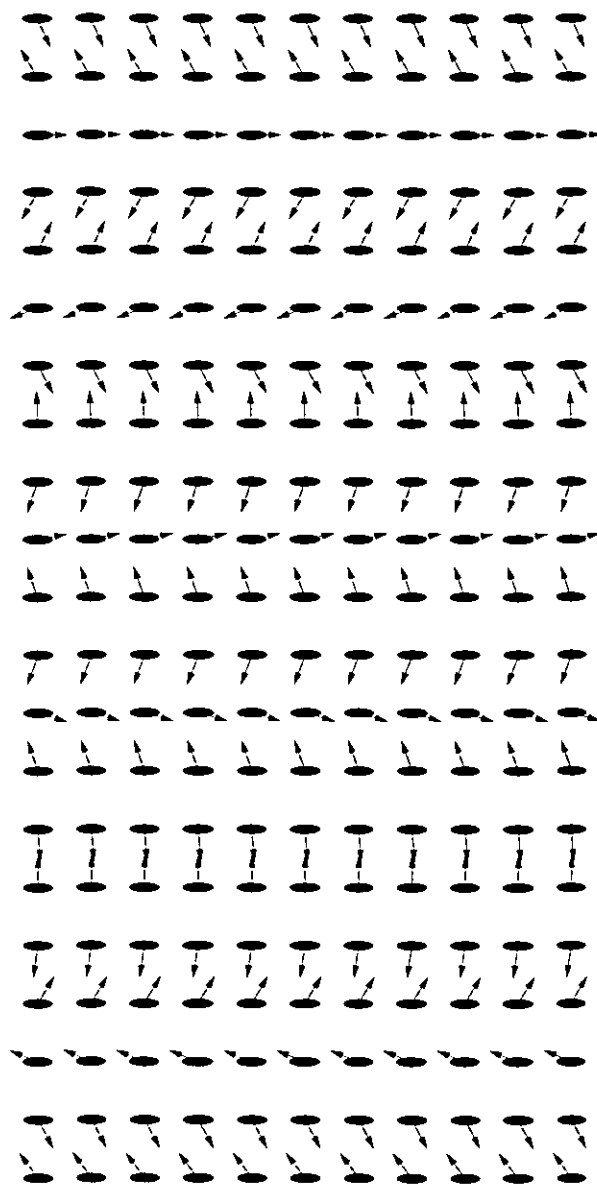


**Figure 2.27b** *Layers 210 - 230 in a 1000 layer magnetic multilayer structure which gives rise to the chaotic phase portrait presented in Figure 2.27a. The magnetic spins appear to be randomly orientated.*

## 2.7 Summary Of Interactions In Magnetic Multilayers

Upon reformulating the problem of a discrete nonlinear set of equations (12) to an iteration problem of a 2-dimensional map (21), we find three characteristically different types of trajectories which may be classified as periodic, quasiperiodic and chaotic.

The periodic magnetic structures are spin-density waves [18] where the orientation of the magnetic moments of each layer changes regularly. Typically, these structures only exist for certain values of the parameter  $\beta$  – even a slight change in  $\beta$  destroys these periodic structures.

If either  $\phi_0$  or  $\beta$  is changed slightly then we find that instead of regular periodic structures we obtain quasiperiodic structures. These quasiperiodic states can be of two types. The first type is that of irregular spatial oscillations of the direction of the magnetic moments of each layer along the reference axis of the magnetic multilayer. As  $\phi_0$  or  $\beta$  is changed further the magnitude of the oscillation of the magnetic moments becomes larger.

Alternatively, we may obtain the second type of quasiperiodic structure – a domain structure. Here, the individual orientation of the magnetic moments of groups of layers in each domain are all aligned in the same direction and are separated by domain walls. With a further increase of  $\beta$  the domains in this type of structure become smaller and closer together as the domain walls become smaller.

As  $\beta$  is further increased both types of quasiperiodic structures disappear and instead we see the formation of a chaotic spin vortex state. In the latter quasiperiodic structure this occurs due to the eventual disappearance of domains – as the domains get smaller and smaller they eventually vanish – and we end up with a spin vortex structure. In the former quasiperiodic structure – that of spatial oscillations in the direction of magnetisation of the layers – with an increase in  $\phi_0$  or  $\beta$  the oscillations get so large that eventually they transform into rotations of the spin in space – spin vortices – where the orientation of the magnetic moments perform a rotation as we move through the layers. These rotations may have either a positive or a negative sense.

Finally, for  $\beta > 2$  there arise some exotic, chaotic structures. In such structures, together with spin vortices, there are also incomplete spin rotations and even arbitrary spin fluctuations. Such structures arise only at large values of  $\beta$  and may be equivalent to spin glass states which arise in bulk magnetic samples.

In conclusion, we have found that in our discrete nonlinear system of magnetic multilayers there may arise spin density waves, spin vortex states and chaotic magnetic structures.

## 2.8 Developing The Model

The Hamiltonian (9) – used above to describe discrete nonlinear systems of magnetic multilayers – may be studied further by performing a fourth order Taylor expansion of the  $\cos^2 \phi_n$  term for  $\phi_n \ll 1$ . Doing so gives

$$H = JM^2 \sum_n 1 - \frac{JM^2}{2} \sum_n (\phi_n - \phi_{n+1})^2 + KM^2 \sum_n \left( 1 - \frac{\phi_n^2}{2} + \frac{\phi_n^4}{24} \right)^2 \quad (22)$$

where the terms involving  $\sum_n 1$  are constants. Expanding the quadratic anisotropy term gives

$$H \approx JM^2 \sum_n 1 - \frac{JM^2}{2} \sum_n (\phi_n - \phi_{n+1})^2 + KM^2 \sum_n \left( 1 - \phi_n^2 + \frac{\phi_n^4}{3} \right) \quad (23)$$

The energetically favourable states of (23) are given by

$$\frac{\partial H}{\partial \phi_n} = 0 \quad (24)$$

which gives

$$-\frac{JM^2}{2} (-2\phi_{n-1} + 4\phi_n - 2\phi_{n+1}) - 2KM^2\phi_n + \frac{4KM^2}{3}\phi_n^3 = 0 \quad (25)$$

Introducing the variables  $\gamma = -JM^2$ ,  $\alpha = 2KM^2$  and  $c = 4KM^2/3$  gives

$$\gamma(-\phi_{n-1} + 2\phi_n - \phi_{n+1}) - \alpha\phi_n + c\phi_n^3 = 0 \quad (26)$$

which is a second order discrete nonlinear equation with a cubic nonlinearity. This type of equation is applicable to many different types of systems. It is studied and solved analytically in the next chapter.

*'Perfection is a path, not a destination.'*

— Morihei Ueshiba

## 3 Solutions Of The Discrete Nonlinear Schrödinger Equation

### 3.1 Introduction To The Discrete Nonlinear Schrödinger Equation

Modern technology allows the manufacturing and processing of materials and structures in which the intrinsic space between the different constituents of a material influences the behaviour of that system.

One example of such a discrete structure is the semiconductor superlattice (SSL) which can be manufactured in such a way that it can consist of different numbers of layers of differing thickness'. In SSL consisting of say, for example, a sequence of layers of  $GaAs$  and  $Ga_xAl_{1-x}As$ , an electron miniband of width  $t$  may be created, where  $t$  is the overlapping integral for an electron localised in neighbouring quantum wells. The number of levels in this miniband depends on the number of layers the SSL consists of. For example, if the superlattice consists of two quantum wells, there are only two levels associated with the symmetric and antisymmetric wave functions. For each energy level, the probability to find the electron in either well is equally distributed. The same is true when there are many levels in the miniband. However, the situation changes dramatically if electron-phonon interactions are considered. The effect of this interaction may give rise to coupled electrons and phonons where the dimensionless electron-phonon coupling constant of this system is inversely proportional to  $t$  [29]. Since the miniband width, in SSL, is between 1 - 100 meV the electron-phonon coupling is strongly intensified in comparison with conventional bandwidths which are in the region of about 1 eV. Such an intensification in the electron-phonon interaction in narrow band structures may give rise to some novel, self-trapped states of the electron.

This phenomenon of the self-trapping of electrons and excitons in solids, originally predicted theoretically [3, 4, 22, 23, 24], has been observed and well studied in many materials (see, for example, review [22]). It arises, primarily, in low dimen-

sional systems and in systems with a strong electron-phonon interaction.

Traditionally, adiabatic self-trapping has only been studied in continuum models [23, 24] applicable to localised states with a large radius (in comparison to the lattice spacing), except, of course, the exciton self-trapping in rare gas solids [22]. Anti-adiabatic (or non-adiabatic) polarons with a small radius have also been intensively investigated [25].

The (Rashba)-Holstein polaron model [3, 4] is described by a discrete nonlinear Schrödinger equation with a cubic nonlinearity. Other systems which may be described by an equation of this generic form include the wave function of superconducting states in layered superconductors [5], metal insulator transitions in Peierls systems [9] and systems of coupled nonlinear oscillators [6].

Consequently, we study the atomic lattice taking into account a nonlinearity which arises due to the interaction of the electron with acoustic phonons. This gives rise to the creation of some self-trapped (or polaronic) states.

### 3.2 The Hamiltonian And The DNSE

The classical and quantum systems mentioned above may be generally described with the use of the Hamiltonian

$$H = \sum_i |\psi_i - \psi_{i+1}|^2 - \sum_i \frac{c}{2} |\psi_i|^4 - E \sum_i |\psi_i|^2 \quad (27)$$

where  $\psi_i$  is the wave function (state) of the system on the  $i^{th}$  site,  $c$  is some parameter and  $E$  is the energy eigenvalue associated with the state of the system.

For coupled (nonlinear) oscillators the function  $\psi$  describes a lattice distortion. For a self-trapped particle  $|\psi_i|^2$  is proportional to the probability of finding the particle at the  $i$ th lattice site. For quantum systems the wave function must, of course, satisfy the conventional normalisation condition

$$\sum_i |\psi_i|^2 = 1 \quad (28)$$

which is effectively described when the eigenvalue  $E$  is used as a Lagrange multiplier. The parameter  $c$  may have both positive (for self-trapped quantum states) and negative (for nonlinear coupled oscillators) values depending on the system being studied.

The energetically favourable states of a system described by (27) correspond to the minima of (27). These states are described by  $\hat{\nabla} H(\psi) \equiv 0$ , where  $\hat{\nabla}$  is the *differential operator* ie  $\frac{\partial}{\partial \psi_i}$ . Differentiating (27) with respect to  $\psi_i$  gives the conventional discrete nonlinear Schrödinger equation (DNSE) of the form

$$-\psi_{i-1} + 2\psi_i - \psi_{i+1} - c|\psi_i|^2\psi_i = E\psi_i \quad (29)$$

which describes, amongst other things, the interaction of electrons and phonons [3, 4].  $\psi_i$  is the wave function of the polaron (electron localised by interactions with phonons) so that  $|\psi_i|^2$  is the charge density of the polaronic state,  $c$  is the electron-phonon coupling constant and  $E$  is the energy eigenvalue of this state. The normalisation condition then gives the charge of the electron. The electron



associated with a *small* polaron spends most of its time trapped on a single lattice site, that is, the majority of the charge is distributed on the localising site.

For simplicity, only real solutions are discussed and so we take  $\psi_i$  to be real in the DNSE. If we consider the discrete equation describing nonlinear harmonic oscillators we have

$$-x_{i-1} + 2x_i - x_{i+1} + cx_i^3 = ex_i \quad (30)$$

which differs from (29) in the sign of  $c$ . With the aid of the transformation

$$x_n = (-1)^n \psi_n \quad (31)$$

$$e = 4 - E \quad (32)$$

we again get

$$-\psi_{i-1} + 2\psi_i - \psi_{i+1} - c\psi_i^3 = E\psi_i \quad (33)$$

Thus, we find that all solutions and the classification of such solutions for the quantum problem associated with the DNSE with positive coupling constant ( $c > 0$ ) are also the solutions (and corresponding classification) of equations describing classical nonlinear lattices.

The behaviour of these solutions does not depend explicitly on the parameter  $c$ ;  $c$  can be rescaled or even scaled out. For example, for some scaling parameter  $\beta$ ,  $\psi_i$  and  $c$  are related by the similarity transformation:  $\psi_i \rightarrow \beta\psi_i$  and  $c \rightarrow c/\beta^2$  [27]. The normalisation condition is then given by  $\sum_i \psi_i^2 = 1/\beta^2$ .

### 3.3 Iterated Maps

For a very small number of lattice sites we could attempt to solve the set of equations produced for each system. To classify the type of solution obtained we could analyse the structure of the wave vector of this solution. However, for more than two sites the problem is nonintegrable [28] and it is extremely difficult to solve the set of equations which govern larger systems. Traditionally, the alternative method employed to understand the behaviour of a system with a larger number of sites is to follow the methods used in the studies of nonlinear dynamical systems: we can iterate the DNSE (33), after first representing it in the form of a  $2D$  map.

Conversion between Hamiltonian forms and mappings has long been known to be a powerful mathematical tool for the theoretical and numerical analysis of dynamical systems. Indeed, two-dimensional maps allow representation of a stationary configuration of a Hamiltonian of the form (27) by a trajectory of a dynamical system. Therefore, the mathematical situation is *identical* to that of temporal evolution, although the static problem has been formulated in terms of spatial arrangements. That is, we can apply adapted methods from the analysis of chaotic dynamical systems and explore the nature of possible solutions to the DNSE (33) by finding suitable orbits.

The discretised nonlinear Schrödinger equation (DNSE) may be cast to form a first order  $2D$  iterative map in discrete space by introducing the auxiliary variable  $Z_{i+1} = \psi_{i+1} - \psi_i$  (see, for comparison, [9, 8, 7, 6]). This gives

$$Z_{i+1} = Z_i - E\psi_i - C\psi_i^3 \quad \text{and} \quad \psi_{i+1} = \psi_i + Z_{i+1} \quad (34)$$

The total spectrum of solutions depending on the initial conditions  $\psi_0$  and  $Z_0$  cannot be obtained in closed form. In the early eighties [9, 8] it was common to generate possible solutions of (34) by fixing the displacements of two neighbouring particles and then iterating the map, however, the physical stability of the system under small perturbations was often not considered. The map technique provides a variety of stationary solutions of equation (33). However, the accessibility to *all* possible solutions is obviously highly limited by the parameter range where the map is math-

ematically stable. If the iteration procedure is divergent for a particular set of initial conditions then this means that for those values a solution does not exist.

Numerical experiments investigating different trajectories of the  $2D$  map have been performed for different values of the parameters. We find that there are essentially only three types of phase portraits produced by iterating (34). There can be *regular* (periodic) orbits where only a small number of points in the phase space are visited. There are also *irregular commensurate* (quasiperiodic) orbits in the form of closed loops. These loops consist of a number of points being visited. As the commensurability decreases the points visited in the phase space become more and more dense and an elliptic orbit is mapped. Finally, we have *irregular incommensurate* (chaotic) orbits where the previous closed loops seem to be (stochastically) dispersed and a large number of points in the phase space are visited.

These simulations, which are in agreement with previous work on the subject ([9, 8, 7, 6]), indicate that in this system there are three qualitatively different types of orbits which depend on the values of the parameters: 1) periodic, 2) quasiperiodic and 3) chaotic. It is well known that the regular/commensurate solutions may be transformed into the quasiperiodic or chaotic type structures by a slight change of initial conditions or parameters.

Below we discuss an alternative method for solving (33) and present the spectrum of (33) in the large  $c$  limit. We then go on to apply a numerical method to our system of DNSEs and obtain results which we cannot reproduce with the above mapping procedure. These results are contrasted with those obtained using the iterated map technique and in this way the spatial structure of the wave function is examined.

### 3.4 Exact Solutions Of The DNSE

Up until now the DNSE has been analysed using the method of iterated maps or by making the continuum approximation and solving the resultant second order differential equation. The continuum limit of equation (29)

$$-\frac{\partial^2 \psi}{\partial x^2} - c|\psi|^2 \psi(x) = E\psi(x) \quad (35)$$

may be solved by substituting the trial solution  $\psi(x) = A \exp(ikx)$  (where  $A$  is a constant of normalisation and  $k$  is some wave number). Doing so gives

$$E = k^2 - c \quad (36)$$

The constant  $A$  is obtained from the normalisation condition  $\int |\psi|^2 dx = 1$  and  $k$  is obtained from the boundary conditions imposed on the system.

As well as these plane wave solutions, the continuum approximation of (33) also has a localised solution [3, 4]. Consider the second order nonlinear differential equation

$$-\frac{\partial^2 \psi}{\partial x^2} - c\psi^3 = E\psi \quad (37)$$

multiplying through by  $\frac{\partial \psi}{\partial x}$  gives

$$\frac{\partial^2 \psi}{\partial x^2} \frac{\partial \psi}{\partial x} + c\psi^3 \frac{\partial \psi}{\partial x} + E\psi \frac{\partial \psi}{\partial x} = 0 \quad (38)$$

which may be rewritten as

$$\frac{\partial}{\partial x} \left[ \frac{1}{2} \left( \frac{\partial \psi}{\partial x} \right)^2 + \frac{c}{4} \psi^4 + \frac{E}{2} \psi^2 \right] = 0 \quad (39)$$

and can be integrated to give

$$\left( \frac{\partial \psi}{\partial x} \right)^2 + \frac{c}{2} \psi^4 + E\psi^2 = h \quad (40)$$

where  $h$  is some constant of integration. The solutions to (40) are the elliptic integrals the simplest of which is the hyperbolic cosine solution. For a well behaved solution we require that  $\psi(\pm\infty) \rightarrow 0$  and  $\psi'(\pm\infty) \rightarrow 0$ . Hence  $h = 0$ , giving

$$\frac{\partial \psi}{\partial x} = \sqrt{-E\psi^2 - \frac{c}{2}\psi^4} \quad (41)$$

With the substitution  $\sigma^2 = \frac{-c}{2E}$  this may be alternatively expressed as

$$\int \frac{d\psi}{\psi \sqrt{1 - \sigma^2 \psi^2}} = \sqrt{-E} \int dx \quad (42)$$

Substituting  $y = \sigma\psi$  (and  $d\psi = dy/\sigma$ ) gives

$$\int \frac{dy}{y \sqrt{1 - y^2}} = \sqrt{-E} \int dx \quad (43)$$

which may be integrated to give

$$\ln \left( \frac{y}{1 + \sqrt{1 - y^2}} \right) = \sqrt{-E}(x - x_0) \quad (44)$$

where  $x_0$  is some constant of integration. This equation may be exponentiated to give

$$y = \exp \left( \sqrt{-E}(x - x_0) \right) + \sqrt{1 - y^2} \exp \left( \sqrt{-E}(x - x_0) \right) \quad (45)$$

which may be rearranged to give

$$y^2 \left( 1 + \exp \left( \sqrt{-E}(x - x_0) \right) \right)^2 - 2y \exp \left( \sqrt{-E}(x - x_0) \right) = 0 \quad (46)$$

This equation is satisfied for either  $y = 0$  (trivial solution) or

$$y = \frac{2}{\exp \left( \sqrt{-E}(x - x_0) \right) + \exp \left( -\sqrt{-E}(x - x_0) \right)} \quad (47)$$

Substituting  $\sigma\psi = y$  gives

$$\psi = \sqrt{\frac{-2E}{c}} \frac{1}{\cosh \left( \sqrt{-E}(x - x_0) \right)} \quad (48)$$

This is the solution of the localised state of a continuum system described by (35). The corresponding eigenvalue may be obtained from the normalisation condition

$$\int_{-\infty}^{\infty} \left[ \sqrt{\frac{-2E}{c}} \frac{1}{\cosh(\sqrt{-E}(x - x_0))} \right]^2 dx = 1 \quad (49)$$

which gives  $E = -c^2/16$ . This solution was originally used to describe the self-trapping of an electron by phonons [3, 4]. It corresponds to an electron localised on an atomic lattice.

The localised and plane wave solutions described above are all solutions to the nonlinear equation (35) where it is acceptable to use infinitesimal differences (derivatives) to model a nonlinear system. However, our recent work [29, 30] shows that the continuum approximation is insufficient in describing discrete systems where the intrinsic discreteness is an important characteristic of that system.

Equation (33) may also be solved exactly whilst maintaining the discrete nature of the equation [29, 30]. To illustrate, consider some examples having exact solutions. The simplest is a double well structure ie a 2-site lattice problem. The eigenvalues of this lattice are  $E = -c/2$ ,  $E = 4 - c/2$  and  $E = 2 - c$  with corresponding eigenvectors  $\psi_1 = \psi_2 = \pm 1/\sqrt{2}$ ,  $\psi_1 = -\psi_2 = \pm 1/\sqrt{2}$  and  $\psi_1 = \pm \frac{\sqrt{1+\alpha}}{\sqrt{2}}$ ,  $\psi_2 = \pm \frac{\sqrt{1-\alpha}}{\sqrt{2}}$  where  $\alpha = \sqrt{1 - \frac{A}{c^2}}$ , with  $A = 16$  for periodic boundary conditions (PBC) or  $A = 4$  for open boundary conditions (OBC). This last solution bifurcates from the homogeneous solution at  $c = 4$  and corresponds to the lowest energy state of the system for  $c > 4$ . In this state the symmetry between the first site and the second site is broken and the value of  $\psi$  is larger at one site than the other: the wave function becomes localised on one site. Note that  $\alpha = 1$  only when  $c = \infty$ , that is the wave function can be completely localised only when  $c = \infty$ . This localisation is due to the effect of the (cubic) nonlinearity in the system. If this nonlinearity were not present ( $c = 0$ ) then the only solutions that would exist are the first two solutions (which are also the solutions of the linear equation) – the so-called band solutions – where the amplitude of the wave function is the same on all the sites.

Note that there is a degeneracy within the system. The above 3 eigenvalues actually correspond to 8 possible realisations of the configuration of the wave function on the 2-site lattice. There are in fact a total of 9 (degenerate) solutions which satisfy the 2 equations describing the 2-site system but one of these is the trivial

solution which does not satisfy the normalisation condition. These 9 solutions arise because we are considering a cubic equation for a 2-site lattice. A cubic equation has 3 solutions and 2 such equations gives rise to a total of  $3^2$  degenerate realisations of the wave function on the lattice.

When a three site PBC lattice structure (or superlattice layers or quantum wells) was considered it was found that the ground state is again characterised by the localisation of the wave function on a single site in the same manner as in the double well structure. With an increase in the value of  $c$  this state rapidly saturates to the limit  $\{\psi_1, \psi_2, \psi_3\} = \{0, 1, 0\}$  or  $\{0, 0, 1\}$  or  $\{1, 0, 0\}$ . These three states are degenerate due to the translational symmetry associated with PBC and correspond to the ground state which in the limit  $c \rightarrow \infty$  takes the simple form  $E = 2 - c$ , ie the same eigenvalue as for the double well structure.

Another, excited state of the system, which for  $c \gg 1$  has the (degenerate) structure  $\{\psi_1, \psi_2, \psi_3\} = \{1/\sqrt{2}, 0, 1/\sqrt{2}\}$  or  $\{1/\sqrt{2}, 1/\sqrt{2}, 0\}$  or  $\{0, 1/\sqrt{2}, 1/\sqrt{2}\}$  and corresponds to the localisation of the wave function on two neighbouring lattice sites; the eigenvalue of this state is  $E = 1 - \frac{c}{2}$ .

In total 5 exact solutions – valid for all values of  $c$  – have been found for the system of 3 lattice sites with PBC. Three of these solutions are localised and two are band solutions. However, unlike the 2-site problem, the dependence of these 5 solutions on the parameter  $c$  is not representable in a simple analytic form and so instead the spectrum of eigenvalues of these exact solutions is presented graphically in Figure 3.1.

The dependence of the eigenvalues on  $c$  appears to be virtually linear for most values of  $c$  and so each eigenvalue may be readily described by an empirical formula for large  $c$ . Note that there is a degeneracy within the system caused by the rotational invariance of this system. The 5 solutions graphically depicted actually correspond to  $3^3 - 1$  possible realisations of the configuration of the wave function on the lattice – the trivial solution is ignored.

When the same system is considered with OBC the rotational invariance – due to PBC – is broken and the rotational degeneracy is lifted from the system; the

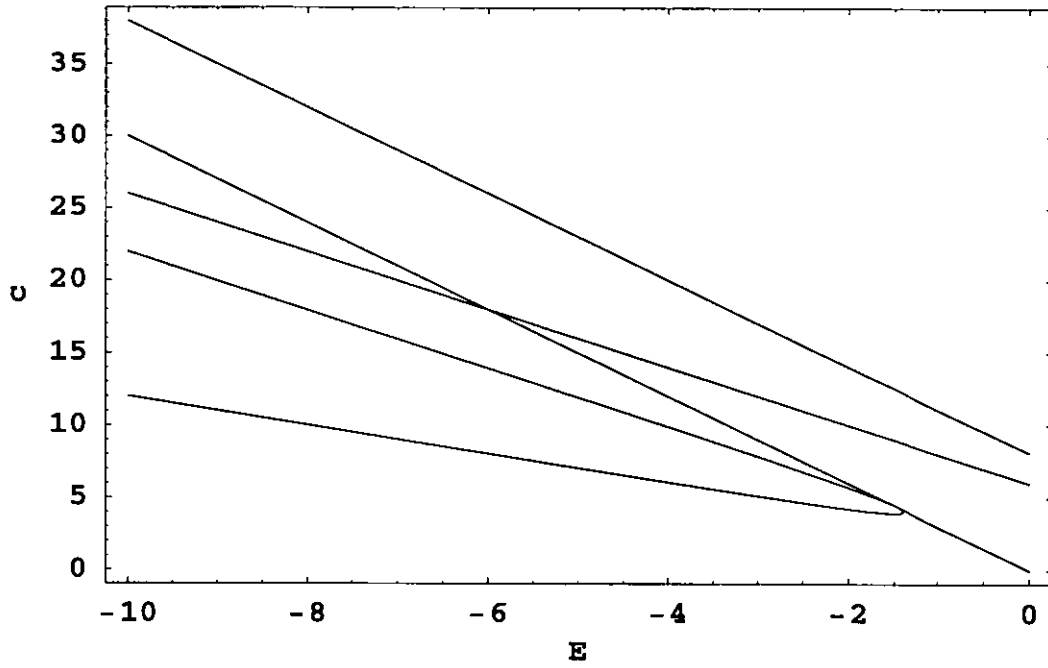
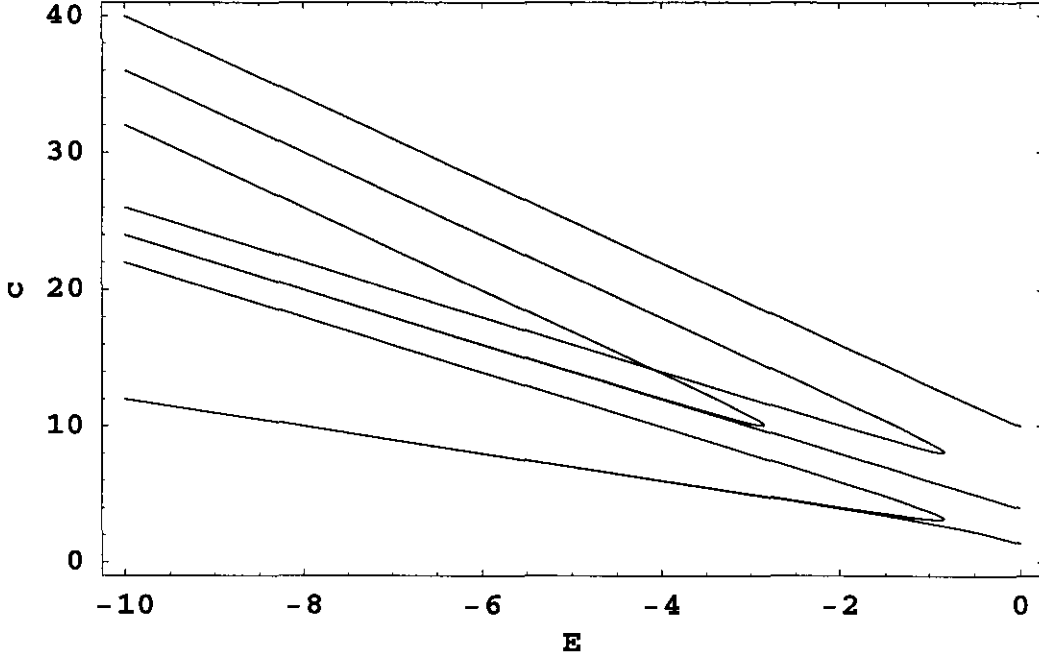


Figure 3.1 The dependence of energy spectrum on the parameter  $c$  for a triple quantum well structure obtained for PBC. The lines of the spectrum correspond to (from bottom up on left hand side) the eigenvalues  $E = 2 - c$ ,  $E = (2 - c)/2$ ,  $E = (6 - c)/2$ ,  $E = -c/3$  and  $E = (8 - c)/3$ .





**Figure 3.2** *The dependence of energy spectrum on the parameter  $c$  for a triple quantum well structure obtained for OBC. The lines of the spectrum correspond to (from bottom up on LHS) the eigenvalues  $E = 2 - c$ ,  $E = (2 - c)/2$ ,  $E = (4 - c)/2$ ,  $E = (6 - c)/2$ ,  $E = (2 - c)/3$ ,  $E = (6 - c)/3$  and  $E = (10 - c)/3$ .*

number of energy eigenvalues increases due to a *splitting* of some of the energy levels associated with the PBC lattice. The spectrum for the triple quantum well structure with OBC is presented in Figure 3.2.

The new eigenvalues may also be described empirically for  $c \gg 1$ . For example, the eigenvalue  $E = (4 - c)/2$  appears and is associated with the localised solutions  $\{\frac{\pm 1}{\sqrt{2}}, 0, \frac{\pm 1}{\sqrt{2}}\}$ . The eigenvalue  $E = \frac{2-c}{3}$  corresponds to the homogeneous solution for OBC. The eigenvalues  $\frac{6-c}{3}$  and  $\frac{10-c}{3}$  are both equivalent to the PBC eigenvalue  $(8 - c)/3$  but the change in boundary conditions has caused this energy level to split.

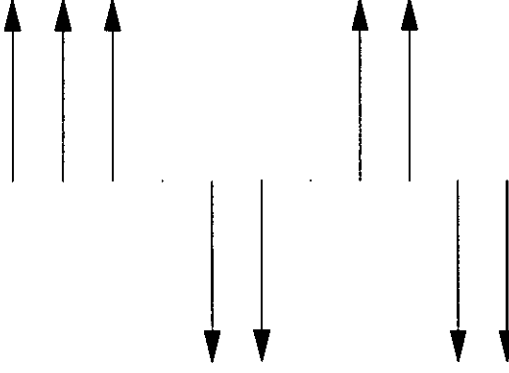
An amazing agreement between the complicated expressions of the exact spectra (presented graphically for simplicity) and the empirical formulae for  $c \gg 1$  is seen. In particular a linear dependence of  $E$  on  $c$  is observed. From the examples discussed above, it is noticed that in the limit  $c \rightarrow \infty$ , the spectrum has some special features

associated with the pattern of the localised states. The spectrum depends on how large the set of localising sites is and how many spots (regions of neighbouring, localising sites) this set is separated into. The lowest eigenvalue always has the form  $E = 2 - c$  and is associated with the localisation of the wave function on a single site. The next eigenvalue,  $E = \frac{(2-c)}{2}$ , is associated with the localisation of the wave function in a single spot consisting of two neighbouring sites. However, when the localisation occurs in two separate sites, so that there are two spots each consisting of one site, the energy eigenvalue is  $E = \frac{(4-c)}{2}$ . With the localisation of the wave function on three neighbouring sites the associated eigenvalue may be written as  $E = \frac{2-c}{3}$ .

These observations can be used to derive exact solutions associated with an arbitrary localisation pattern of the wave function on a lattice consisting of  $n$  sites. Initially, with  $c \gg 1$ , assume that the wave function is localised on a single site of an  $n$  site lattice, say the  $k^{th}$  site, so that  $|\psi_k|^2 = 1$  and  $|\psi_j|^2 = 0$  for all possible  $j \neq k$ . Upon making this substitution into the DNSE and after some algebraic manipulation, we see that this substitution corresponds to a solution with the eigenvalue  $E = 2 - c$ . Similarly, if it is assumed that the wave function is localised on two neighbouring sites, say, the  $k^{th}$  and  $(k+1)^{th}$ , and we substitute into the DNSE  $\psi_k = \frac{1}{\sqrt{2}}$ ,  $\psi_{k+1} = \frac{1}{\sqrt{2}}$  and  $\psi_j = 0$  for  $j \neq k, k+1$  then (after some algebra) the eigenvalue  $E = \frac{2-c}{2}$  is obtained. For the localisation of the wave function on 3 neighbouring sites, we make the substitution  $\psi_k = \psi_{k+1} = \psi_{k+2} = \frac{1}{\sqrt{3}}$  and  $\psi_n = 0$  for all other sites. This then yields  $E = \frac{2-c}{3}$ . Repeating the same procedure for the wave function localised on  $N$  neighbouring sites, we derive the eigenvalue  $E = \frac{2-c}{N}$ .

The same procedure may be applied for a wave function localised in two distinct spots, consisting of, say,  $N_1$  and  $N_2$  sites. Surprisingly, we find that in this case,  $E = \frac{(4-c)}{N}$ , where  $N = N_1 + N_2$ . If this localisation occurs in  $m$  distinct regions, and each of these regions consists of  $N_m$  neighbouring sites, the associated eigenvalue is  $E = \frac{(2m-c)}{N}$ , where  $N = \sum_m N_m$ .

However, this is still not a complete set of solutions. If the wave function is localised in a single spot consisting of  $N = 2N_0$  neighbouring sites, then the wave



function may change sign for the different sites of this region. For example, if for the first  $N_0$  neighbouring sites the wave function has a positive sign and for the remaining  $N_0$  sites the wave function is negative, then the associated eigenvalue is  $E = \frac{2+4-c}{N}$ . Similarly, if there are two changes in the sign of the wave function which is localised in a single spot then the eigenvalue associated with this structure is  $E = \frac{2+8-c}{N}$ . In general, if the wave function changes sign  $l$  times in one or several spots of the  $n$  site lattice described by the DNSE then, in the limit  $c \rightarrow \infty$ , the energy eigenvalue of this structure takes the form

$$E_{N,m,l} = \frac{2m + 4l - c}{N} \quad (50)$$

where  $E$  intrinsically depends on both the structure of the wave function on the lattice – described by  $m, l, N$  – and on the parameter  $c$ . The structure of the wave function is such that it is localised,  $\psi_i \neq 0$ , on just  $N$  sites of the  $n$  site lattice ( $N \leq n$ ); on the remaining  $n - N$  sites the wave function is zero,  $\psi_i = 0$ . Note that on each site where the (normalised) wave function is localised it takes a value of either  $\psi_i = \pm 1/\sqrt{N}$  for all  $N$  sites – no other values are taken. These  $N$  localising sites are separated into  $m$  spots – regions of neighbouring lattice sites on which the wave function is localised – and  $l$  kinks – change in the sign of the wave function on adjacent lattice sites – inside these spots. Between the spots the wave function is vanishing. Both  $m$  and  $l$  are less than or equal to  $N$ .

For example, in the above diagram if the up arrows represent a positive value and the down arrows represent a negative value of wave function then the wave function

is localised on  $N = 9$  sites. These 9 sites are separated into  $m = 3$  spots – the first spot consisting of 3 up arrows, the second spot consisting of 2 down arrows and the third spot consisting of 2 up and 2 down arrows. This last spot contains  $l = 1$  kink where the wave function changes sign. Hence, the eigenvalue of this structure is  $E = \frac{10-c}{N}$ .

Since the spectrum (50) is associated with a local localisation pattern, it is universal and does not depend on the type of boundary conditions imposed on the lattice. It describes both systems with periodic boundary conditions and systems with open boundary conditions.

In contrast with previous work on this subject, where the continuum approximation is made and only one localised solution is obtained, we find that there are in fact a whole host of solutions which correspond to localised structures of the discrete system. The eigenvalues corresponding to these discrete solutions all have a linear dependence on  $c$  as shown by (50). The eigenvalues of the plane wave solutions of the continuum model also have a linear dependence on  $c$ . However, the eigenvalue corresponding to the hyperbolic cosine solution has a quadratic dependence on  $c$  which indicates that this continuum localised solution is somehow characteristically different from the discrete localised solutions.

This suggests that **the continuum approximation is insufficient in describing discrete systems**. In a discrete nonlinear system there exists a whole host of states which simply do not arise in the continuum limit.

Equation (50), obtained in the limit  $c \rightarrow \infty$ , has been compared with the numerical solutions for various systems consisting of different numbers of sites. In all these cases and for nearly all values of  $c$  (except small regions of critical values where the self-trapped solutions originate) there is perfect agreement with the spectrum (50). However, in contrast with this perfect agreement between eigenvalues, a decrease in the value of  $c$  leads to a noticeable deviation in the wave functions from those obtained in the limit  $c \rightarrow \infty$ . As  $c$  decreases the localisation spots smear out and the boundaries between localising sites and sites where the wave function vanishes become less distinct. The structure of the wave function for smaller values of  $c$  only

has qualitative features of the corresponding wave function obtained in the limit  $c \rightarrow \infty$ .

Although the structure of the wave function for  $c > 1$  does not strongly agree with the structure of the wave function in the limit  $c \rightarrow \infty$ , we find that the wave function may be approximated reasonably well by an exponential function. This is only valid if the peaks in the wave function structure are separated sufficiently so that there is little or no interaction between the tails.

For lattice sites sufficiently far away from the localised site we can assume that in equation (33) the value of the wave function is small so that the cubic nonlinear term is negligible,  $\psi_i^3 \approx 0$ . Then, to get an indication of the type of behaviour of the wave function sufficiently far away from a localising site, we may take the continuum limit and obtain a second order linear differential equation which may be expressed as

$$-\frac{\partial^2 \psi}{\partial x^2} = E\psi(x) \quad (51)$$

Equation (51) has the asymptotic solution

$$\psi = A \exp(-\sqrt{-E}x) \quad (52)$$

where  $A$  is some parameter. Hence, far away from a localising site the wave function decays exponentially. Therefore the neglected nonlinear term  $\sim A^3 \exp(-3\sqrt{-E}x)$  is very small, that is, this asymptotic approximation is a self-consistent one.

### 3.5 First Order Perturbation Corrections

If a small perturbation in the asymptotic limit ( $c \rightarrow \infty$ ) wave function  $\Psi = (\psi_1, \psi_2, \dots, \psi_i, \dots, \psi_N)$  and energy eigenvalue  $E$  is considered then a correction to the wave function is revealed.

Let

$$\psi_i = p_i + x_i \quad (53)$$

and

$$E = E_0 + E_1 \quad (54)$$

where  $p_i$  is the zero order approximation wave function,  $x_i$  is a small perturbation in the wave function,  $E_0$  is the zero approximation energy eigenvalue and  $E_1$  is a small perturbation in the energy eigenvalue. Substituting this into (33) and ignoring the terms which involve cross-products of the perturbation terms gives

$$-p_{i-1} - x_{i-1} + 2p_i + 2x_i - p_{i+1} - x_{i+1} - cp_i^3 - 3cp_i^2x_i \approx E_0p_i + E_0x_i + E_1p_i + E_1x_i \quad (55)$$

In matrix form the system of  $n$  equations becomes

$$\mathbf{TX} = \mathbf{F} \quad (56)$$

where  $\mathbf{F}$  and  $\mathbf{X}$  are vectors with  $n$  components ( $n$  is the number of lattice sites). The components of  $\mathbf{F}$  are  $F_i = E_0p_i + cp_i^3 + p_{i-1} - 2p_i + p_{i+1}$ , the components of  $\mathbf{X}$  are  $X_i = x_i$  ie  $\mathbf{X}$  is the wave vector of first order corrections to the zero approximation wave function. Finally, (for 3 or more sites)  $\mathbf{T}$  is a tridiagonal  $n \times n$  matrix with diagonal elements  $T_{i,i} = 2 - E_0 - 3cp_i^2$ , elements on either side of the diagonal  $T_{i,i-1}, T_{i,i+1} = -1$  and top-right and bottom-left elements  $T_{1,N}, T_{N,1} = -1$  for periodic boundary conditions (PBC). The terms involving  $E_1$  have been ignored for the meanwhile because we know from above that  $E_0$ , as given by (50), is in excellent agreement with the actual value of  $E$  for nearly all values of  $c$ .

Premultiplying equation (56) by  $\mathbf{T}^{-1}$  gives the first order corrections to the wave vector:

$$\mathbf{X} = \mathbf{T}^{-1}\mathbf{F} \quad (57)$$

Now that we have the first order perturbation corrections to the wave function we can substitute these in equation (55) to calculate the first order correction to the energy eigenvalue,  $E$ . Assuming PBC and summing equation (55) over all  $i$  (neglecting the nonlinear terms in  $x_i$  as  $x_i^2 \ll x_i$ ), we obtain the first order correction to the energy eigenvalue

$$E_1 = \frac{-c \sum_i p_i^3 - 3c \sum_i p_i^2 x_i - E_0 \sum_i p_i - E_0 \sum_i x_i}{\sum_i p_i + \sum_i x_i} \quad (58)$$

To see how the perturbation corrections compare to actual solutions we compare these corrections with exact solutions of equation (33). For a 2-site system with PBC we know that the exact solutions correspond to the eigenvalues  $E = -c/2$ ,  $E = (8 - c)/2$  and  $E = 2 - c$ . The corresponding eigenvectors are

$$\text{for } E = -c/2 \quad \begin{bmatrix} \frac{1}{\sqrt{2}} \\ \frac{1}{\sqrt{2}} \end{bmatrix}$$

$$\text{for } E = (8 - c)/2 \quad \begin{bmatrix} \frac{1}{\sqrt{2}} \\ -\frac{1}{\sqrt{2}} \end{bmatrix}$$

$$\text{for } E = 2 - c \quad \begin{bmatrix} \frac{\sqrt{1 \pm \alpha}}{\sqrt{2}} \\ \frac{\sqrt{1 \mp \alpha}}{\sqrt{2}} \end{bmatrix}$$

where  $\alpha = \sqrt{1 - \frac{16}{c^2}}$  and lies in the range  $0 \leq \alpha \leq 1$ . This solution only exists for  $c > 4$ . The above three eigenvalues (obtained analytically) are precisely the same as those given by equation (50) if the appropriate wave function structures are substituted. Note that for  $E = -c/2$  and  $E = (8 - c)/2$  we have no spots ie  $m = 0$ ; there are no sites where the wave function is zero. If OBC were considered (instead of PBC) then, due to the nature of the boundary conditions,  $m = 1$ .

For the solutions which correspond to the eigenvalues  $E = -c/2$  and  $E = (8 - c)/2$  we know that there are no corrections to the wave function and energy eigenvalue. Thus, we expect that  $x_i = 0$  and  $E_1 = 0$  for both of these solutions. Substituting for  $E_0$  and  $p_i$  in equations (55), (58) we find that this is indeed the case.

Doing the same for the symmetry breaking solution gives no first order correction to the localised component of the wave function (but does give a correction of  $-2/c^2$  for  $c \gg 1$ ) and a first order correction of  $2/c$  to the vanishing component. To compare these results with the exact solutions we must expand the surd (in inverse powers of  $c$ ) for both the localised and vanishing components of the wave function.

Doing so gives

$$\frac{\sqrt{1 + \sqrt{1 - \frac{16}{c^2}}}}{\sqrt{2}} \approx 1 - \frac{2}{c^2} - \frac{10}{c^4} - \frac{84}{c^6} - \dots \quad (59)$$

$$\frac{\sqrt{1 - \sqrt{1 - \frac{16}{c^2}}}}{\sqrt{2}} \approx 0 + \frac{2}{c} + \frac{4}{c^3} + \frac{28}{c^5} + \frac{264}{c^7} + \dots \quad (60)$$

which agree completely with the results from our perturbation analysis. Note that in the limit  $c \rightarrow \infty$  the corrections are all zero and the zero approximation solutions are obtained. Although there is excellent agreement in the wave functions, the same is not true regarding the energy eigenvalue. We know that the eigenvalue  $E = 2 - c$  is exact and consequently there should be no corrections to  $E_0$ . However, we obtain the correction  $E_1 \approx -4/c$ . This is because we did not take into consideration all orders of correction. We have only used first order corrections and neglected higher order corrections. Clearly, higher order corrections do exist and these too must be considered for complete agreement. Thus, the correction in the energy eigenvalue,  $E_1$ , is zero to an order of  $(c)^0 \sim 1$ .

The first order corrections to the wave function obtained with the use of perturbation theory are of the order of  $1/c$ . Once we have obtained the first order corrections to the wave function and eigenvalues we can then investigate higher order corrections. From the 2-site PBC example discussed above we expect that the



next correction to the wave function will, in general, be of order  $\sim 1/c^2$ .

### 3.6 Exact Numerical Solutions For Finite $c$

We can modify the above procedure by finding the first order correction to the zero order approximation wave function obtained in the limit  $c \rightarrow \infty$  as detailed above. We then find the next order correction to this new wave function. That is we repeat the above procedure and determine the next order correction to the ‘corrected’ wave function. This iterative procedure (which is reminiscent of the Newton-Raphson procedure) is repeated until the successive corrections to the wave function become negligible. This means that the value of the wave function converges to some limit. This limit is an exact, numerical solution of the DNSE (33).

This exact solution is obtained by following an analogous procedure to that used to obtain (57). If  $\psi_i(k)$  is our wave function iterated  $k$  times then we again have

$$\mathbf{T}\mathbf{X} = \mathbf{F} \quad (61)$$

where  $\mathbf{F}$  and  $\mathbf{X}$  are again vectors with  $n$  components associated with the number of lattice sites. The components of  $\mathbf{F}$  are now  $F_i = E_0\psi_i(k) + c\psi_i^3(k) + \psi_{i-1}(k) - 2\psi_i(k) + \psi_{i+1}(k)$  and the components of  $\mathbf{X}$  are  $X_i = x_i$  the  $(k+1)$ th iterative corrections to the wave function iterated to  $k^{th}$  order. Finally,  $\mathbf{T}$  is again a tridiagonal  $n \times n$  matrix with diagonal elements  $T_{i,i} = 2 - E_0 - 3c\psi_i^2(k)$ .

Premultiplying equation (61) by  $\mathbf{T}^{-1}$  gives the  $(k+1)$ th iteration corrections to the wave vector:

$$\mathbf{X} = \mathbf{T}^{-1}\mathbf{F} \quad (62)$$

This iterative procedure may be represented in an alternative (but equivalent) form. The linear approximation to the wave function on the lattice may be written as

$$\Psi(k+1) = \Psi(k) + \delta\Psi(k) \quad (63)$$

where  $\Psi(\mathbf{k})$  is our wave function (vector) consisting of  $n$  components ( $n$  lattice sites) iterated  $k$  times; if  $k = 0$  then it is simply the wave function in the asymptotic limit.

Similarly,

$$E(k+1) = E(k) + \delta E(k) \quad (64)$$

so that the counterpart of (55), after  $k$  iterations, may be written in the form

$$\hat{\nabla}H(\Psi(k+1)) - \hat{\nabla}H(\Psi(k)) \approx \hat{\nabla}^2H(\Psi(k))(\Psi(k+1) - \Psi(k)) \quad (65)$$

where  $\hat{\nabla}^2H(\Psi(k))$  is (for 3 or more sites) a tridiagonal  $n \times n$  matrix with diagonal elements  $2 - E - 3c\psi_i^2(k)$ , elements on either side of the diagonal  $= -1$  and top-right and bottom-left elements  $= -1$  for PBC.

Then (61) can be expressed in the form

$$\hat{\nabla}^2H(\Psi(k))\delta\Psi(k) = \hat{\nabla}H(\Psi(k)) \quad (66)$$

with  $\mathbf{F} = \hat{\nabla}H(\Psi(k))$ ,  $\mathbf{T} = \hat{\nabla}^2H(\Psi(k))$  and  $\mathbf{X} = \delta\Psi(k)$  so that

$$\Psi(k+1) = \Psi(k) - [\hat{\nabla}^2H(\Psi(k))]^{-1} \hat{\nabla}H(\Psi(k)) \quad (67)$$

This procedure is used until the correction to the wave function becomes negligible. Note that, as the corrections are of the form of a series with negative integral powers of  $c$ , in the limit  $c \rightarrow \infty$  the corrections are all zero and the asymptotic solutions are obtained. The Mathematica programme for this procedure is presented in Appendix 2 [21].

Analogous to (58), the energy eigenvalue (for PBC) after each iteration step is given by

$$E(k) = \frac{-c \sum_i \psi_i^3(k)}{\sum_i \psi_i(k)} \quad (68)$$

and the value of  $E(k)$  converges towards  $E$  for most values of  $c \gg 1$  except for small neighbourhoods of  $c$  where the localised states originate. Even in these sensitive regions the value of  $E(k)$  is in fairly close agreement with  $E$ .

This process is, however, not always convergent. The wave vector may change structure when different eigenvalues have the same value or when the structure

obtained from the asymptotic limit does not exist for a range of  $c$ . For example, for a 3 site system with PBC two of the eigenvalues are  $-c/3$  and  $(6-c)/2$ . Both of these eigenvalues have the same numerical value for  $c = 18$  but the corresponding wave functions have very different structures. It is possible for the initial wave vector structure corresponding to one energy eigenvalue to change during the iteration process to another structure which corresponds to a different energy eigenvalue. However, this new structure does also exist and is also a solution of the DNSE (33).

If during the iterative process there is a drastic change in  $E$  then this indicates that the wave function structure has changed and the iteration process will converge to some other limit.

Applying this method to (33) for finite  $c$  taking the asymptotic solutions (which are exact in the limit  $c \rightarrow \infty$ ) as the initial condition we may compare the results obtained by successively applying the perturbation procedure with the results obtained by the use of  $2D$  iterated maps. For such a comparison, however, we have to introduce the new *phase space function*  $\psi_{i+1} - \psi_i$  for the perturbation procedure applied to the discrete system of equations and plot  $\psi_{i+1} - \psi_i$  against  $\psi_i$ . This then allows us to compare the wave function structures obtained with the use of the perturbation procedure and the  $2D$  iterated maps discussed in Section 3. We find that as well as obtaining results from the two different methods which are consistent with each other we also obtain results from the perturbation procedure which we could not obtain with the  $2D$  maps.

As well as periodic, quasiperiodic and chaotic structures of the wave function on a lattice, we also find evidence for the existence of fractal-like structures. That is discrete nonlinear systems described by (33) may exhibit behaviour on one scale which is similarly echoed on another scale.

### 3.7 Results

In the previous section we have reformulated our problem of the solution of a discrete nonlinear set of equations, (33), to a (discrete generalised Newton-Raphson) iterative problem. This gives possible criteria for the classification of the solutions obtained. Following this iteration procedure we find that there exist different types of structures of the wave function; nonlinear localised solutions arise for  $E < 0$ . Our results indicate that there exist both regular and irregular types of structure of the wave vector for negative values of  $E$ . These structures may be akin to periodic, quasiperiodic and (deterministic) chaotic structures.

Of course for finite systems, quasiperiodic and chaotic structures are not well defined because these are, strictly speaking, well defined only for systems of infinite size. However, we may still indicate analogous features, for example, with the aid of phase portraits adopted for finite size systems which are possibly equivalent to regular commensurate, irregular commensurate and irregular incommensurate structures of the wave function on the lattice.

#### 3.7.1 Periodic Structures

Consider the initial structure where the normalised wave function is located on only 4 equidistant sites, ie there are only 4 sites where the wave function is not zero. These 4 sites are equally spaced on a lattice consisting of a total of 32 sites with PBC. Each of the localised sites is separated by 7 sites where the wave function is zero. From (50) the energy eigenvalue of this structure is given by  $E = (8 - c)/4$ .

Taking the coupling constant to be  $c = 12$  and successively applying the Perturbation Procedure to this initial structure of the normalised wave function, until the corrections to the wave function become negligible, we obtain the solution presented in Figure 3.3a. This shows a periodic behaviour of the wave function on the lattice. The corresponding phase portrait of the quantum state, Figure 3.3b, indicates that this initial structure gives rise to a regular, commensurate period-8 structure. The phase portrait consists of only 8 points as the wave function oscillates regularly. The wave function will occupy each 8th site with a greater probability  $\sim |\psi_i|^2$  than

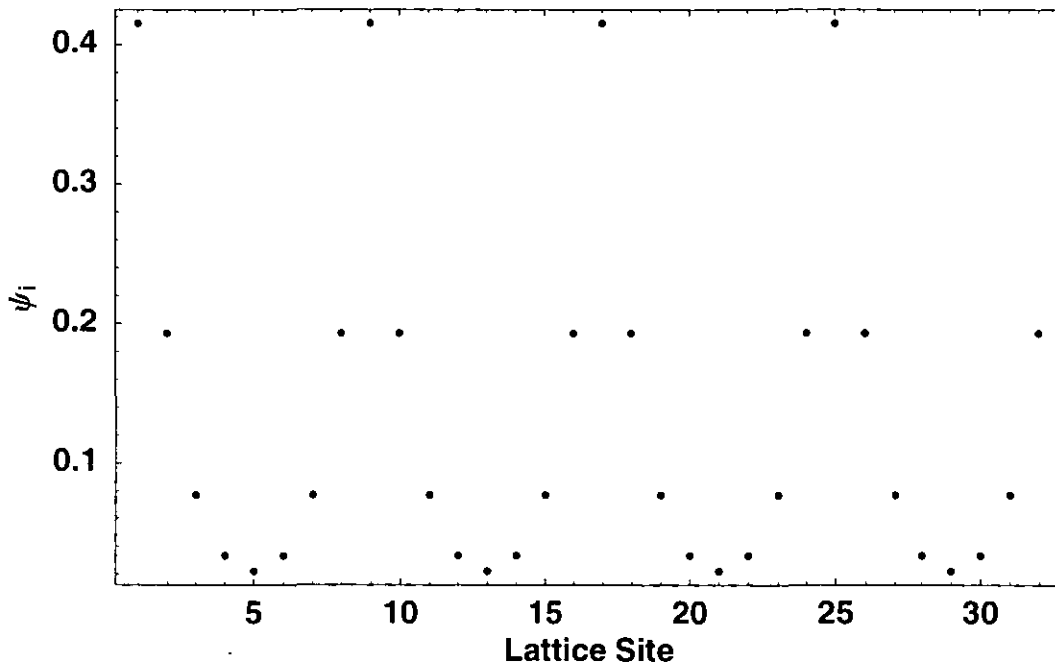


**Figure 3.3a** *The converged behaviour of a periodic wave function on a 32 site lattice obtained by the Perturbation Procedure for PBC. The initial conditions were  $c = 12$  and  $E = -0.5$  with the initial, normalised wave function value of  $\psi = 1/2$  at only 4 equidistant sites. Between these localised sites the value of the wave function was zero.*

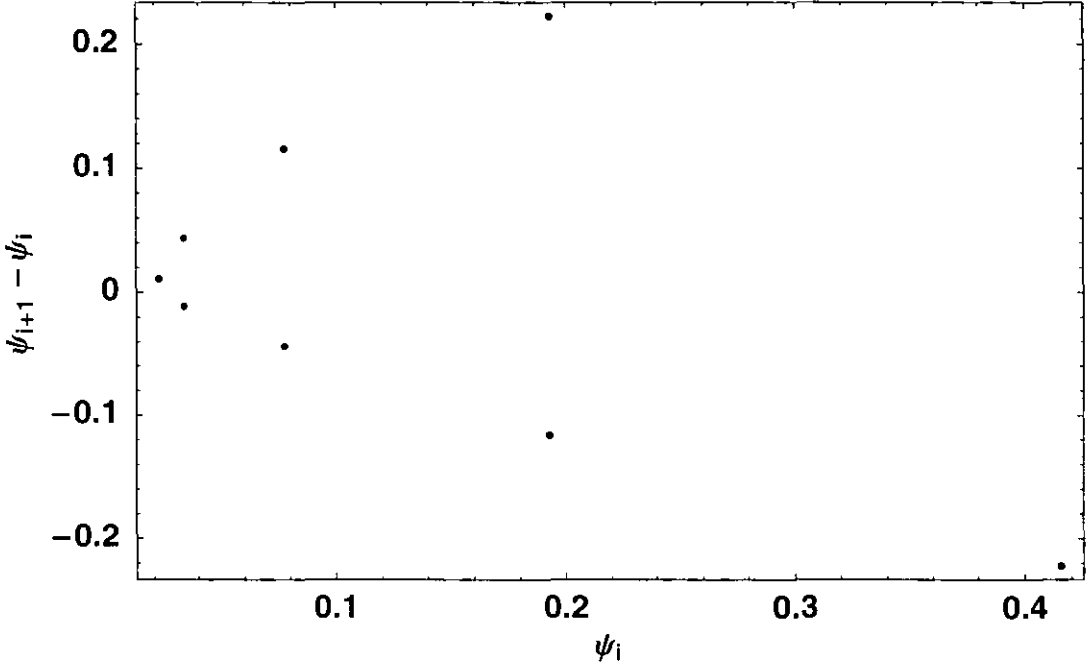


**Figure 3.3b** *The phase portrait corresponding to the wave function shown in Figure 3.3a. Only 8 points are visited in this phase portrait indicating a period-8 structure.*

the other 7 sites. Therefore, this structure of the wave function corresponds to a regular class of behaviour. In the limit  $c \rightarrow \infty$  we will obtain our initial structure of the wave function being completely localised on 4 sites and zero everywhere else. Note that in this limit the corresponding phase space consists of just 3 points: one at the origin  $(\psi_i, \psi_{i+1} - \psi_i) = (0, 0)$ , one at  $(\psi_i, \psi_{i+1} - \psi_i) = (0, 1/\sqrt{N})$  and one at  $(\psi_i, \psi_{i+1} - \psi_i) = (1/\sqrt{N}, -1/\sqrt{N})$ . These points represent the only permissible changes in the structure of the wave function between adjacent lattice sites in the limit  $c \rightarrow \infty$ .

Consider an initial structure consisting of a normalised wave function localised on only 10 sites, all equally spaced. Each of these localised sites is separated by 9 sites where the wave function is zero. The sign of the wave function of these 10 sites alternates ie if it is positive at a particular site then the sign of the wave function 10 sites before or 10 sites after is negative. This gives rise to a period-20 structure on a 100 site lattice. The corresponding energy eigenvalue (given by (50)) is  $E = (20-c)/10$ . Taking the coupling constant to be  $c = 24$  and successively applying

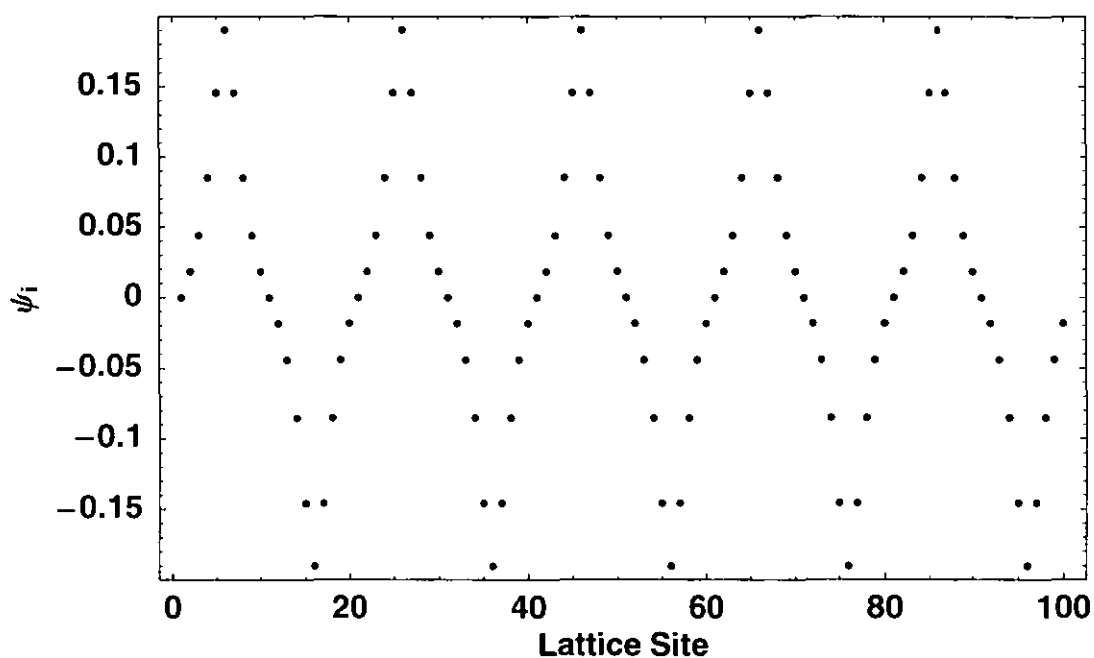
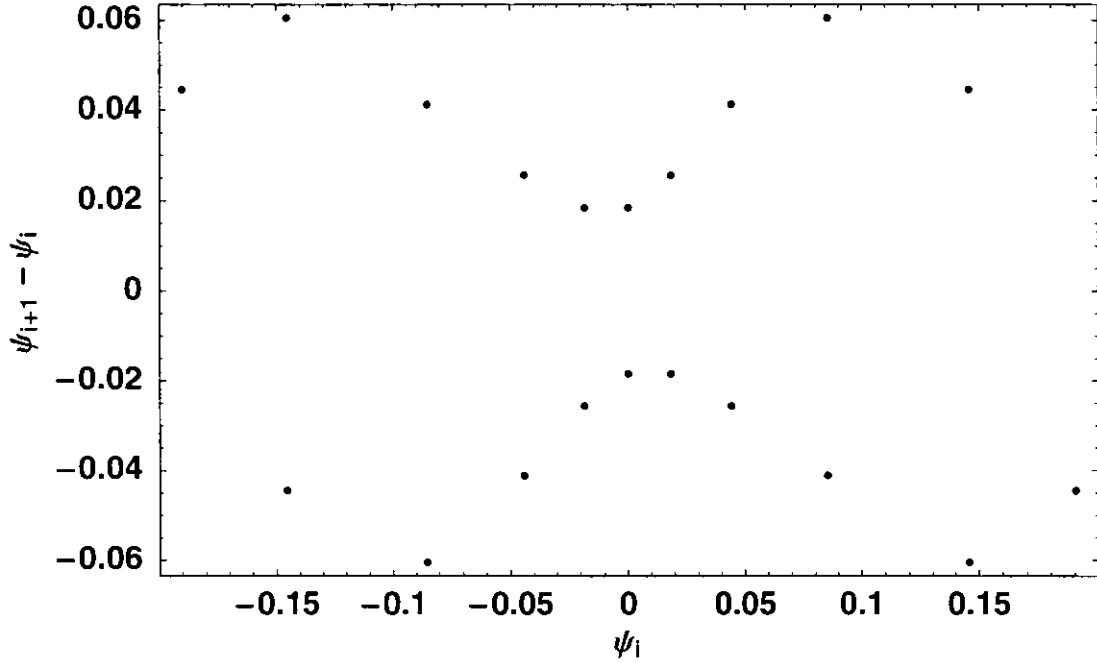


Figure 3.4a *The converged behaviour of a periodic wave function on a 100 site lattice with PBC. The initial structure consisted of a normalised wave function being localised on only 10 sites all equally spaced apart with alternating sign. Between these localised sites the value of the wave function was zero. The initial conditions were  $c = 24$  and  $E = -0.4$ .*





**Figure 3.4b** *The phase portrait corresponding to the wave function shown in Figure 3.4a. The 20 points visited in this phase portrait indicate a period-20 structure.*

the Perturbation Procedure to this initial structure of the normalised wave function, we obtain the solution presented in Figure 3.4a. This shows a periodic behaviour of the wave function through the lattice (as expected from the initial conditions). The corresponding phase portrait, Figure 3.4b, indicates that this initial structure gives rise to a regular commensurate period-20 structure. The phase portrait consists of only 20 points as the wave function oscillates regularly.

Figure 3.5a shows what happens as  $c$  is increased to  $c = 30$ . The oscillations in the structure of the wave function grow. The width of the peaks and troughs decreases and the height or depth increases, respectively. The wave function becomes more localised. In the limit  $c \rightarrow \infty$ , we obtain our initial structure of the wave function being completely localised on the original 10 sites and zero everywhere else. Note that in this limit the corresponding phase space consists of just 5 points: the origin  $(\psi_i, \psi_{i+1} - \psi_i) = (0, 0)$ ,

$$(\psi_i, \psi_{i+1} - \psi_i) = (0, 1/\sqrt{N}),$$

$$(\psi_i, \psi_{i+1} - \psi_i) = (0, -1/\sqrt{N}),$$

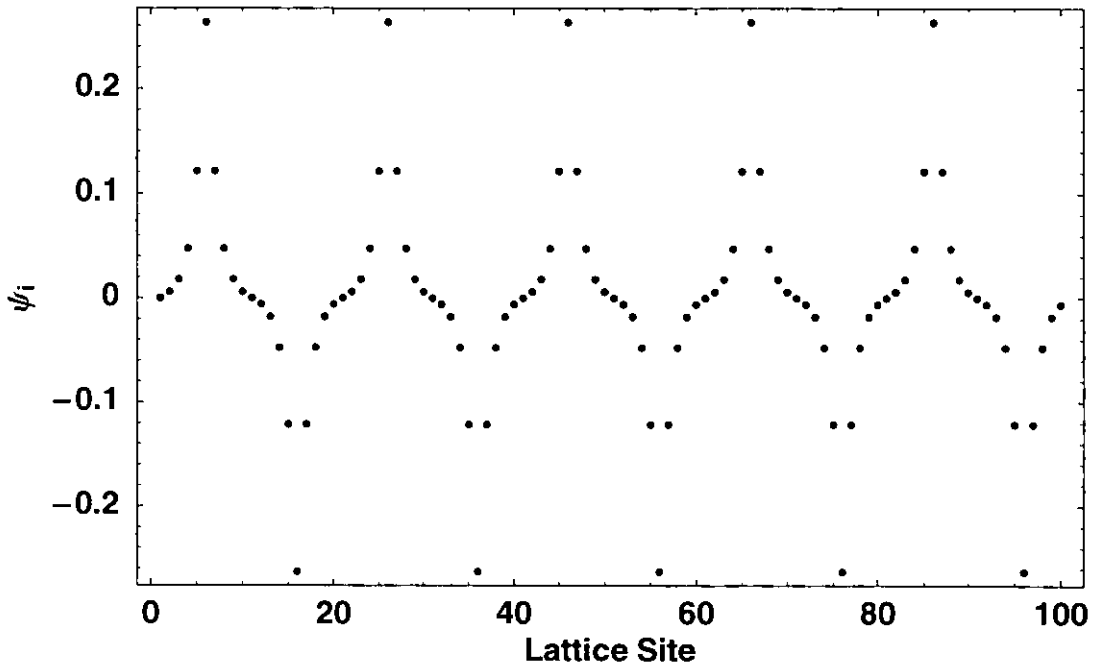


Figure 3.5a As in Figure 3.4a but with  $c = 30$  and so  $E = -1$ .

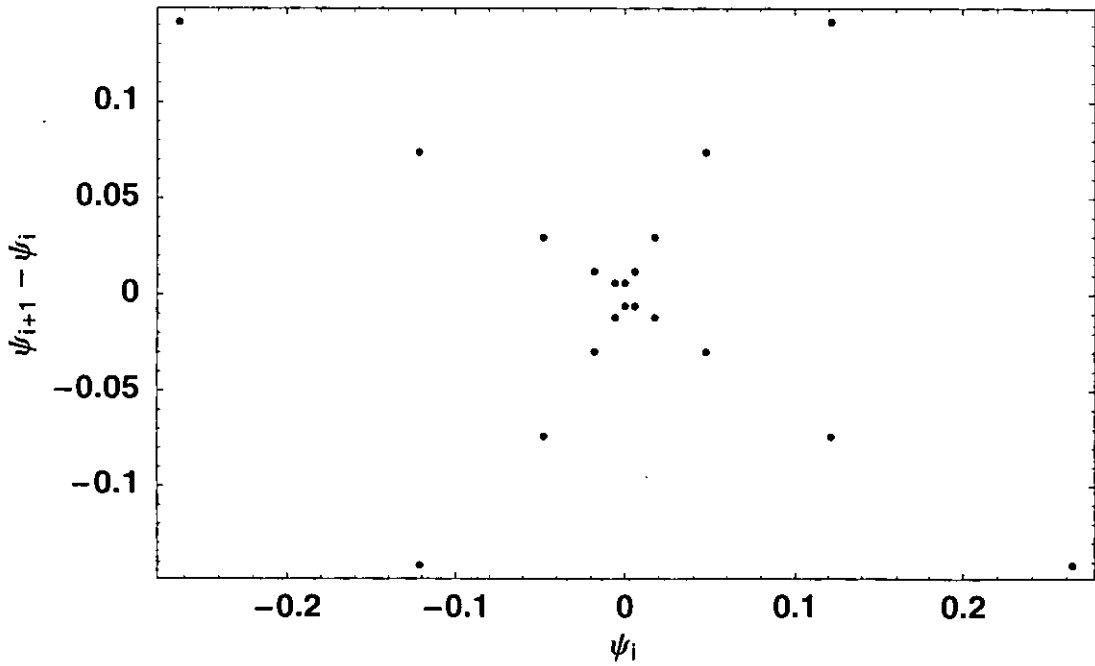


Figure 3.5b The phase portrait corresponding to the wave function shown in Figure 3.5a. The 20 points in the phase portrait again indicate a period-20 solution.

$$(\psi_i, \psi_{i+1} - \psi_i) = (1/\sqrt{N}, -1/\sqrt{N})$$

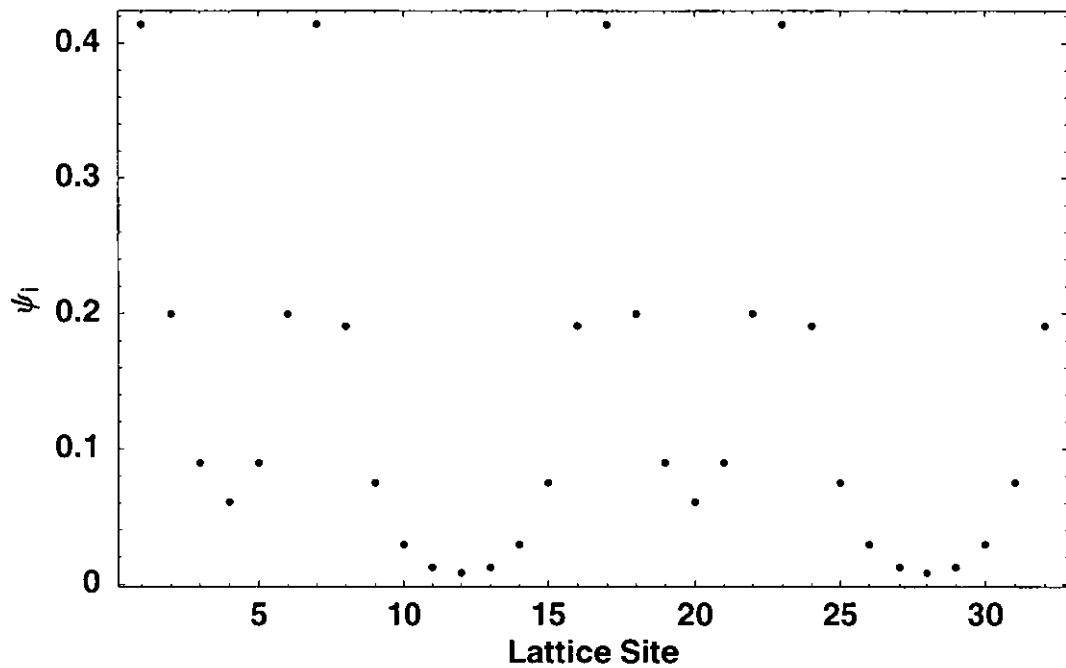
and  $(\psi_i, \psi_{i+1} - \psi_i) = (-1/\sqrt{N}, 1/\sqrt{N})$ . Again, these points represent the only permissible changes in the structure of the wave function between adjacent lattice sites in the limit  $c \rightarrow \infty$ .

### 3.7.2 Quasiperiodic Structures

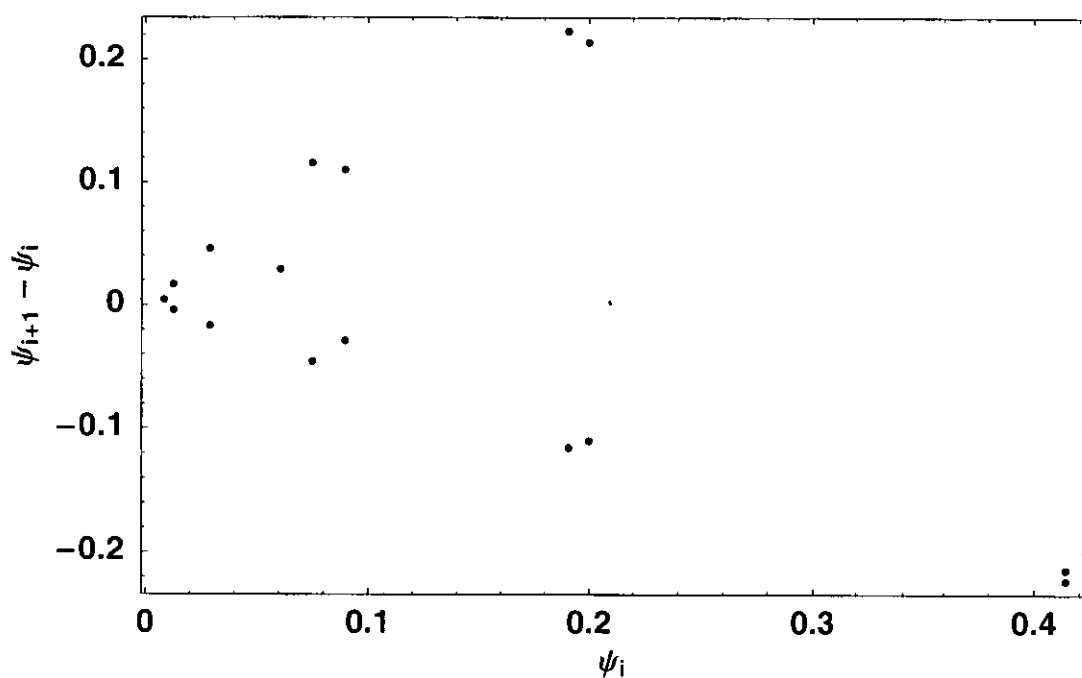
If the initial structure of the wave function in Figure 3.3 – 4 localising sites on a 32 site lattice with PBC – is altered slightly, so that the 4 localised sites are not equidistant, then we see a deviation from the regular periodic behaviour of the wave function. The 4 sites on which the wave function is localised are either 6 or 10 lattice sites apart. These lattice sites are separated by either 5 or 9 lattice sites, respectively, on which the wave function is zero. From (50) the energy eigenvalue is still given by  $E = (8 - c)/4$ .

Figure 3.6a depicts the wave function, obtained by successively applying the Perturbation Procedure until the corrections to the wave function become negligible, for  $c = 12$ . We see some interference develop between the different peaks. This gives an irregular structure which has periods which deviate slightly from one another but are, nevertheless, commensurate with the lattice. This deviation of the periods is illustrated in the phase portrait of this structure Figure 3.6b where we see a dispersion of the points in the phase space. The previous regular period-8 structure of the lattice no longer exists. Two different structures arise which correspond to two different sets of points being visited in the phase space. The deviation in these formerly regular structures indicates the on-set of quasiperiodicity or even chaoticity within the system due to an interaction of different spots. Specifically, it is easy to imagine a larger lattice with a greater number of interfering spots. Here, the number of points visited in the phase space of the discrete nonlinear system will increase and the mapped closed loop will be dense. This would be indicative of a quasiperiodic solution. If this closed loop is dispersed then this would indicate a stochastic structure which is reminiscent of classical chaotic motion.

If the value of the parameter  $c$  decreases then the energy eigenvalue becomes less



**Figure 3.6a** *The converged behaviour of an irregular wave function on a 32 site lattice. The initial conditions were  $c = 12$  and  $E = -1$  with the initial, normalised wave function value of  $\psi = 1/2$  at only 4 sites. These 4 sites were not separated uniformly but had either 5 or 9 sites where  $\psi = 0$  separating the localised sites giving an 'irregular' structure.*



**Figure 3.6b** *The phase portrait corresponding to the wave function shown in Figure 3.6a. The 16 points visited in the phase space no longer lie on a simple closed loop and so this arrangement of points is associated with an irregular class of behaviour of the wave function.*

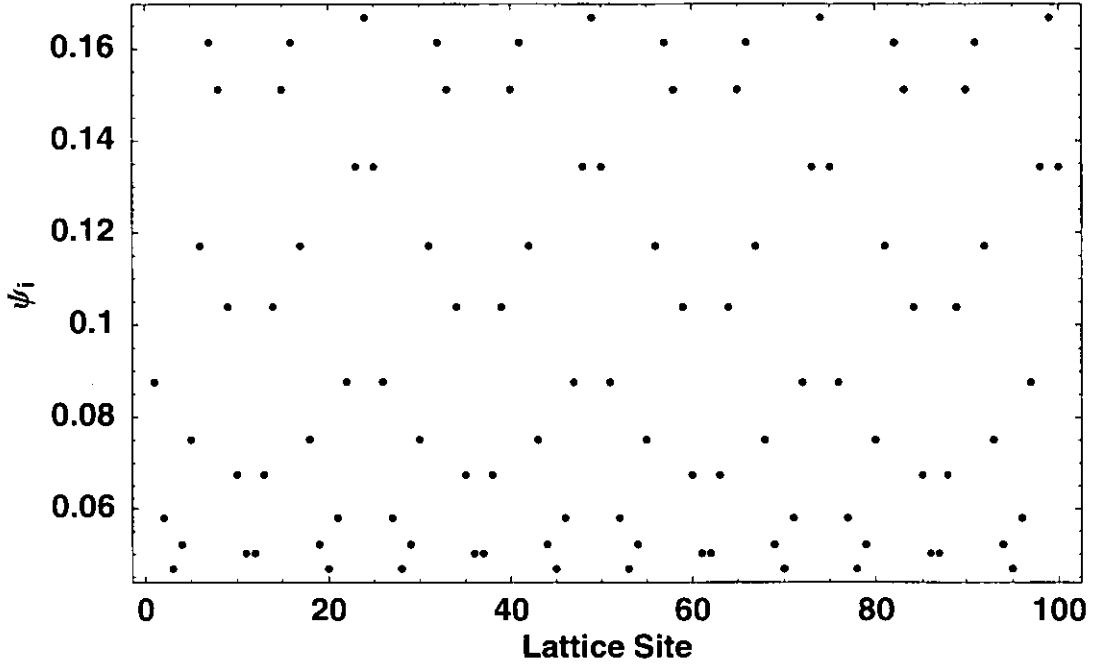


**Figure 3.7a** *The converged behaviour of an apparently random wave function on a 100 site lattice with PBC. The initial conditions were  $c = 29$  and  $E = -0.416$  with the initial, normalised wave function value of  $\psi = 1/\sqrt{12}$  at 12 sites. These 12 sites were separated into 12 spots which were further separated by either 6, 7 or 9 'empty' sites. This structure was repeated every 25 sites.*

negative, ie closer to zero but still negative, and the interaction between the spots intensifies. The width of the peaks widens and their height decreases. Similarly, if the value of  $c$  is increased then the width of the peaks lessens and their height increases. Consequently, the interaction between the spots is reduced.

Figure 3.7a depicts the converged state of a wave function initially localised on 12 lattice sites in 12 different spots on a 100 site lattice with PBC. The number of empty lattice sites separating the localised sites varies cyclically. There are, respectively, 6, 7 and 9 empty lattice sites between the localised sites. This pattern is repeated systematically every 25 sites. The energy eigenvalue of this structure is  $E = (24 - c)/12$ . After applying the Perturbation Procedure until the corrections to the wave function become negligible, for  $c = 29$  we obtain a wave function structure which at first seems to have no order. Figure 3.7b shows the underlying pattern of

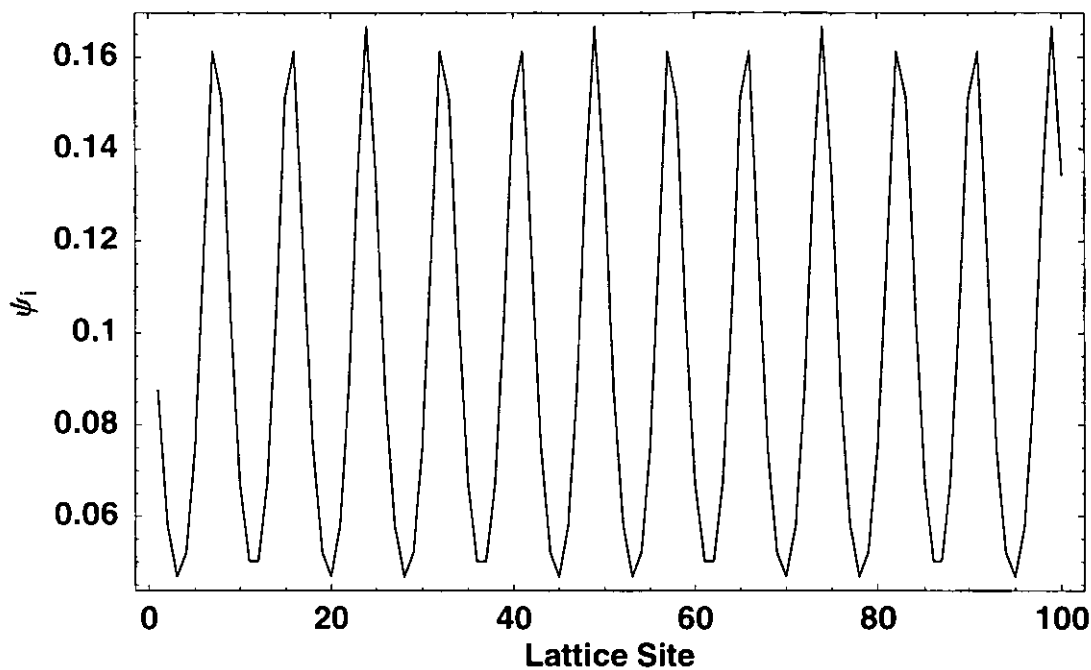


Figure 3.7b The underlying pattern manifest in the structure presented in Figure 3.7a. The pattern is repeated every 25 sites as expected.

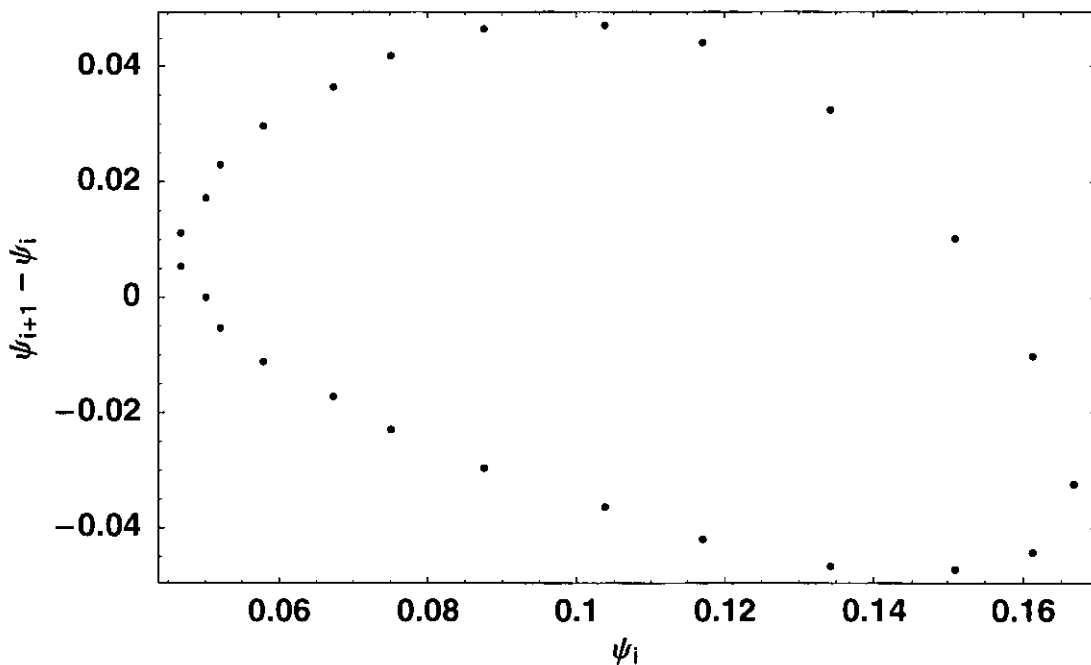
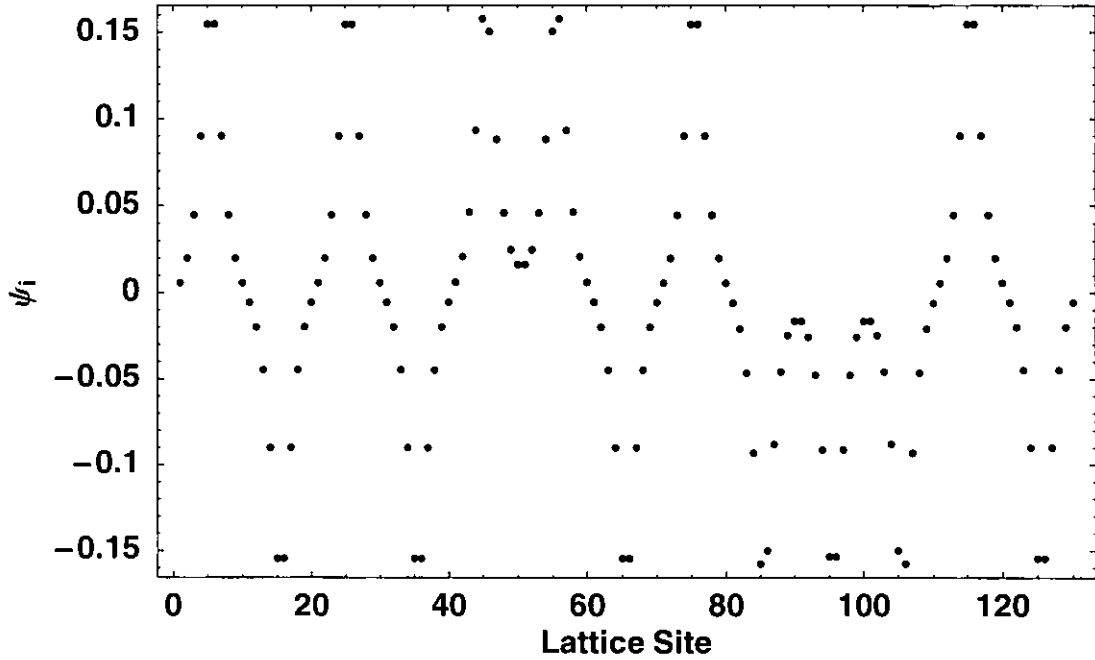


Figure 3.7c The phase portrait corresponding to the wave function shown in Figure 3.7a. A closed loop is traced out by the 25 points visited in the phase space. However, this loop corresponds to three distinct orbits; one for each of the three peaks in the wave function every 25 lattice sites.



**Figure 3.8a** *The converged behaviour of an irregularly oscillating wave function on a 130 site lattice with PBC. The initial conditions were  $c = 40$  and  $E = -0.53846$  with the initial, normalised wave function value of  $\psi = 1/\sqrt{26}$  at 26 sites. These 26 sites are grouped into 13 spots.*

this structure.

The phase portrait of this system, Figure 3.7c, consists of 25 points and so indicates a period-25 structure. This periodicity is due to the structure being systematically repeated every 25 lattice sites. Figure 3.7b shows that there are actually three peaks of the wave function which occur over 25 lattice sites. That is the loop plotted in Figure 3.7c must actually consist of 3 sets of points; each set orbits the phase space of the phase portrait. These sets of points are not regular but they are still commensurate with the lattice. Thus, in Figure 3.7c we see something akin to an irregular commensurate structure of the wave function.

Figure 3.8a shows the converged state of a wave function on a 130 site lattice with PBC. The initial structure consisted of a normalised wave function being localised on 26 sites separated into 13 spots, each of which consists of two localising sites with the same sign of wave function. The sign of the wave function of different spots is



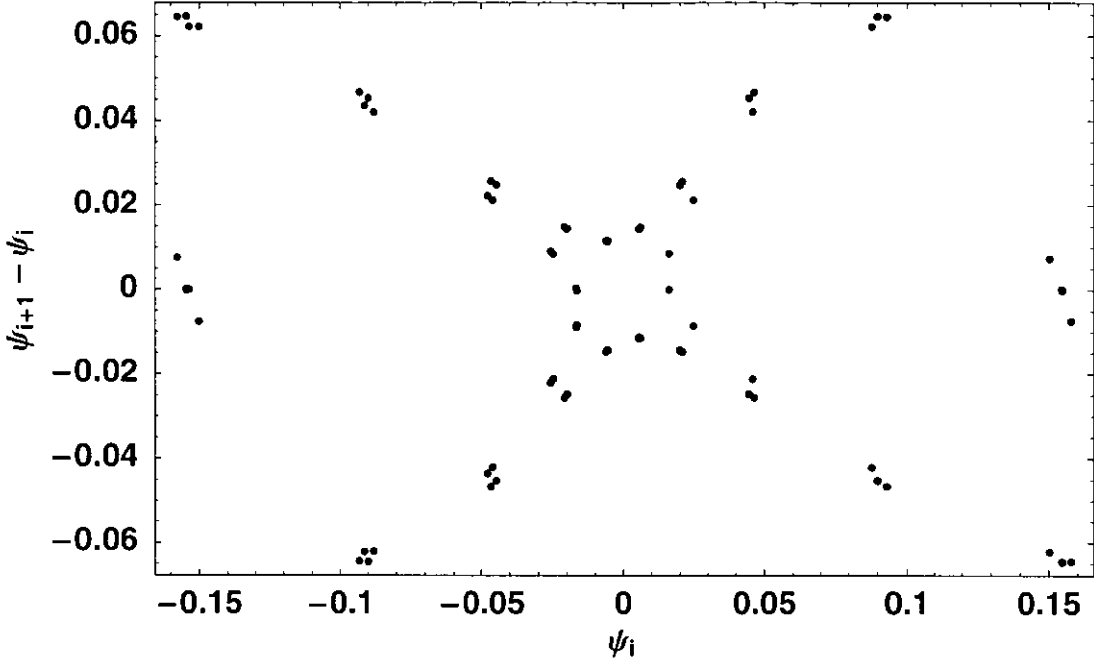


**Figure 3.8b** *The phase portrait corresponding to the wave function shown in Figure 3.8a which maps out a dispersed double loop.*

either positive or negative. However, the sign of the wave function of different spots does not vary regularly throughout the lattice. These 13 spots are equally spaced apart and separated from each other by 8 sites where the initial value of the wave function is zero. The corresponding energy eigenvalue is  $E = (26 - c)/26$ . Taking the coupling constant to be  $c = 40$  and applying the procedure described above to this initial structure of the normalised wave function we obtain the solution presented in Figure 3.8a. This shows an irregular oscillation of the wave function through the lattice although each of the peaks and troughs, respectively, are similar to one another. The corresponding phase portrait, Figure 3.8b, maps out a double loop and near the origin is reminiscent of a hyperbolic point.

Again as  $c$  is increased the wave function becomes more localised and in the limit  $c \rightarrow \infty$  we again obtain our initial structure of the wave function being completely localised on the original 26 sites and zero everywhere else. Note that in this limit the corresponding phase space will consist of 7 points: the five listed above and two more:  $(\psi_i, \psi_{i+1} - \psi_i) = (1/\sqrt{N}, 0)$

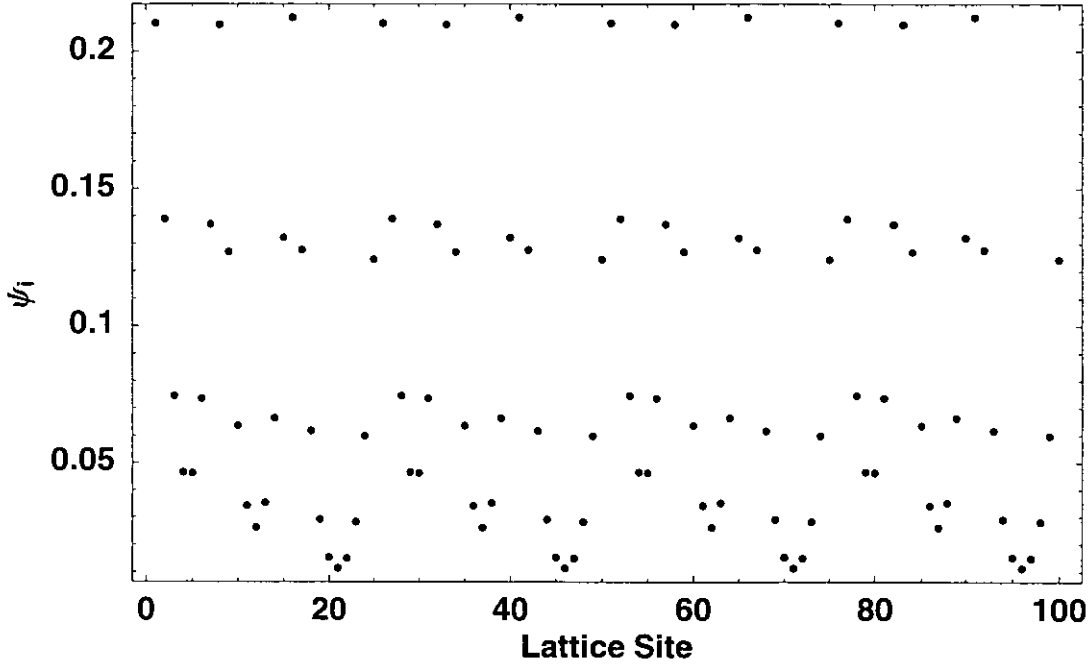


**Figure 3.9a** *The converged behaviour of an oscillating wave function on a 100 site lattice with PBC. The initial conditions were  $c = 32$  and so  $E = -0.6$  with the initial, normalised wave function value of  $\psi = 1/\sqrt{12}$  at 12 sites. These 12 sites were separated into 12 spots which were further separated by either 6, 7 or 9 'empty' sites. The converged wave function appears to be separated into zones at the top, middle and bottom.*

and  $(\psi_i, \psi_{i+1} - \psi_i) = (-1/\sqrt{N}, 0)$ .

### 3.7.3 Chaotic Structures

Figure 3.9a shows the behaviour of the wave function on the lattice as  $c$  is increased to  $c = 32$  for the same zero approximation structure as that in Figure 3.7a. The energy eigenvalue (from (50)) is still  $E = (24 - c)/12$  but because  $c$  is increased it becomes more negative.

The wave function structure, Figure 3.9a, has split into three regions; top, middle and bottom. Figure 3.9b shows the underlying pattern of this wave function structure. As expected, the structure repeats itself every 25 sites and the corresponding phase space, Figure 3.9c, is in the form of another dispersed closed loop. In each set

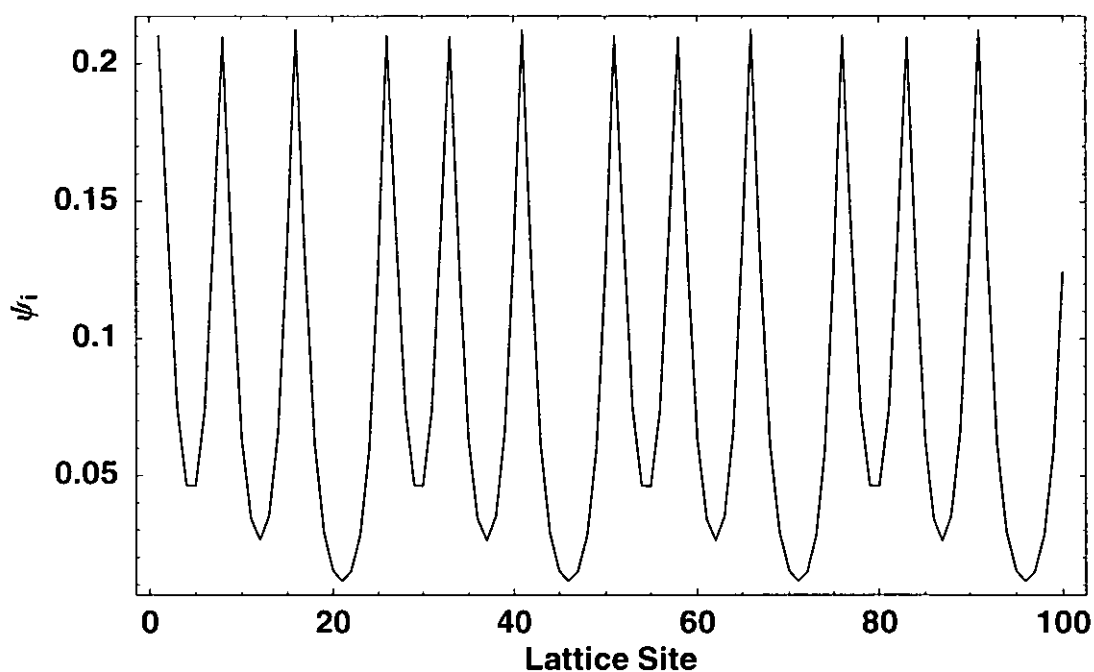


Figure 3.9b *The underlying pattern manifest in the structure presented in Figure 3.9a.*

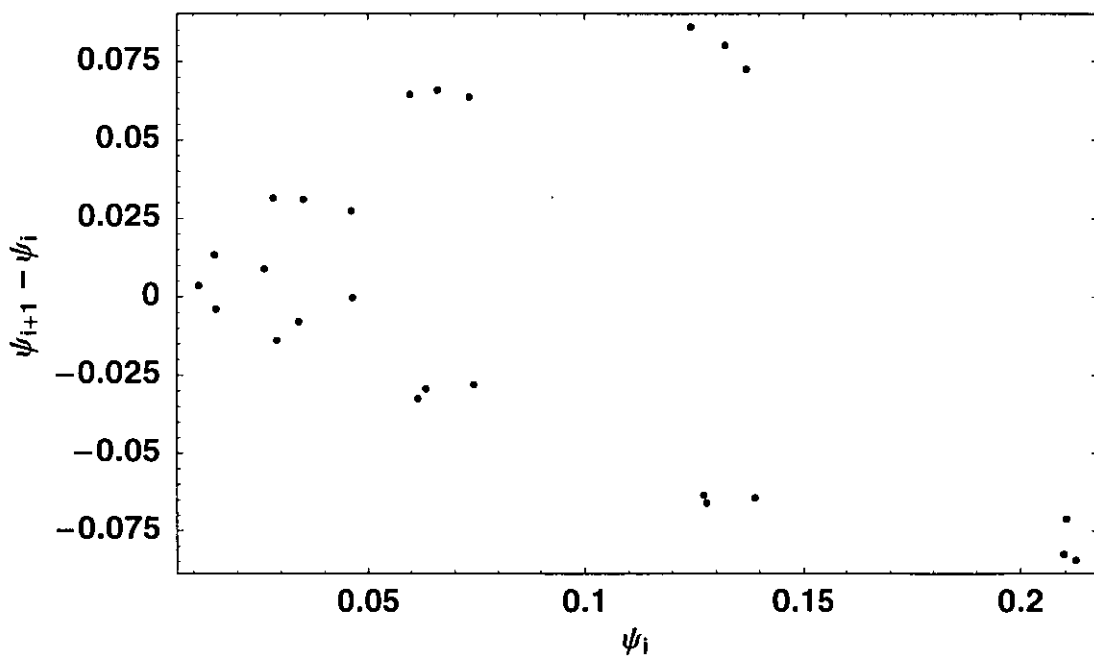


Figure 3.9c *The phase portrait corresponding to the wave function shown in Figure 3.9a. Most of the points visited in this phase space occur in sets of three.*

of 25 lattice sites the wave function has three peaks. From Figure 3.9b one can see that now the interactions between the spots has decreased. The peaks are narrower and higher. The phase space of this structure, Figure 3.9c, comprises of sets of three points.

This structure is due to the interaction of different localisation spots. The appearance of a dispersed orbit demonstrates a chaotic behaviour and indicates the effects of irregular incommensurability of the wave function on the lattice. Upon further inspection of Figure 3.9a, which shows the value of the wave function throughout the lattice, we see that the different horizontal regions in Figure 3.9a actually correspond to the different points of the orbits which span the phase space of this structure. Figure 3.9c has 8 sets of three points and on closer inspection of Figure 3.9a we see that it is actually organised into 8 horizontal sets; one at the top, two in the middle and five at the bottom.

Figure 3.10a shows the behaviour of the wave function on the lattice for the same zero approximation wave function structure as  $c$  is increased to  $c = 36$ . The interaction between the spots decreases further as the energy eigenvalue becomes more negative. The wave function is again divided into three distinct regions at the top, middle and bottom. These distinct regions correspond to the dispersed points in Figure 3.10b. The dispersion of these points has now reduced and they are beginning to converge towards different limits. This indicates that the incommensurate wave function structure is becoming commensurate. The structure of the wave function in Figure 3.10a is separated into different sets which correspond to the different convergence limits in the phase portrait.

As  $c$  is further increased the wave function structure now begins to resemble the initial condition where the wave function is localised on 12 sites in 12 spots. Note that this initial structure can only exist in the limit  $c \rightarrow \infty$ .

Figure 3.11a shows the wave function structure for  $c = 84$ . The value of the wave function now has three specific domains; at the top, near the bottom and at the bottom. These domains correspond to the different states of the system as depicted in Figure 3.11b. The wave function structure now indicates regular

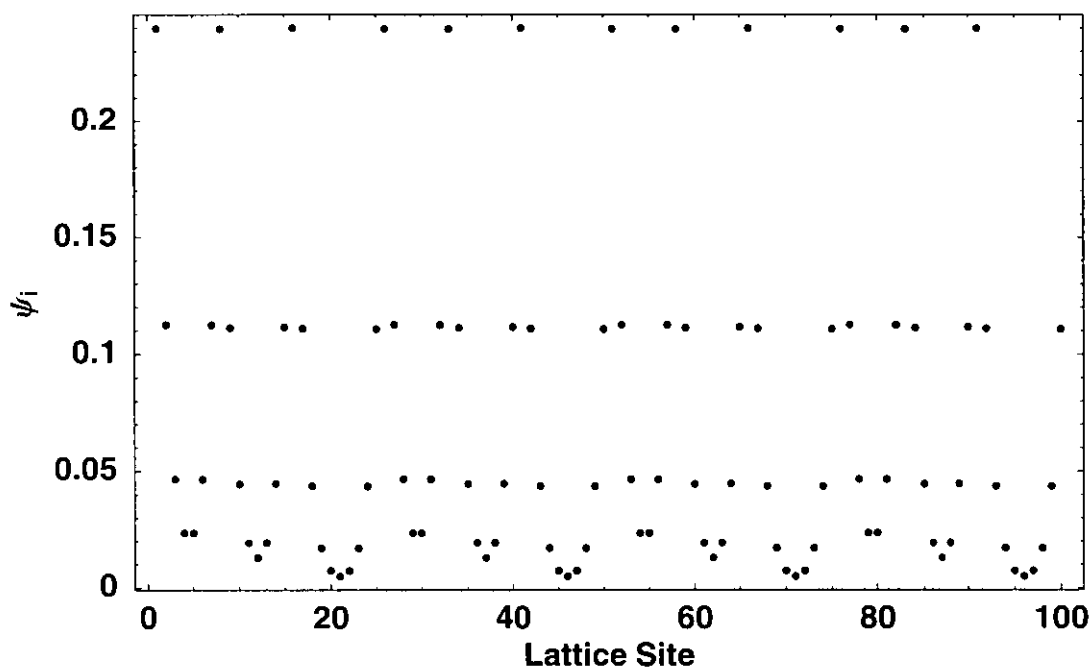


**Figure 3.10a** *The converged behaviour of an oscillating wave function on a 100 site lattice with PBC. The initial conditions were  $c = 36$  and so  $E = -1$  with the initial, normalised wave function value of  $\psi = 1/\sqrt{12}$  at 12 sites. These 12 sites were separated into 12 spots which were further separated by either 6, 7 or 9 'empty' sites. The zones the wave function is separated into become much more distinct and further apart as  $c$  increases.*

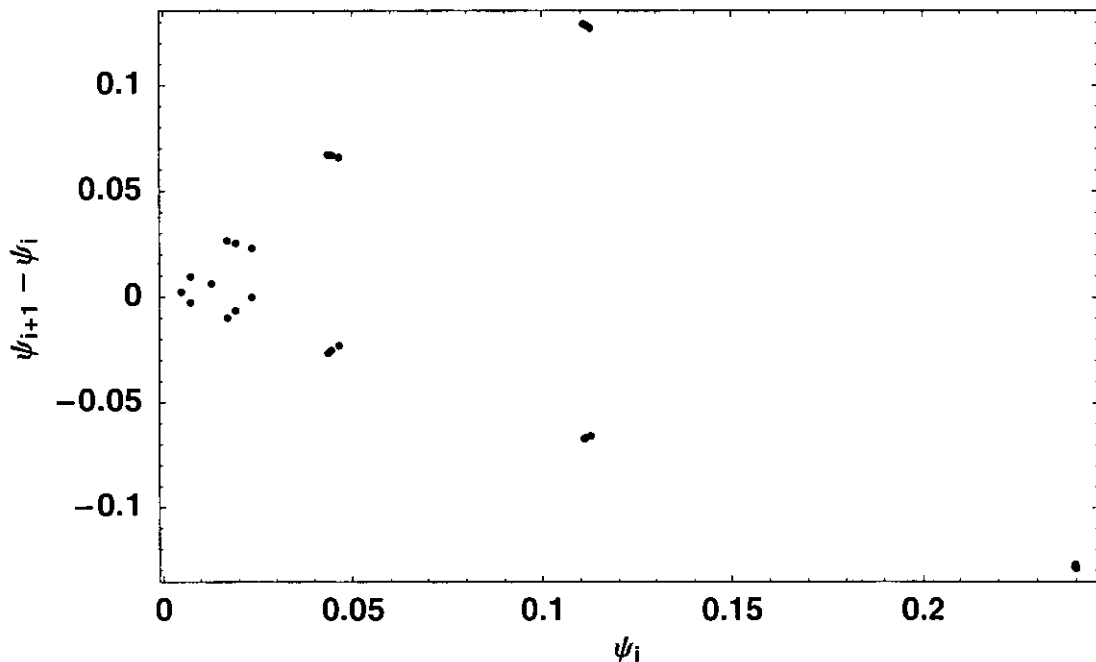


Figure 3.10b *The phase portrait corresponding to the wave function shown in Figure 3.10a. It is clear that as  $c$  increases the dispersion of the sets of points decreases.*

commensurability. Note that the sets of three points which are evident in Figure 3.9c and corresponded to three separate orbits spanning the phase space have converged as  $c$  has increased. Now there is only one orbit which spans the phase space as the previous dispersion of points has vanished. In fact, a careful study of Figure 3.11b indicates a period-9 structure; there are actually three points closely located at the origin. If the value of  $c$  were further increased then these points too would converge to a single point at the origin.

Figure 3.12a shows the converged state of a wave function on a 208 site lattice for an arbitrary initial configuration. The energy eigenvalue of this structure – given by (50) – is  $E = (86 - c)/63$ . Taking  $c = 260$  and applying the Perturbation Procedure until the corrections to the wave function become negligible, we obtain Figure 3.12a where the behaviour of the wave function appears disordered. The wave function structure has split into three regions: top, middle and bottom. Figure 3.12b shows the underlying pattern manifest in the wave function which consists of narrow peaks and troughs arranged in a pattern without any long-range order. The corresponding

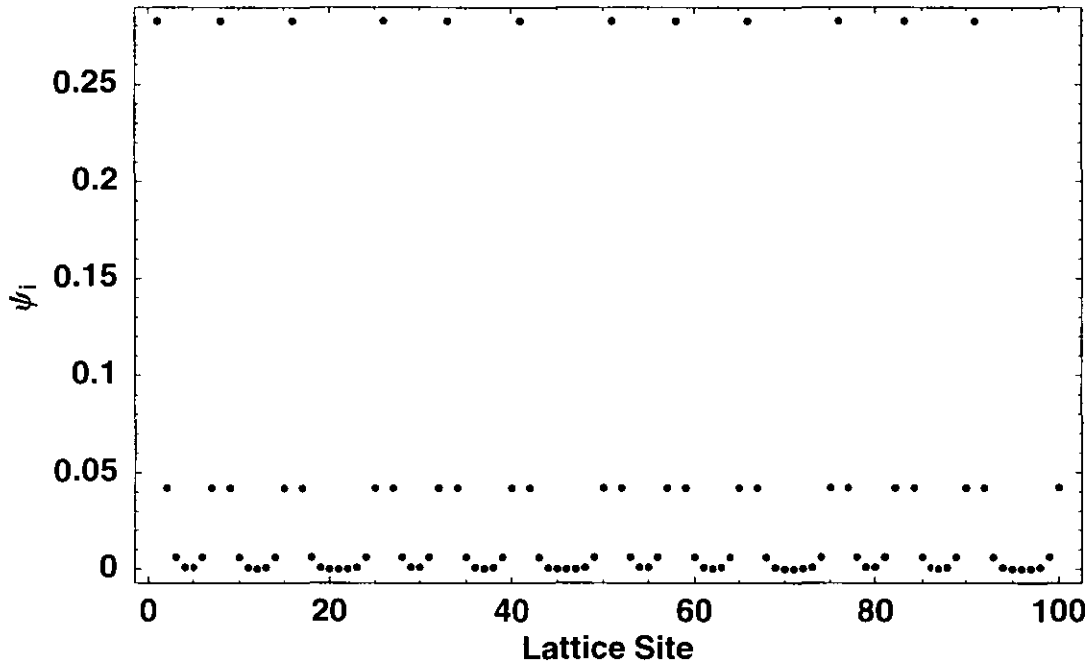


Figure 3.11a *The converged behaviour of a wave function on a 100 site lattice with PBC. The initial conditions were  $c = 84$  and so  $E = -5$  with the initial, normalised wave function value of  $\psi = 1/\sqrt{12}$  at 12 sites. These 12 sites were separated into 12 spots which were further separated by either 6, 7 or 9 'empty' sites. The wave function separates into zones at the top, near the bottom and at the bottom as  $c$  has increased further.*

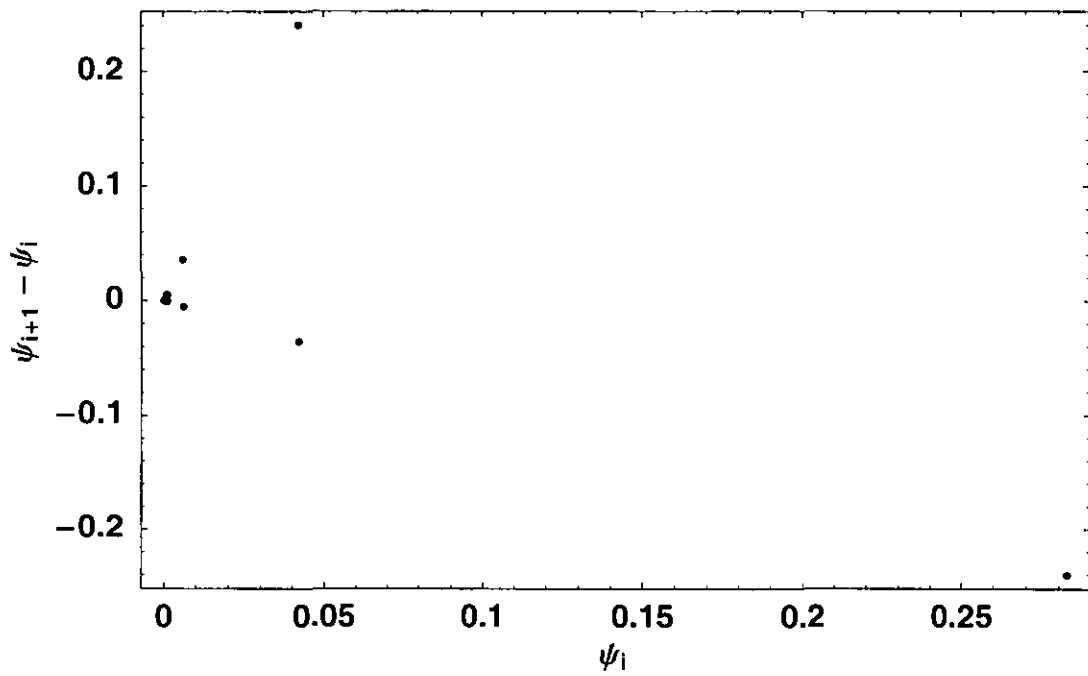


Figure 3.11b *The phase portrait corresponding to the wave function shown in Figure 3.11a.*

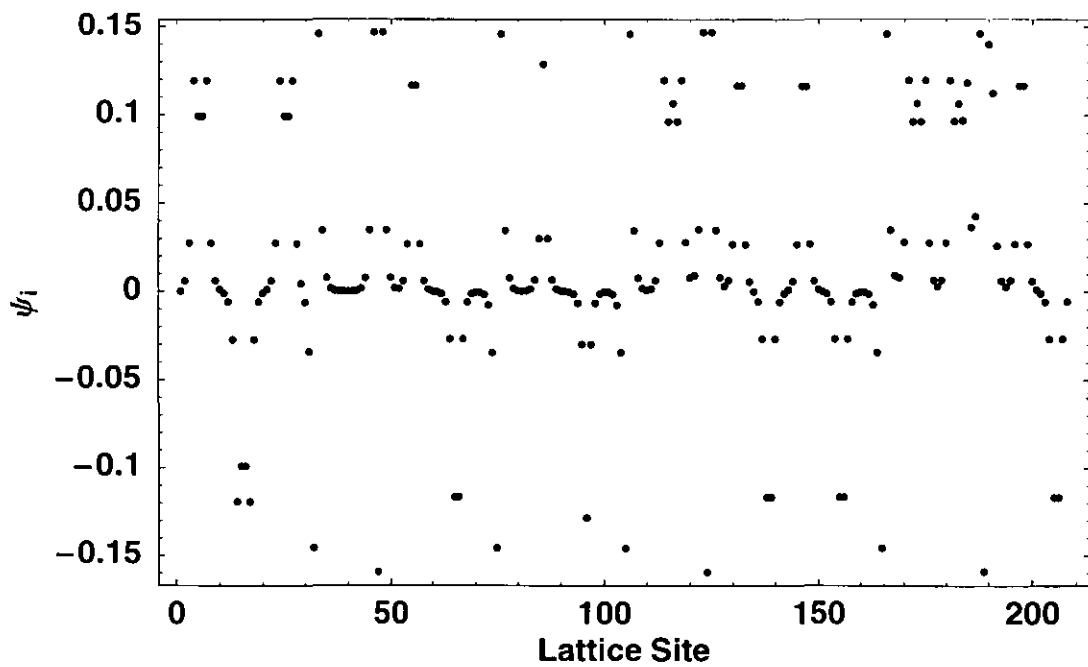


Figure 3.12a *The converged behaviour of a chaotic wave function on a 208 site lattice with PBC. The initial conditions were  $c = 260$  and  $E = -2.7619$  for an arbitrary starting configuration.*



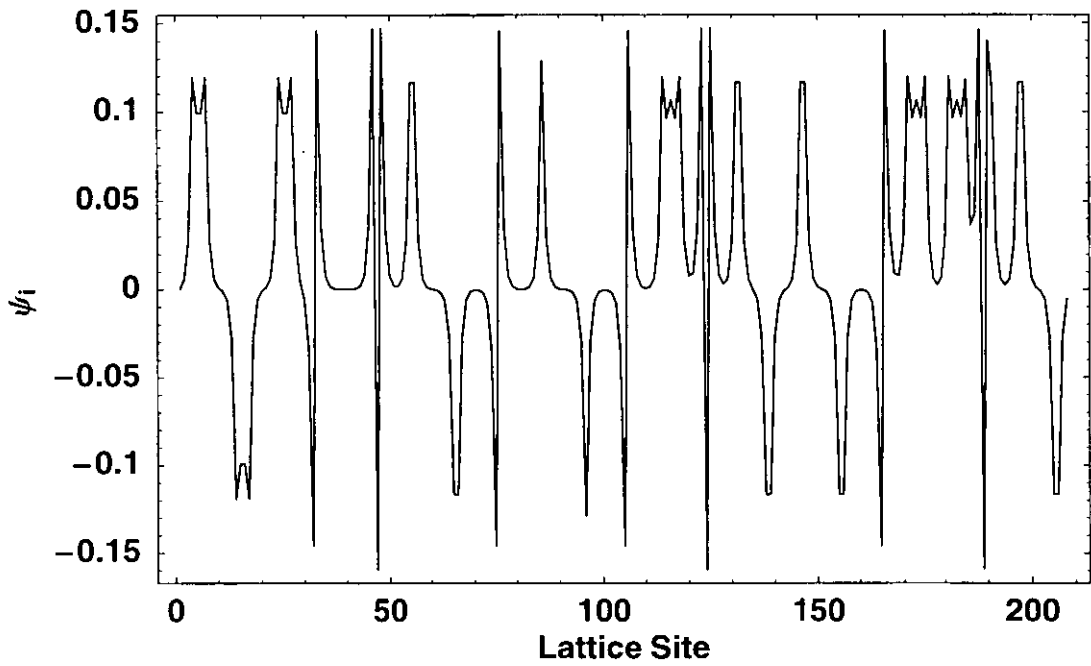


Figure 3.12b *The underlying pattern manifest in the structure presented in Figure 3.12a.*

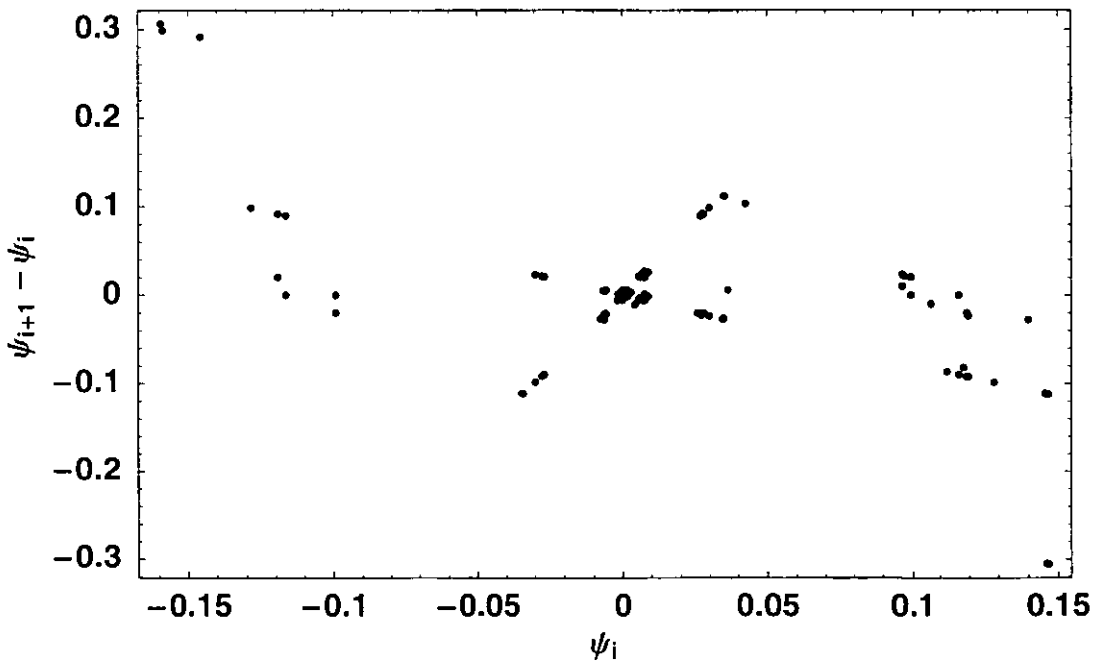
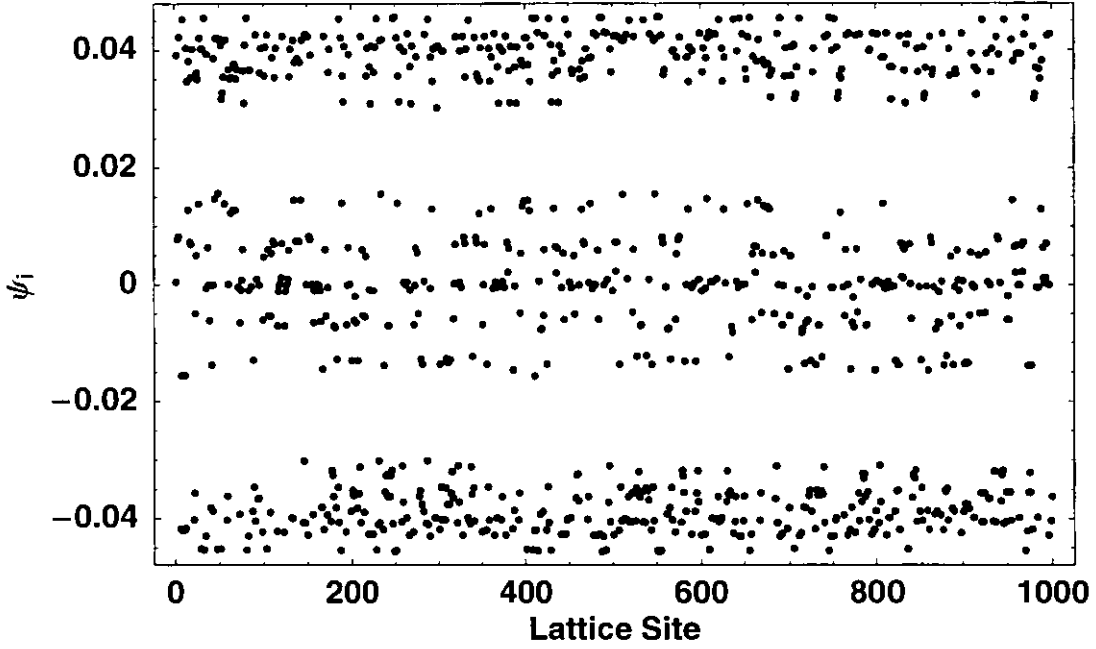


Figure 3.12c *The phase portrait corresponding to the wave function shown in Figure 3.12a. The dispersed orbit is reminiscent of chaos in classical systems.*



**Figure 3.13a** *The converged behaviour of a wave function on a 1000 site lattice with PBC. The initial conditions were  $c = 4000$  and  $E = -4.342767$  for a random starting configuration. The wave function has split into three regions.*

phase space, Figure 3.12c, is in the form of a dispersed closed loop. This structure (which is reminiscent of chaos in classical systems) is due to the interaction of different localisation spots. The appearance of a dispersed orbit indicates the effects of irregular incommensurability of the wave function on the lattice.

#### 3.7.4 Fractal Structures

Figure 3.13a shows the converged state of a wave function on a 1000 site lattice. The initial configuration was generated (pseudo-) randomly [21] from the integers  $-1, 0, 1$  and then normalised. The energy eigenvalue (from (50)) is  $E = (1238 - c)/636$  and a value of  $c = 4000$  gives the wave function structure shown in Figure 3.13a. Again the wave function structure has split into top, middle and bottom. Figure 3.13b shows the (dense) oscillations of the wave function and Figure 3.13c is the phase portrait for this wave function. The points in this phase portrait do not lie on an obvious closed loop or even a dispersed closed loop but rather a smeared curve. As

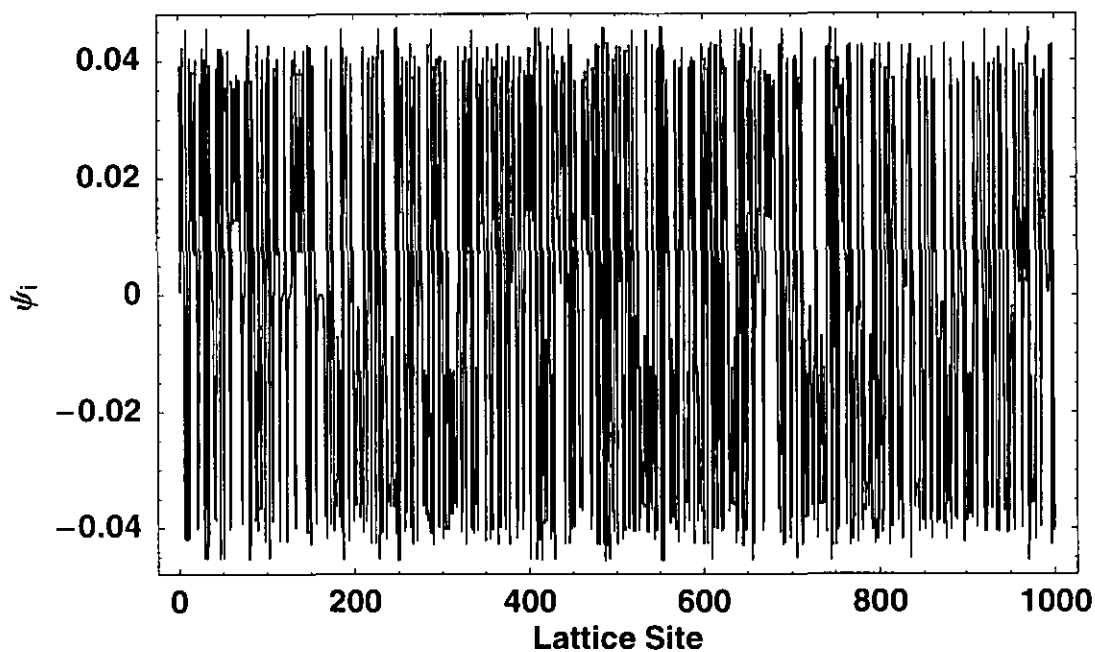


Figure 3.13b *The underlying pattern manifest in the structure presented in Figure 3.13a. The points are nested within each section.*

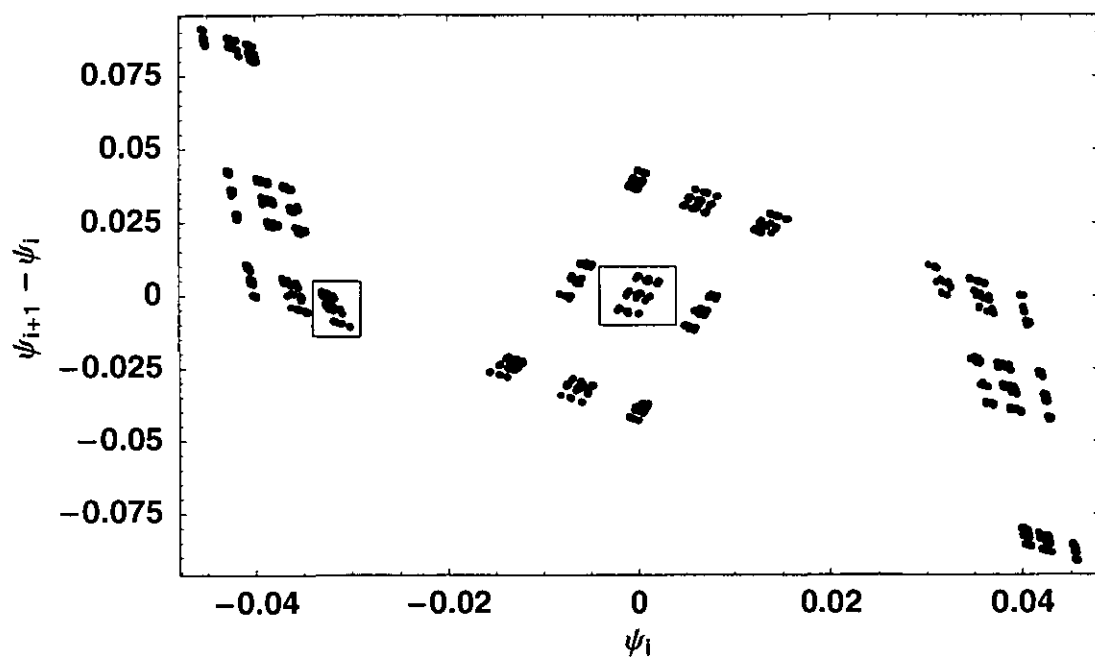
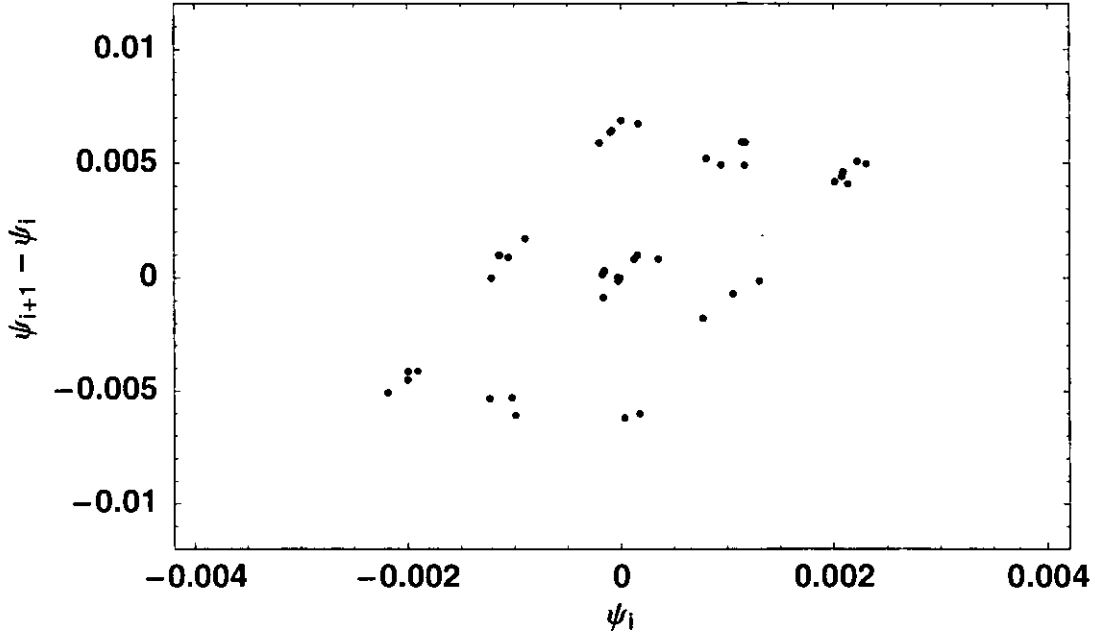


Figure 3.13c *The phase portrait corresponding to the wave function shown in Figure 3.13a.*



**Figure 3.13d** *A magnification of the boxed central region of the phase portrait presented in Figure 3.13c.*

this structure has no definite period it could be a possible candidate for a chaotic state of the system. The phase portrait is split into three parts: top-left, centre and bottom-right. Each of these three sections is further divided into sub-sections in which there appears a ‘nesting’ of points. Something which is especially noticeable in the central part of this phase portrait is that each of the sub-sections are similar to the larger section in which they are contained.

For example, the boxed sub-section of nested points at the origin, which is magnified in Figure 3.13d, is similar to the central section of Figure 3.13c. The same trend can also be observed in other parts of the phase portrait, for example Figure 3.13e is a magnification of the boxed region in the top-left segment of Figure 3.13c. Both of these examples indicate a self-similarity in the structure of the wave function on a lattice. That is, similar structures of the wave function exist on different length scales which suggests a fractal nature of the wave function on the lattice.

As the value of  $c$  is increased, the different points visited in the phase space converge until only a maximum of nine points exist. These nine points which corre-

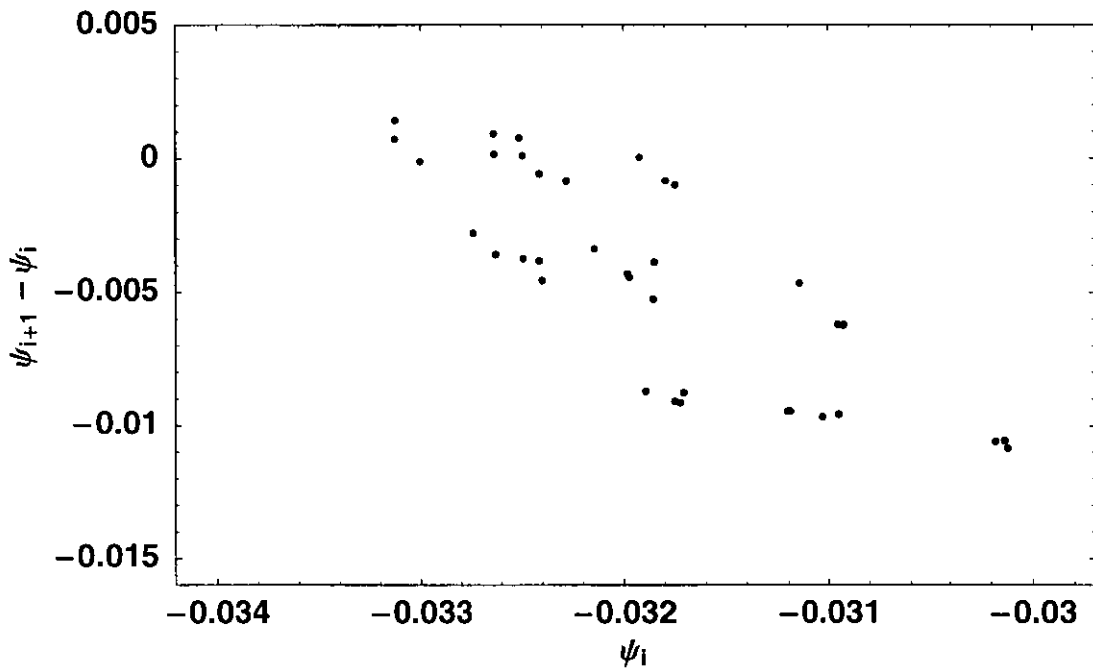


Figure 3.13e A magnification of the boxed top-left region of the phase portrait presented in Figure 3.13c.

spond to the wave function structure in the limit  $c \rightarrow \infty$  are

$$(\psi_i, \psi_{i+1} - \psi_i) = (0, 0),$$

$$(\psi_i, \psi_{i+1} - \psi_i) = (0, 1/\sqrt{N}),$$

$$(\psi_i, \psi_{i+1} - \psi_i) = (0, -1/\sqrt{N}),$$

$$(\psi_i, \psi_{i+1} - \psi_i) = (1/\sqrt{N}, 0),$$

$$(\psi_i, \psi_{i+1} - \psi_i) = (1/\sqrt{N}, -1/\sqrt{N}),$$

$$(\psi_i, \psi_{i+1} - \psi_i) = (1/\sqrt{N}, -2/\sqrt{N}),$$

$$(\psi_i, \psi_{i+1} - \psi_i) = (-1/\sqrt{N}, 0),$$

$$(\psi_i, \psi_{i+1} - \psi_i) = (-1/\sqrt{N}, 1/\sqrt{N}),$$

$$(\psi_i, \psi_{i+1} - \psi_i) = (-1/\sqrt{N}, 2/\sqrt{N}).$$

### 3.8 Summary

Thus, we obtain that, in the limit  $c \rightarrow \infty$ , there arises a number of localised solutions associated with different localisation states of the wave function of the DNSE (27) which consist of empty lattice sites (where the wave function is vanishing) and lattice sites where the wave function is localised. These localisation patterns, which can be viewed as soliton type structures, have many different configurations. When the value of  $c$  is not infinite different localisation spots within the pattern start to interfere with each other and modify the behaviour of the wave function. This leads to the existence of many different states in this discrete nonlinear system.

We go on to apply Perturbation Theory to this system of discrete nonlinear equations where, starting with the asymptotic solutions and perturbing, the  $\Psi(k+1)$  iteration is a better approximation to the solution of (33) than the  $\Psi(k)$  iteration for finite  $c$ . This solution gives the structure of the wave function on the lattice and suggests the possible existence of fractal structures where the wave function structure at one scale is echoed at another scale.

For example, consider a single electron which interacts strongly with phonons on a 1D chain of atoms. Here equation (33) describes the (Rashba)-Holstein self-trapping model. In the continuum limit, this system has only one soliton type solution which corresponds to the self-trapped state. However, our studies on discrete systems indicate that there are many different localised solutions to the characteristic equation and consequently there are many different self-trapped states. As well as the ground state, there also exist excited localised states of the whole system. We also find that the wave function of these self-trapped states (charge density distribution of the electron) can have either regular or irregular structure and may even possess a fractal structure.

Such different states may be experimentally observed in semiconductor superlattices (SSL). Here an electron may be trapped by a deformation of the SSL over one or several quantum wells. This localised spot with a trapped electron can interact strongly with sound waves which themselves are deformations of the lattice. Inside a spot the deformation  $\sim 1/N$  and vanishes outside and so each spot may be

viewed as a sound wave resonator. The resonant frequency and the wavelength of this resonator is related to the size of the spot. The size of a spot consisting of  $n_i$  quantum wells is  $n_i d$  where  $d$  is the period of SSL and so the resonance wavelength will also be  $\lambda_i = n_i d$ . Sound waves (acoustic phonons) with wave vector  $2\pi/(n_i d)$  will be especially strongly scattered or trapped by this spot.

Consequently, when a sound wave moving through a SSL passes the self-trapped spot there will be a transfer of momentum from the sound wave to the spot. As a result of this scattering, acoustic phonons with wave vector  $q = 2\pi/(n_i d)$  will be absorbed forcing the trapped electron to propagate through the lattice. Such motion may give rise to the creation of current induced by sound.

The level of interaction between the solitons (spots) is essentially governed by the radius of the solitons and their separation. If the radius of the solitons is much smaller than their separation then we have regular, commensurate behaviour of the wave function on the lattice. In this case the interaction between the solitons is very weak. As the radius of the solitons increases and the separation remains constant, the interaction between the solitons increases and the behaviour of the wave function on the lattice becomes less regular. Finally, when the radius of the solitons is about the same as the separation of the solitons we have strong interactions between the solitons. This results in strong incommensurability of the behaviour of the wave function on the lattice.

We find that the interference between the localised spots can give rise to three qualitatively different structures: periodic, quasiperiodic and chaotic. To indicate such structures in the quantum state the methods used in the studies of classical chaos were applied to the quantum system. A phase portrait was built up which consists of the amplitudes of the wave functions and of residues of these amplitudes associated with neighbouring sites. That is a projection of the 'phase space of our discrete nonlinear system' in the plane, the set  $\{\psi_{i+1} - \psi_i, \psi_i\}$ , is studied.

In the regular periodic and quasiperiodic solutions the wave function amplitudes replicate with some period equal to some integer number of lattice constants or creates aperiodic structures, respectively. However, there is also the appearance of

structures analogous to the those arising in classical chaos which gives rise to self-similar structures of the wave function on the lattice at different length scales. The destruction of the periodic and quasiperiodic orbits, which has been ascribed to the creation of spatial chaotic structure in the wave function, is also exhibited by the system. That is, the creation of a structure which has no definite period has been found.



*'The mountain does not laugh at the river because it is lowly,  
nor does the river speak ill of the mountain because it cannot move about.'*

— Koichi Tohei

## 4 Solutions To A First Order Discrete Cubic Equation

### 4.1 Exact Solutions Of The Discrete Equation

The work presented in the previous section on the spectrum of eigenvalues of the DNSE and the corresponding solutions may be extended and applied to any number of similar discrete nonlinear systems. To study further the solutions which arise in systems described by a similar set of equations we decided to investigate a first order, discrete nonlinear equation of the form

$$x_i - x_{i+1} - cx_i^3 = Ex_i \quad (69)$$

with the normalisation condition  $\sum_i x_i^2 = 1$ .

The solutions of equation (69) for the 2-site problem with periodic boundary conditions (PBC) are  $\{x_1 = x_2 = \pm 1/\sqrt{2}\}$  for  $E = -c/2$ ,  $\{x_1 = -x_2 = \pm 1/\sqrt{2}\}$  for  $E = 2 - c/2$  and  $\{x_1 = \pm \frac{\sqrt{1 \pm \alpha}}{\sqrt{2}}, x_2 = \pm \frac{\sqrt{1 \mp \alpha}}{\sqrt{2}}\}$ , where  $\alpha = \sqrt{1 - \frac{4}{c^2}}$ , for  $E = 1 - c$ . This last solution bifurcates from the homogeneous solution at  $c = 2$  and corresponds to the lowest energy state of the system for  $c > 2$ .

The solutions to the 2-site problem with open boundary conditions (OBC) cannot be expressed as simply but the equations describing the system can be solved and the dependence of the different eigenvalues on the parameter  $c$  can be plotted. This is presented in Figure 4.1. The dependence of the eigenvalues on  $c$  is linear for most values of  $c$  and so each eigenvalue may be readily described by an empirical formula for large  $c$ .

Again an amazing agreement between the complicated expressions of the exact spectra (presented graphically in Figure 4.1) and the empirical formulae is seen. Note that, for the state described by the eigenvalue  $E = 1 - c$ ,  $x_i$  is either 0 or 1 for  $c \gg 1$ . For the state described by the eigenvalue  $E = (1 - c)/2$ , the function has the value  $\{x_1 = x_2 = \pm 1/\sqrt{2}\}$ . For  $E = (3 - c)/2$ ,  $x_i$  takes the values  $\{x_1 = -x_2 = \pm 1/\sqrt{2}\}$ .

As in the previous chapter, we can extend this work to 3 sites. Figure 4.2

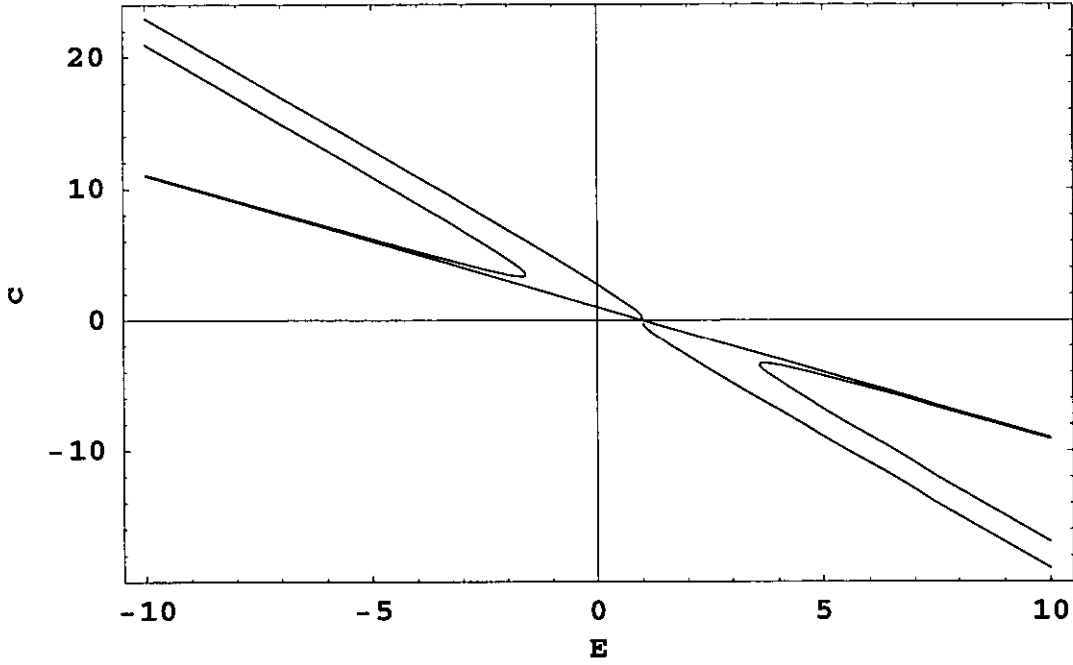


**Figure 4.1** The dependence of energy spectrum on the parameter  $c$  for a 2-site problem with OBC. The lines of the spectrum correspond to (from bottom up on the left hand side) the eigenvalues  $E = 1 - c$ ,  $E = (1 - c)/2$  and  $E = (3 - c)/2$ .

shows the energy spectrum for the discrete nonlinear equation (69) for the 3 site problem with periodic boundary conditions – again a linear dependence of  $E$  on  $c$  is observed. The solutions of equation (69) for the 3-site problem with PBC in the limit  $c \rightarrow \infty$  are  $\{x_1, x_2, x_3\} = \{0, \pm 1, 0\}$  for  $E = 1 - c$ ,  $\{x_1, x_2, x_3\} = \{\pm 1/\sqrt{2}, \pm 1/\sqrt{2}, 0\}$  for  $E = (1 - c)/2$ ,  $\{x_1, x_2, x_3\} = \{\pm 1/\sqrt{2}, \mp 1/\sqrt{2}, 0\}$  for  $E = (3 - c)/2$ ,  $\{x_1, x_2, x_3\} = \{\pm 1/\sqrt{3}, \pm 1/\sqrt{3}, \pm 1/\sqrt{3}\}$  for  $E = -c/3$  and  $\{x_1, x_2, x_3\} = \{\pm 1/\sqrt{3}, \mp 1/\sqrt{3}, \pm 1/\sqrt{3}\}$  for  $E = (4 - c)/3$ .

Similarly, Figure 4.3 shows the energy spectrum for (69) for the 3-site problem with open boundary conditions. Again we find an amazing agreement between the complicated expressions of the exact spectra (presented graphically for simplicity) and the empirical formulae for  $c \gg 1$ . The solutions of equation (69) for the 3-site problem with OBC in the limit  $c \rightarrow \infty$  are  $\{x_1, x_2, x_3\} = \{0, \pm 1, 0\}$  for  $E = 1 - c$ ,  $\{x_1, x_2, x_3\} = \{\pm 1/\sqrt{2}, \pm 1/\sqrt{2}, 0\}$  for  $E = (1 - c)/2$ ,  $\{x_1, x_2, x_3\} = \{\pm 1/\sqrt{2}, 0, \pm 1/\sqrt{2}\}$  for  $E = (2 - c)/2$ ,  $\{x_1, x_2, x_3\} = \{\pm 1/\sqrt{2}, \mp 1/\sqrt{2}, 0\}$  for  $E =$

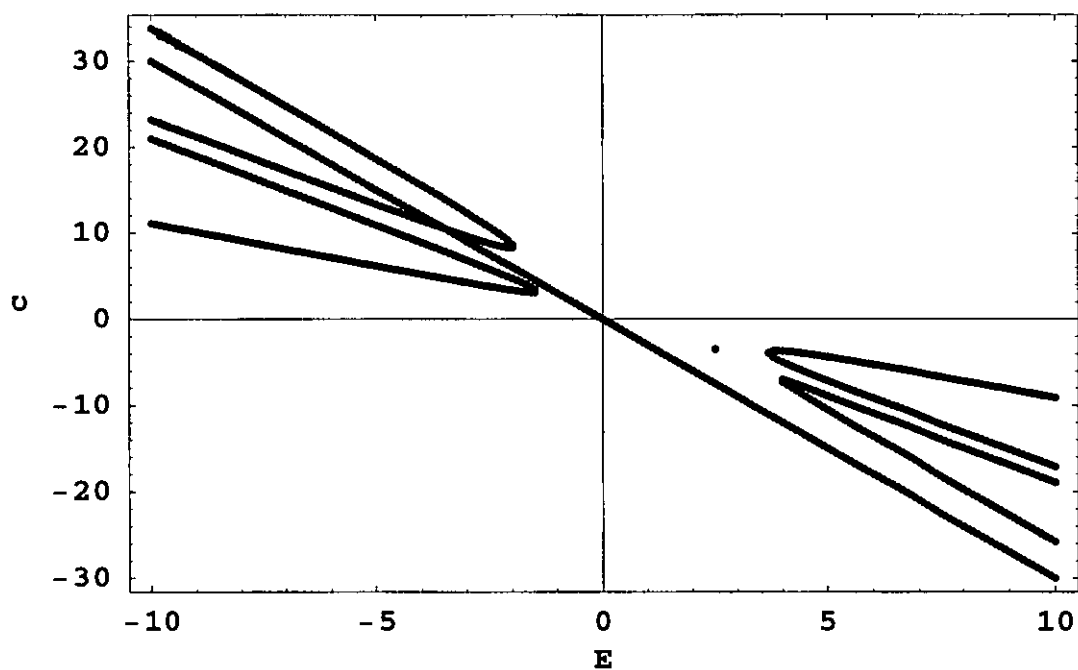


**Figure 4.2** *The dependence of energy spectrum on the parameter  $c$  for a 3-site problem with PBC. The lines of the spectrum correspond to (from bottom up on the left hand side) the eigenvalues  $E = 1 - c$ ,  $E = (1 - c)/2$ ,  $E = (3 - c)/2$ ,  $E = -c/3$  and  $E = (4 - c)/3$ .*

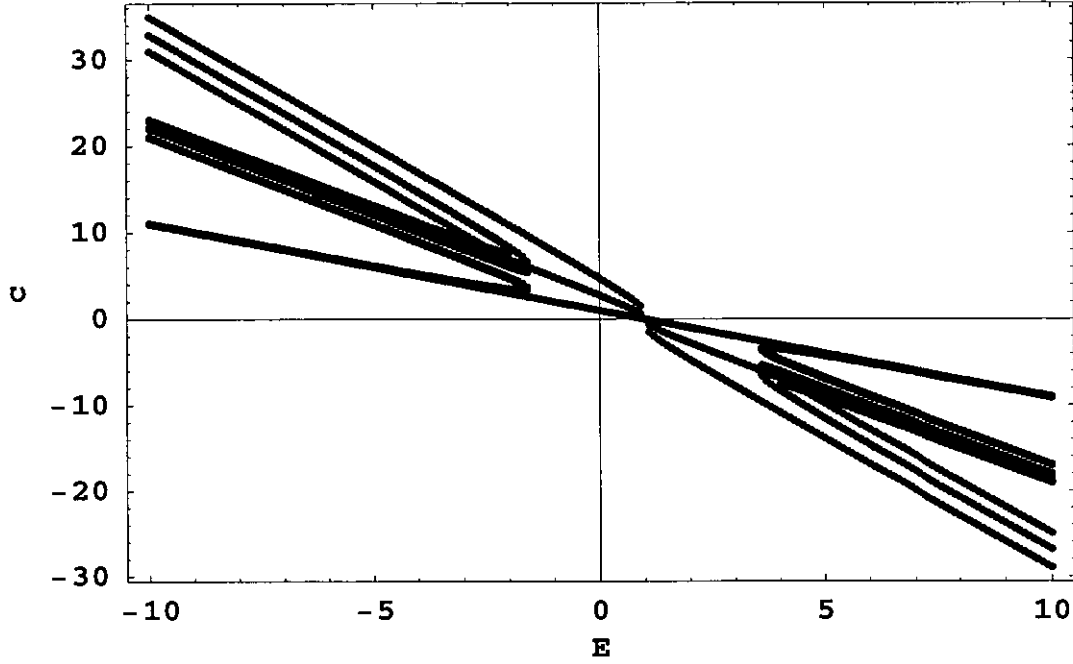


**Figure 4.3** The dependence of energy spectrum on the parameter  $c$  for a 3-site problem with OBC. The lines of the spectrum correspond to (from bottom up on the left hand side) the eigenvalues  $E = 1 - c$ ,  $E = (1 - c)/2$ ,  $E = (2 - c)/2$ ,  $E = (3 - c)/2$ ,  $E = (1 - c)/3$ ,  $E = (3 - c)/3$  and  $E = (5 - c)/3$ .

$(3 - c)/2$ ,  $\{x_1, x_2, x_3\} = \{\pm 1/\sqrt{3}, \pm 1/\sqrt{3}, \pm 1/\sqrt{3}\}$  for  $E = (1 - c)/3$ ,  $\{x_1, x_2, x_3\} = \{\pm 1/\sqrt{3}, \pm 1/\sqrt{3}, \mp 1/\sqrt{3}\}$  for  $E = (3 - c)/3$  and  $\{x_1, x_2, x_3\} = \{\pm 1/\sqrt{3}, \mp 1/\sqrt{3}, \pm 1/\sqrt{3}\}$  for  $E = (5 - c)/3$ .

Analogously to the work presented in the previous chapter, it is noticed that in the limit  $c \rightarrow \infty$  the spectrum again has some special features associated with the pattern of the localised states. The value  $x_i$  of the function at site  $i$  again only takes three distinct values  $-0, \pm 1/\sqrt{N}$  where – as before –  $N$  is the number of sites where the function is localised. The elementary spectrum of (69) depends on how large this set of localising sites is and how many spots –  $m$  – and kinks –  $l$  – this set is separated into.

In the limit  $c \rightarrow \infty$ , the spectrum of eigenvalues takes the form

$$E_{N,m,l} = \frac{m + 2l - c}{N} \quad (70)$$

which is very similar to the spectrum of the DNSE presented in Chapter 2. The considerable amount of success enjoyed in solving first and second order discrete nonlinear equations with cubic nonlinearity suggests that this method of studying discrete nonlinear equations may be applied to solve discrete equations with any order difference and cubic nonlinearity.

*'Time is that gift of nature which keeps everything from happening at once.'*

— C. J. Overbeck

## 5 Conclusion and Outlook

### 5.1 Conclusion

Having started my PhD in October 1997 in the Department Of Physics at Loughborough University with Professor Feodor Kusmartsev I worked on mainly two projects associated with the investigation of solutions of discrete nonlinear equations and their physical applications.

One of these equations is the discrete nonlinear Schrödinger Equation (or Discrete Self-trapping Equation) which may generically be applied to many physical phenomena including the (Rashba)-Holstein polaron model [3, 4], superconducting states in layered superconductors [5], systems of coupled nonlinear oscillators [6], metal insulator transitions in Peierls systems [9], electron locking in layered structures [29], [31] and magnetic multilayer systems. This equation takes the form

$$-\psi_{i-1} + 2\psi_i - \psi_{i+1} - c|\psi_i|^2\psi_i = E\psi_i \quad (71)$$

where  $\psi_i$  is the wave function on the  $i^{th}$  site,  $c$  is some coupling constant and  $E$  is the energy eigenvalue. Previously this equation has been studied by either making the continuum approximation and solving the resultant second order differential equation [3, 4] or representing this equation in the form of a 2D map and iterating [6, 7, 8, 9].

However, we found that the DNSE may, in the limit  $c \rightarrow \infty$ , be solved exactly whilst maintaining the discrete nature of the equation [29, 30]. The spectrum of this equation takes the elegant form

$$E_{N,m,l} = \frac{2m + 4l - c}{N} \quad (72)$$

where  $N, m, l$  are integer numbers describing the structure of the wave function. The wave function is localised on  $N$  sites with equal amplitude in a pattern consisting of  $m$  spots and  $l$  kinks.

These results were applied to electron-phonon interactions in layered structures



[29], [31]. The lowest energy corresponds to the trapping of an electron in a single quantum well but other states may potentially be thermally activated.

Magnetic multilayer systems may also be described by the other equation studied [19]

$$-2\phi_{n-1} + 4\phi_n - 2\phi_{n+1} + \beta \sin 2\phi_n = 0 \quad (73)$$

In the framework of this model, we characterised the possible interlayer magnetic structures created in magnetic multilayers – by representing this equation in the form of a 2D map and iterating – and found three qualitatively different types of structures: periodic (spin density waves), quasiperiodic (spin oscillations and domains) and chaotic (spin vortices and spin glass) states. The magnetic structures created depend on  $\beta$ , the parameter associated with the interlayer magnetic moment interactions. As  $\beta$  is increased the periodic structures first transform into the quasiperiodic and then into the chaotic glass states. The same tendency arises with  $\phi_0$ , the depolarization of the magnetic moments of the first layer deposited on the substrate of the magnetic multilayer.

## 5.2 Future Work

Previous work on the DNSE, which has been done in the continuum limit, suggests that the DNSE has only one localised solution. Our work – which takes into account the *discrete* nature of the system – suggests that the continuum approximation is insufficient because it does not describe the possible states which may emerge in a discrete nonlinear system; there are a whole host of states which simply do not exist in the continuum limit!

Taking these additional states into consideration there are many issues which should be investigated – or reinvestigated – to improve our understanding of discrete nonlinear systems: the conditions for the existence and the hierarchy of the rich variety of structures; the influence of an external force on the system and how this affects the types of structures created and their hierarchy; the dynamical evolution and stability of these structures; and finally the thermodynamics and statistical mechanics of these discrete systems. All this could be generalised to two and three dimensions and related to physically measurable quantities.

### 5.2.1 Static Magnetic Multilayer Structures

For the example of a discrete nonlinear system of magnetic multilayers, it should be possible – using the results of previous work [29, 30] – to discuss collinear structures (where the amplitude of the magnetisation of each layer is the same) for  $c \gg 1$ . From preliminary studies, we anticipate that the homogeneous structure will have the lowest energy, but what of the existence and hierarchy of excited states? In addition, the structures created within each magnetic layer should also be investigated. This then gives rise to the possible appearance of skyrmions.

### 5.2.2 Influence Of A Magnetic Field On Magnetic Multilayers

The obvious step forward to extend the previous work is by applying an external magnetic field to the magnetic multilayer system and studying what effect this has on the type of structures which arise and their hierarchy. This can be done by

including a Zeeman term  $-\mathbf{M}_i \cdot \mathbf{H}$  in the Hamiltonian describing the system where  $\mathbf{M}_i$  is the magnetisation of the  $i$ th magnetic layer and  $\mathbf{H}$  is the magnetic field.

### 5.2.3 Dynamics Of Discrete Nonlinear Systems

The time dependent behaviour of discrete nonlinear systems may also be interesting and give a greater understanding of the stability of structures which arise in these systems. For example the existence of spatially-localised excitations, ie discrete breathers [32] is plausible. Breathers exist in a variety of nonlinear lattices [33] including arrays of Josephson junctions where they have been observed experimentally [34, 35] and studied theoretically [36]. These arrays may also be described by some model associated with (dynamical) discrete nonlinear systems. For the example of magnetic multilayers it is possible that there also exist (breather excitation) states where the magnetisation of one of the layers is varying with time while the magnetisation of the other layers does not change.

This issue could be investigated by including a second order time derivative (similar to [37]) in the equations which describe the system

$$-\psi_{i-1} + 2\psi_i - \psi_{i+1} - c\psi_i^3 = \frac{\partial^2 \psi_i}{\partial t^2} \quad (74)$$

### 5.2.4 Statistical Mechanics Of Discrete Nonlinear Systems

The different states of any system are difficult to analyse in detail. Even if we knew the initial state of the system and its evolution *and* could solve the resulting system, it is unlikely that we could use the vast amount of data practically. Classically, the possible states of a macroscopic system are treated by some averaging procedure that allows the prediction of the important (thermodynamic) variables, for example, energy and entropy, of that system. However, this averaging procedure is not well-defined for discrete systems.

Previous work on the statistical mechanical properties of a discrete nonlinear system [38] has made use of the continuum approximation discussed earlier. However, we find [30] that there exist a multitude of states in a discrete system which

simply do not exist in the continuum limit. These additional states may significantly modify the statistical mechanical properties of the discrete system and therefore this issue should be reinvestigated.

With the use of the exact solutions discussed in Chapter 2 it should be possible to obtain the partition function of the discrete system

$$z = \sum_{i=1}^w \exp(-\beta E_i) \quad (75)$$

where there are a total of  $w$  configurations of the system.

In this suggested work the principal emphasis should lie on the *discrete* nature of the system and then a contrast with continuum results made. After calculating the discrete partition function of the system, one could obtain expressions for quantities such as magnetisation and susceptibility for the example of magnetic multilayers and compare the predicted theoretical results with experimental results.

The results of the study of the statistical mechanics of discrete nonlinear systems will be widely applicable to a variety of scientific areas including electron-phonon interactions, magnetic multilayers, semiconductor superlattices, layered superconductors and neural networks. This work may even suggest alternative approaches to the conceptual and quantitative study of spatially discrete systems.

## References

- [1] H. S. Dhillon (unpublished)
- [2] R. C. Hilborn, *Chaos And Nonlinear Dynamics*, Oxford University Press, New York, 1994
- [3] E. I. Rashba, *Opt. Spectr.* **2**, 78, **2**, 88 (1957)
- [4] T. Holstein, *Ann. Phys.* **8**, 343 (1959)
- [5] W. E. Lawrence and S. Doniach, in *Proceedings Of 12th International Conference On Low Temperature Physics*, ed. E. Kanda (Academic Press Of Japan) (1971)
- [6] K. E. Kürten, in *Condensed Matter Theories*, ed. J. da Providencia and B. Malik (Plenum, New York) Vol. 13 (1998)
- [7] F. V. Kusmartsev and K. E. Kürten, *Effects of Chaos in Quantum Lattice Systems in Lecture Notes in Physics*, ed. J. W. Clark and M. L. Ristig (Springer-Verlag, New York Heidelberg Berlin) Vol. 284 (1997)
- [8] S. Aubry, *J. de Physique* **44** 147 (1983)
- [9] P. Bak and V. L. Pokrovsky, *Phys. Rev. Lett.* **47** 958 (1981)
- [10] M. A. Howson, *Contemporary Physics* **35** 347 (1994)
- [11] Oxford Reference, *A Concise Dictionary Of Physics*, (Oxford University Press, Oxford, New York, 1990)
- [12] F. J. Keller, W. E. Gettys, M. J. Skove, *Physics: Classical and Modern*, (McGraw-Hill Inc., 1993)
- [13] D. E. G. Williams, *The Magnetic Properties of Matter*, (Longmans, 1966)
- [14] C. Kittel, *Introduction to Solid State Physics*, (John Wiley & Sons, Inc., New York, Chichester, Brisbane, Toronto, Singapore, 1996)

- [15] W. J. Duffin, *Electricity and Magnetism*, (McGraw-Hill Inc., 1973)
- [16] N. W. Ashcroft, N. D. Mermin, *Solid State Physics*, (Saunders College, 1976)
- [17] A. Geim, *Physics Today*, **51** 36 (1998)
- [18] P. M. Chaikin, T. C. Lubensky, *Principles of condensed matter physics*, (Cambridge University Press, Cambridge, 1995)
- [19] F. V. Kusmartsev, H. S. Dhillon, M. D. Crapper, *JMMM* **198-199** 743 (1999)
- [20] S. Aubry, P. Y. Le Daeron, *Physica* **D 8**, 381, (1983)
- [21] S. Wolfram, *The Mathematica Book*, (Wolfram Media/Cambridge University Press, 1999)
- [22] E. I. Rashba, in: *Excitons*, ed. by E. I. Rashba and M. D. Sturge, North-Holland (Amsterdam) 1982, p.543
- [23] F. V. Kusmartsev, *Phys. Rev.* **B43**, 1345 (1991)
- [24] F. V. Kusmartsev et al, *Europhys. Lett.* **42** 547 (1998)
- [25] A. S. Alexandrov and N. F. Mott, *Polarons and Bipolarons* (WS, Singapore) (1995)
- [26] E. I. Rashba, *Synth. Met.* **64**, 255 (1994)
- [27] F. V. Kusmartsev, E. I. Rashba, *Sov. Phys.- JETP* **59**, 668 (1984)
- [28] M. Johansson, M. Hörnquist, R. Riklund, *Phys. Rev.* **B 52**, 231 (1995)
- [29] F. V. Kusmartsev, H. S. Dhillon, *Phys. Rev.* **B 60**, 6208 (1999)
- [30] H. S. Dhillon, F. V. Kusmartsev, K. E. Kürten, *JNLMP*, **8** 38 (2001)
- [31] H. S. Dhillon, F. V. Kusmartsev, *Physica* **B 284**, 1780, (2000)
- [32] S. Flach, C. R. Willis, *Phys. Rep.* **295** 181 (1998)

- [33] C. Baesens, R. S. MacKay, *Nonlinearity* **7**, 59 (1994)
- [34] E. Trias, J. J. Mazo, T. P. Orlando, *Phys. Rev. Lett.* **84**, 741 (2000)
- [35] P. Binder, D. Abraimov, A. V. Ustinov, *Phys. Rev. Lett.* **84**, 745 (2000)
- [36] R. T. Giles, F. V. Kusmartsev, *Physica B* **284**, 1850 (2000), F. V. Kusmartsev  
(private communications)
- [37] C. I. Christov, G. Nicolis, *Physica A* **228**, 326 (1996)
- [38] J. A. Krumhansl, J. R. Schrieffer, *Phys. Rev. B* **11**, 3535 (1975)

*'The way we have to describe Nature is generally incomprehensible to us.'*

— Richard Feynman



## Appendices

## Appendix 1

### Mathematica Programme Used To Study Magnetic Multilayers

```
(* Setting initial conditions to generate phase portraits *)
```

```
x = 1.0;
```

```
beta1 = 2.5;
```

```
z = 0;
```

```
func = {};
```

```
func00 = {};
```

```
func1 = {};
```

```
(* Iteration to obtain phase portraits *)
```

```
(* Do[ x = N[ Mod[x , 2 Pi, -Pi ], 200];
```

```
AppendTo[func00, x];
```

```
AppendTo[func, z];
```

```
AppendTo[func1, {x, z}];
```

```
z = N[ z + (beta1/2) Sin[2 x]];
```

```
x = N[ x + z, 200],
```

```
{j, 1000}]; *)
```

```
Do[
```

```
x = N[ Mod[x , 2 Pi, -Pi ], 200];
```

```
AppendTo[func00, x];
```

```
AppendTo[func, z];
```

```
AppendTo[func1, {x, z}];
```

```
z = N[ z + (beta1/2) Sin[2 x]];
```

```
x = N[ x + z, 200],
{j, 1000}];
```

```
(* To plot phase portraits *)
```

```
ListPlot[func1, PlotRange -> All, PlotJoined -> False, Axes -> False,
Frame -> True, ImageSize -> 72 7, TextStyle -> {FontWeight -> "Bold"},
FrameLabel -> { Subscript[ $\phi$ ], n], Subscript[Z, n] }]
```

```
(* create arrays for iteration to draw structures *)
```

```
func = {};
```

```
funcz = {};
```

```
funca = {};
```

```
func00 = {};
```

```
func1 = {};
```

```
func1a = {};
```

```
func4a = {};
```

```
func4b = {};
```

```
func4c = {};
```

```
func4d = {};
```

```
func4e = {};
```

```
func4f = {};
```

```
func4g = {};
```

```
func4h = {};
```

```
func4i = {};
```

```

func4j = {};
func4k = {};

(* setting initial conditions *)

beta1 = 2.5;
x = 1.0;
z = 0;

p = 0; (* p = counter when using LPVectField *)

(* Iteration Procedure *)

Do[ AppendTo[ func00, x];
  AppendTo[ funcz, {x, z}];

  AppendTo[ func, {p, 0, Sin[x], Cos[x]}];

  (* AppendTo[ func1a, {p, Cos[x]}];
  AppendTo[ func1b, {p, Sin[x]}];
  AppendTo[ func2a, {Cos[x], z}];
  AppendTo[ func2b, {Sin[x], z}]; *)

  (* *)

  (* a1 is horizontal spacing factor in plots *)

  (* a2 is vertical spacing factor in plots *)

  a1 = 1.25;

```

```
a2 = 1.25;
```

```
AppendTo[ func4a, {0, 1.25 p, Sin[x], Cos[x]}];  
AppendTo[ func4b, {1 a1, 1.25 p, Sin[x], Cos[x]}];  
AppendTo[ func4c, {2 a1, 1.25 p, Sin[x], Cos[x]}];  
AppendTo[ func4d, {3 a1, 1.25 p, Sin[x], Cos[x]}];  
AppendTo[ func4e, {4 a1, 1.25 p, Sin[x], Cos[x]}];  
AppendTo[ func4f, {5 a1, 1.25 p, Sin[x], Cos[x]}];  
AppendTo[ func4g, {6 a1, 1.25 p, Sin[x], Cos[x]}];  
AppendTo[ func4h, {7 a1, 1.25 p, Sin[x], Cos[x]}];  
AppendTo[ func4i, {8 a1, 1.25 p, Sin[x], Cos[x]}];  
AppendTo[ func4j, {9 a1, 1.25 p, Sin[x], Cos[x]}];  
AppendTo[ func4k, {10 a1, 1.25 p, Sin[x], Cos[x]}];
```

```
z = z + (beta1/2) Sin[2x];  
x = Mod[x + z , 2 Pi, -Pi];  
p = p + 1, {j, 1000}}];
```

```
(* Transform structure of data to enable pictures to be plotted *)
```

```
f1a = Flatten[ func];  
f2a = Partition[ f1a, 2];  
f3a = Partition[ f2a, 2];  
f3a1 = Take[ f3a, {1, 100}];  
f3a2 = Take[ f3a, {101, 200}];  
f3a3 = Take[ f3a, {201, 300}];  
f3a4 = Take[ f3a, {301, 400}];  
f3a5 = Take[ f3a, {401, 500}];  
f3a6 = Take[ f3a, {501, 600}];  
f3a7 = Take[ f3a, {601, 700}];
```

```
f3a8 = Take[ f3a, {701, 800}];
f3a9 = Take[ f3a, {801, 900}];
f3a10 = Take[ f3a, {901, 1000}];
```

(\* To plot 10 pictures \*)

```
g1 = ListPlotVectorField[f3a1, Axes -> None, ImageSize -> 72 7,
  AspectRatio -> 0.15, ScaleFactor -> 0.8];
g2 = ListPlotVectorField[f3a2, Axes -> None, ImageSize -> 72 7,
  AspectRatio -> 0.15, ScaleFactor -> 0.8];
g3 = ListPlotVectorField[f3a3, Axes -> None, ImageSize -> 72 7,
  AspectRatio -> 0.15, ScaleFactor -> 0.8];
g4 = ListPlotVectorField[f3a4, Axes -> None, ImageSize -> 72 7,
  AspectRatio -> 0.15, ScaleFactor -> 0.8];
g5 = ListPlotVectorField[f3a5, Axes -> None, ImageSize -> 72 7,
  AspectRatio -> 0.15, ScaleFactor -> 0.8];
g6 = ListPlotVectorField[f3a6, Axes -> None, ImageSize -> 72 7,
  AspectRatio -> 0.15, ScaleFactor -> 0.8];
g7 = ListPlotVectorField[f3a7, Axes -> None, ImageSize -> 72 7,
  AspectRatio -> 0.15, ScaleFactor -> 0.8];
g8 = ListPlotVectorField[f3a8, Axes -> None, ImageSize -> 72 7,
  AspectRatio -> 0.15, ScaleFactor -> 0.8];
g9 = ListPlotVectorField[f3a9, Axes -> None, ImageSize -> 72 7,
  AspectRatio -> 0.15, ScaleFactor -> 0.8];
g10 = ListPlotVectorField[f3a10, Axes -> None, ImageSize -> 72 7,
  AspectRatio -> 0.15, ScaleFactor -> 0.8];
```

(\* To generate one picture \*)

```
Show[ GraphicsArray[ {{g1}, {g2}, {g3}, {g4}, {g5}, {g6},
{g7}, {g8}, {g9}, {g10}}], ImageSize -> {500, 700}]
```

```
(* n1 = lower level of MML, n2 = higher level of MML *)
```

```
n1 = 101;
```

```
n2 = 120;
```

```
(* Take data between n1 and n2 *)
```

```
d1a = Flatten[ func4a];
```

```
d2a = Partition[ d1a, 2];
```

```
d3a = Partition[ d2a, 2];
```

```
td3a = Take[ d3a, {n1, n2}];
```

```
d1b = Flatten[ func4b];
```

```
d2b = Partition[ d1b, 2];
```

```
d3b = Partition[ d2b, 2];
```

```
td3b = Take[ d3b, {n1, n2}];
```

```
d1c = Flatten[ func4c];
```

```
d2c = Partition[ d1c, 2];
```

```
d3c = Partition[ d2c, 2];
```

```
td3c = Take[ d3c, {n1, n2}];
```

```
d1d = Flatten[ func4d];
```

```
d2d = Partition[ d1d, 2];
```

```
d3d = Partition[ d2d, 2];
```

```
td3d = Take[ d3d, {n1, n2}];
```

```
d1e = Flatten[ func4e];  
d2e = Partition[ d1e, 2];  
d3e = Partition[ d2e, 2];  
td3e = Take[ d3e, {n1, n2}];
```

```
d1f = Flatten[ func4f];  
d2f = Partition[ d1f, 2];  
d3f = Partition[ d2f, 2];  
td3f = Take[ d3f, {n1, n2}];
```

```
d1g = Flatten[ func4g];  
d2g = Partition[ d1g, 2];  
d3g = Partition[ d2g, 2];  
td3g = Take[ d3g, {n1, n2}];
```

```
d1h = Flatten[ func4h];  
d2h = Partition[ d1h, 2];  
d3h = Partition[ d2h, 2];  
td3h = Take[ d3h, {n1, n2}];
```

```
d1i = Flatten[ func4i];  
d2i = Partition[ d1i, 2];  
d3i = Partition[ d2i, 2];  
td3i = Take[ d3i, {n1, n2}];
```

```
d1j = Flatten[ func4j];  
d2j = Partition[ d1j, 2];  
d3j = Partition[ d2j, 2];  
td3j = Take[ d3j, {n1, n2}];
```



```

d1k = Flatten[ func4k];
d2k = Partition[ d1k, 2];
d3k = Partition[ d2k, 2];
td3k = Take[ d3k, {n1, n2}];

j3 = Join[ td3a, td3b, td3c, td3d, td3e, td3f, td3g, td3h, td3i, td3j, td3k];

(* To plot data *)

graph1 = ListPlotVectorField[ j3, ImageSize -> 72 4,
ScaleFunction -> (0.7 &), AspectRatio -> 2]

graph2a =
Graphics[
Table[ Disk[{ a1 m1, 1.25 n1 + 1.25 m2}, {0.35, 0.1}],
{m1, 0, 10}, {m2, -1, n2 - n1 - 1}]]

Show[ graph1, graph2a]

```

## Appendix 2

### Mathematica Programme Used To Study The DNSE

(\* to generate initial unnormalised pattern p1 \*)

```
SeedRandom[0];  
p1 = Table[ Random[ Integer, {-1, 1}], {1000}];
```

```
Length[p1]
```

(\* to calculate initial > 'zero approximation' wave function pattern, p2,  
energy eigenvalue, e1 and specify coupling constant, c \*)

```
n = p1.p1;
```

```
p2 = p1 / Sqrt[n];
```

```
m1a = RotateLeft[p1];
```

```
m2a = (p1 - m1a) ^ 2;
```

```
m = Count[m2a, 1] / 2;
```

```
l = Count[m2a, 4];
```

```
Clear["c"];  
e1 = (2m + 4l - c) / n
```

```
c = 84 (* for example *)
```

```

(* numerical value of energy *)

N[e1]

(* to iterate the wave function and generate figures *)

funcx2 = {};

Do[ {

(* wave function n + 1 *)

p2l = RotateLeft[p2];

(* wave function n - 1 *)

p2r = RotateRight[p2];

(* wave vector f RHS of vector equation  $T x = f$ 
where T is matrix & x is wave vector corrections *)

Clear["f1"];
f1 = Simplify [ (e1 p2 + c p2 ^ 3 + p2l - 2 p2 + p2r)];

(* size of tmatrix is related to system size, s *)

s = Length[p2];

(* tmatrix = T in vector equation
depends on size of system

```

to set all elements of T to zero \*)

```
Clear["tmatrix"] ;
```

```
Do[ tmatrix[i, j] = 0, {i, s}, {j, s}];
```

(\* terms on leading diagonal \*)

```
Do[ tmatrix[i, i] = 2. - 3 c (p2[[i]]) ^ 2 - e1, {i, s}];
```

(\* terms just below leading diagonal \*)

```
Do[ tmatrix[i, i - 1] = - 1., {i, s}];
```

(\* terms just above leading diagonal \*)

```
Do[ tmatrix[i, i + 1] = - 1., {i, s}];
```

(\* PBC give non - zero terms on end elements of off - diagonal \*)

```
tmatrix[1, s] = -1; tmatrix[s, 1] = -1;
```

```
Clear["t1"]; t1 = Array[ tmatrix, {s, s} ] ;
```

(\* inverse of tmatrix \*)

```
Clear["t2"]; t2 = Inverse[t1];
```

(\* corrections to wave vector \*)

```

Clear["x1"]; x1 = Simplify[t2.f1];

(* non - normalised wave vector with corrections ready for
use for next iteration: rnfl = renormalisation factor *)

p2 = p2 + x1;

x2 = x1.x1;
AppendTo[funcx2, x2];

rnfl = Sqrt[p2.p2];

(* p2 = p3/rnfl; *)

(* to map z against wave function psi *)

$TextStyle = {FontFamily -> "Helvetica", FontWeight -> "Bold",
FontSize -> 12};
psi = p2 ;
psil = RotateLeft[psi];
z1 = Simplify[ psil - psi];
func1 = {}; Do [ AppendTo[func1, {psi[[i]], z1[[i]]}], {i, s
}];

ListPlot[ psi, PlotRange -> All, FormatType -> TraditionalForm ];

ListPlot[ func1, PlotRange -> All, Axes -> False, Frame -> True,
FormatType -> TraditionalForm ];

(* energy, e, with next order corrections *)

```

```

sump1 = Apply[Plus, p2];

sump3 = Expand[ Apply[Plus, p2 ^ 3]];

e2 = Simplify[(- c sump3) / sump1];

Print[e2];

Print[rnf1];

Print[x2];

Print[iter];

}, {iter, 10}]

ListPlot[ funcx2, PlotRange -> All, Axes -> False, Frame -> True,
FormatType -> TraditionalForm ];

```



